OFFICE OF CIVILIAN RADIOACTIVE WASTE MANAGEMENT

MODEL COVER SHEET

1. QA: QA

Complete Only Applicable Items

2. Type of Mathematical Model
Process Model ☒ Abstraction Model ☐ System Model ☐
Describe Intended Use of Model:

To be used as Input to License Application

Technical Contact/Department: Stephen Lu/Waste Package

3. Title:
Stress Corrosion Cracking of the Drip Shield, the Waste Package Outer Barrier, and the Stainless Steel Structural Material

4. DI (Including Rev. No. and Change No., if applicable):
ANL-EBS-MD-000005 REV 01 ICN 00

5. Total Attachments:
N/A

6. Attachment Numbers – No. of Pages in Each:
N/A

	Printed Name	Signature	Date
7. Originator	Stephen Lu	SIGNATURE ON FILE	7/15/03
8. CSO	David Stahl	SIGNATURE ON FILE	7/15/03
9. Checker	Tyzh-Chiang Sun	SIGNATURE ON FILE	7/16/03
10. QER	Charles Warren	SIGNATURE ON FILE	7/16/03
11. Responsible Manager/Lead	Tammy Summers	SIGNATURE ON FILE	7/16/03
12. Responsible Manager	Curtis Glower	SIGNATURE ON FILE	7/16/03

13. Remarks:

Applicable Technical Error Reports are TER-02-0024 and TER-02-0051.

MODEL REVISION RECORD

2. Model Title:
Stress Corrosion Cracking of the Drip Shield, the Waste Package Outer Barrier, and the Stainless Steel Structural Material

3. DI (including Rev. No. and Change., if applicable):
ANL-EBS-MD-000005 REV 01 ICN 00

4. Revision/Change No.	5. Description of Revision/Change
00	Initial Issue
00/01	PCG Back Check and Design Review Copy. This AMR has been changed to include “no backfill” design and more data in support of analysis in the Waste Package Degradation PMR ICN 01 (WP PMR) and SR-CR. Vertical bars in the right margin of the text indicate the changes made in ANL-EBS-MD-000006 REV 00 ICN 01.
00 ICN 01	Interim Change Notice is to remove TBV-4897. Assumption 5.5 added, and Sections 6.3.3 and 8.1 modified. The input statuses of some of the references in the Document Input Reference System (DIRS) report have been revised. Changes made in this Analysis and Model Report are indicated by vertical lines in the right margin.
01A Draft 04B	The new complete draft of REV 01 submitted for CSO Review on 2/20/03.
01A Draft 04C	CSO Review Comment Resolution Copy (3/6/03). Per CSO review comments, (1) high-level criteria identified in NRC's YM Review Plan were added to Section 4.2; (2) assumptions 2, 3, & 4 were removed from Section 5; and (3) Section 6.5.3 was revised. Approved by CSO on 3/6/03.
01A Draft 04E	Technical Check Copy (3/26/03) which is similar to REV 01A Draft 04C.
01B	QER Check Copy (4/15/03). This is the result of intensive rewriting to incorporate comments from informal peer reviews with the following major changes from REV 01A Draft 04E: (1) The discussion of crack initiation and manufacturing flaws has been placed ahead of discussing the crack growth model; (2) Kiscc is no longer an alternative model but part of the base-case crack growth model; (3) Clarification has been added to identify the currently recommended WP design, the WP design configurations used in calculating stress and stress intensity factor profiles, and the basis for using these calculations for the current design; (4) Figures and equations are numbered from 1 to N; (5) Tables 8-1 through 8-5 have been added in Section 8 to summarize output data of the SCC AMR; and (6) References have been added, deleted, and checked for consistency between the listing and quote in the text.
01C	Technical Back Check Copy (4/23/03) which is REV 01B plus changes to incorporate technical checker's comments marked in REV 01A Draft 04E.
01D	Back Check Copy / QER Back Check Copy (5/9/03). The entire document has been revised per checker's and QER's comments.
01E	QER Back Check Copy (5/21/03). Changes made in Sections 1, 2, 3, 6.2.1, 6.3.4, 6.3.5, 6.4.2.2, 6.5.2, 7.4, 8, and 9 for resolution of additional QER's comments applicable to REV 01D.
01F	Back Check Copy (6/11/03). The document was revised mainly to incorporate changes in Sections 4.1 (Table 4.1-5), 6.2.2.2, 6.3.5 (Table 6-3), 6.4.3, 7.4, and 8 (Tables 8-1 and 8-3) resulting from the change of one source (input) DTN (LL021010212251.004), which was superseded by LL030412512251.057. There are also textual changes made for the purpose of clarification as results of additional comments from the checker and review by the responsible manager.
01G	Review Copy (6/12/03). Same as REV 01F. There are no more comments from the Technical Checker and QER’s only comments are related to nonqualified DTN’s, which will be resolved before issuing this document.
01/00	Final Copy (7/13/03). The entire document has been revised. Changes are too extensive to be identified by vertical bars at the right margin of each page.

CONTENTS

Page

FIGURES

Page

ACRONYMS

ACM	Alternative Conceptual Model
AMR	Analyses and Models Report
BWR	Boiling Water Reactor
CEF	Coupled Environment Fracture
CLST	Container Life and Source Term
CRWMS	Civilian Radioactive Waste Management System
CW-GTAW	Cold Wire Feed Gas Tungsten Arc Welding
DCB	Double Cantilever Beam
DOE	U.S. Department of Energy
DS	Drip Shield
DTN	Data Tracking Number
EBS	Engineering Barrier System
EDA	Enhanced Design Alternative
FEP	Features, Events, and Processes
GC	General Corrosion
GEGRC	General Electric Global Research Center
GTAW	Gas Tungsten Arc Welding
HIC	Hydrogen Induced Cracking
HLW	High Level Radioactive Waste
IRSR	Issue Resolution Status Report
IWPD	Integrated Waste Package Degradation
IWPDM	Integrated Waste Package Degradation Model
KTI	Key Technical Issue
LA	License Application
LC	Localized Corrosion
LLNL	Lawrence Livermore National Laboratory
LOF	Lack of Fusion
LOP	Lack of Penetration
LTCTF	Long Term Corrosion Test Facility
MIC	Microbiologically Influenced Corrosion
M&O	Management and Operating Contractor
NACE	National Association of Corrosion Engineers
NDE	Non-destructive Examination

ACRONYMS (continued)

NRC	U.S. Nuclear Regulatory Commission
OCRWM	Office of Civilian Radioactive Waste Management
PA	Performance Assessment
PMR	Process Model Repor
PWR	Pressurized Water Reactor
QA	Quality Assurance
QAP	Quality Administrative Procedures
QARD	Quality Assurance Requirements and Description
QP	Quality Procedure
SCC	Stress Corrosion Cracking
SCE	Saturated Calomel Electrode
SDFR	Slip Dissolution/Film Rupture
SECP	Single Edge Cracked Plate
SIA	Structural Integrity Associates
SIF	Stress Intensity Factor
SNF	Spent Nuclear Fuel
SSRT	Slow Strain Rate Test
TPO	Technical Product Output
TSIF	Threshold Stress Intensity Factor
TSPA	Total System Performance Assessment
TSPA-LA	Total System Performance Assessment for License Application
TWP	Technical Work Plan
UT	Ultrasonic
UTS	Ultimate Tensile Strength
WAPDEG	Waste Package Degradation
WP	Waste Package
WPD	Waste Package Degradation, Waste Package Department
WPML	Waste Package Middle Lid
WPOB	Waste Package Outer Barrier
WPML	Waste Package Middle Lid
YMP	Yucca Mountain Site Characterization Project

1. PURPOSE

1.1 PURPOSE AND BACKGROUND

The current revision of this analysis/model report (AMR), ANL-EBS-MD-000005, was prepared according to the *Technical Work Plan for: Waste Package Materials Data Analysis and Modeling*, TWP-EBS-MD-000005 REV 05 (BSC 2002 [161132]). As directed by the Technical Work Plan, an analysis of the potential degradation by stress corrosion cracking (SCC) of the drip shields and waste packages in the engineered barrier system (EBS) of the proposed repository at Yucca Mountain is to be conducted. This analysis is conducted by the Performance Assessment Project's (PAP) Waste Package Department (WPD) to provide a basis for assessing waste package (WP) and drip shield (DS) degradation by SCC under exposure conditions anticipated in the proposed repository. This analysis will also provide information useful in satisfying requirements of the Yucca Mountain Review Plan (NRC 2002 [158449]). Comments by the Waste Package Peer Review Panel (Beavers, et al. 2002 [158781]) as well as Key Technical Issue (KTI) Agreements raised by the Nuclear Regulatory Commission (NRC) (Reamer 2001 [158380]) were also considered. In the case of the WPOB and DS, the critical environment is conservatively taken as any aqueous environment contacting the metal surfaces including thin aqueous films as well as dripping water and bulk aqueous electrolytes. Further, for any of these environmental cases, SCC can occur over the full expected temperature range for both the WPOB and the DS.

Relevant Features, Events, and Processes (FEPs) considered in this AMR include: FEP 2.1.03.02.0A, *stress corrosion cracking (SCC) of waste packages*, and FEP 2.1.03.02.0B, *stress corrosion cracking (SCC) of drip shields* (DTN: MO0301SEPFEPS1.000). This AMR does not provide a direct basis for the inclusion of the FEPs in the Total System Performance Assessment for License Application (TSPA-LA). Rather, the results of the model/analysis are used by the model document, Integrated Waste Package Degradation Model (IWPDM) (ANL-EBS-PA-000001), which is currently in preparation, to develop a basis for implementing the FEPs in the TSPA-LA. Nevertheless, the technical basis for the inclusion of these FEPs and the process that will be utilized to implement the included FEPs are discussed in Section 6.1.

Technical errors identified in Technical Error Reports TER-02-0024 and TER-02-0051 resulting from the Model Validation Status Review conducted by the U.S. Department of Energy (DOE) (BSC 2001 [156257], Section 6.10 are addressed in Section 7 (Model Validation) of this AMR.

The consequence of an SCC failure of the DS, the waste package outer barrier (WPOB), or the stainless steel structural material is the initiation and propagation of tight, sometimes branching cracks that might be induced by the combination of an aggressive environment and various types of tensile stresses that can develop in the DSs or the WPs. For the current design of the DS and WP, the Type 316 stainless steel inner structural cylinder of the WP will be excluded from the SCC evaluation. The SCC performance assessment will not take credit for the inner cylinder. Therefore, this document provides a detailed description of the process-level models that can be applied to assess the performance of Alloy 22, used for the WPOB, and titanium grade 7 (Ti-7), used for the DS, subjected to the effects of SCC. The possibility of using laser peening or other

residual stress mitigation techniques is considered as a means of mitigating SCC in the WP final closure weld.

Uncertainties (see Sections 6.3.4, 6.3.5, and 6.4.5) and limitations (see Section 6.1) of the process level models associated with SCC are also addressed in this AMR. As indicated in Section 5, no assumption was used to perform the model activity in this AMR.

1.2 MODEL OVERVIEW

SCC is the initiation and propagation of cracks in metal components due to three factors presenting simultaneously: material susceptibility, critical environment, and static (or sustained) tensile stress. Alloy 22, the material used for WPOB, is highly corrosion resistant but it will be shown in this AMR that its susceptibility to SCC cannot be ignored for the Yucca Mountain environment and the co-existing stress conditions described in Section 6.4. For the DS, Section 6.3.7 provides a post-cracking analysis, which forms the technical basis for screening out SCC in the DS. A lifetime modeling scheme is developed to assess the degradation of the WPOB due to SCC. As indicated by the flow diagram shown below, the lifetime modeling considers both crack initiation and pre-existing manufacturing flaws (Section 6.2), the stress conditions that drive the crack initiation and propagation (Section 6.4), the stress threshold that defines the crack initiation (Section 6.2.1), the threshold stress intensity factor (Section 6.3.5) that defines propagation of both initiated incipient cracks and manufacturing flaws, the crack growth model (based on the film rupture/slip dissolution theory) that determines the crack growth rate (Section 3). The SCC model provides all the elements (as summarized in Section 8) needed for the performance of a lifetime prediction of the WPOB subjected to the effects of SCC.

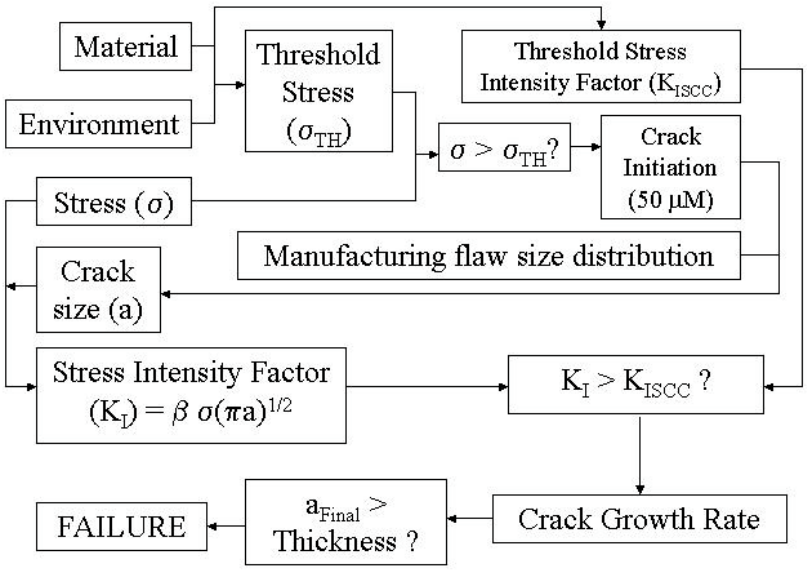

Flow Diagram of SCC Model

2. QUALITY ASSURANCE

The Office of Civilian Radioactive Waste Management (OCRWM) Quality Assurance (QA) program applies to this AMR. The drip shield (DS) was clasiffied (per QAP-2-3) as Quality Level-1 in *Classification of the MGR Uncanistered Spent Nuclear Fuel Disposal Container Syste*m (CRWMS M&O 1999 [106190], p. 8). All types of waste packages were classified per QAP-2-3 as Quality Level-1 based on the conclusion of *Classification of the MGR Uncanistered Spent Nuclear Fuel Disposal Container Syste*m (CRWMS M&O 1999 [105154], p. 7). This classification is still in effect.

This revision of the AMR has been developed per AP-SIII.10Q [162696] procedure under *Technical Work Plan for: Waste Package Materials Data Analyses and Modeling* (BSC 2002 [161132]), which, in turn, was developed in accordance with AP-2.27Q [159604], *Planning for Science Activities*. The applicability of *Quality Assurance Requirements and Description* requirements (DOE 2003 [162903]) is documented in the technical work plan (TWP) (BSC 2002 [161132], Section 8). A process control evaluation was performed in accordance with AP-SV.1Q [160533], *Control of the Electronic Management of Information*., with evaluation results documented in Attachment A of the technical work plan (BSC 2002 [161132]). The process for control of the electronic management of information on evaluation of work activities/processes/process functions, outlined in Section 5.0 of AP-SV.1Q [160533], is followed to ensure accuracy, completeness, and security of information and data used in preparation of this AMR. Examples of process controls mentioned in AP-SV.1Q [160533] are (a) access to the information contained on personal computer is password protected; (b) secured backup copies are appropriately labeled and stored before changes are made and kept until the changes are confirmed and correct; (c) physical electronic media (tape, diskette, CD-ROM, etc.) are appropriately labeled; and (d) for non-physical electronic media, transport mechanisms can be e-mail, TCP/IP, Netbios, etc. and methods of receipt verification may include visual inspection, transmission verification settings, check sums, application information integrity check, etc.

3. COMPUTER SOFTWARE USAGE

No software or computer codes were used directly in developing this AMR. The computer software/code generated data on through-thickness residual stress and stress intensity factor profiles at the welds of the middle and outer lids of the waste package design were obtained by procurement from a qualified vendor. These data, presented in DTN: LL000316205924.142 were developed using vendor (Structural Integrity Inc., San Jose, CA) internally qualified computer software that was accepted by OQA. Accordingly, these data are designated acquired not developed for this AMR.

Microsoft Excel 97 was used to perform support calculations and graphics. *Microsoft Excel 97* is a standardized commercial spreadsheet program designed to assist in routine calculations and graphics. The program provides built-in mathematical functions that can be used to automate the calculation process. It also includes a graphics package to assist in data presentation. *Microsoft Excel* is exempt from software qualification because, in accordance with AP-SI.1Q, *Software Management* [161284], Section 2.1.1, office automation systems such as word processors and spreadsheets are not required to be qualified. Furthermore, according to AP-SI.1Q, *Software Management* [161284], the graphical representation use of Excel can be exempted under Section 2.1.2 and the calculations using built-in mathematical function use can be exempted under Section 2.1.6. When Excel is used for calculations (see Section 6.3.4), information required for an independent person to reproduce the work (including formula or algorithm used, listing of inputs, and listing of outputs) is provided.

4. INPUTS

4.1 DATA AND PARAMETERS

The data providing input for the development of parameters and/or other databases used in the models/analyses documented in this AMR are identified in Table 4.1. While uncertainty in the input data is discussed in Section 6, this table and the accompanying Tables 4.1-1 through 4.1-5 and Figure 1 provide

- A description of the data set(s) used
- A roadmap to what data are in the DTN, if applicable
- A description on how the data are used to develop input parameters for the model/analyses.

The input data are appropriate for using as input to the model/analyses documented in this AMR because they are either qualified acquired or accepted data or qualified and verified test data developed specifically for this AMR. No developed parameters or other input information are used in the model/analyses documented in this AMR. Number of figures used for numerical data in this AMR often exceed that of significant figures for concern of round-off errors.

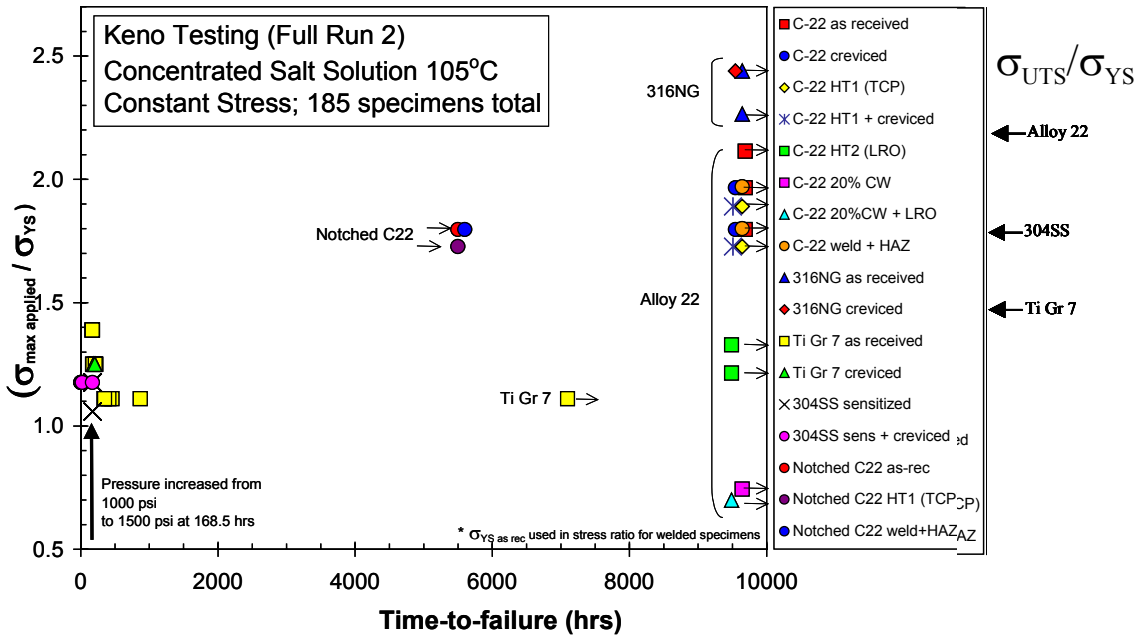

Note: Target test solution composition: 0.27M Na_2CO_3, 0.35M KCl, 0.41M NaCl, 0.013M NaF, 0.43M $NaNO_3$, 0.03M Na_2SO_4, 0.04M $Na_2SiO_3.9H_2O$ (pH = 12.4 at room temperature) and p 94. This composition represents an approximately 15% solution of Basic Saturated Water (BSW) whose target composition is given in DTN: LL021105312251.023, p 3. DTN: LL021105312251.023, Figure 2-1

Figure 1. Failure stress vs. time-to-failure.

Table 4.1. Input Data

Data Name	Data Source	DTN	Discussion
Measured crack growth rates in mm/s for Alloy 22 specimens c153, c144, and c152 tested for stress intensity factors of 30 and 45 MPa√m.	Stress corrosion cracking growth and initiation measurements in for C-22 and Ti-7, General Electric Global Research Center (GECRC) 121202. Submittal date: 01/08/2003	LL021105312251.023	Input data (see Table 4.1-1) are used in Section 6.3.4 for determining the repassivation slope 'n' of the slip dissolution/film rupture model.
Crack initiation measurements for Alloy 22 and titanium grade 7 specimens.	Stress corrosion cracking initiation & growth measurements in environments relevant to high level nuclear waste packages. Submittal date: 01/08/2003	LL021105312251.023	Input data (see Figure 1) are used in Section 6.2.1 for determining the threshold stress for crack initiation for Alloy 22 and titanium grade 7.
Coefficients of stress profiles, A_0, A_1, A_2, and A_3.	Stress corrosion cracking of the drip shield, the waste package outer barrier and the stainless steel structural material. Submittal date: 03/22/2000.	LL000316205924.142	Input data (see Table 4.1-2) are used in Section 6.4.2 for stress profiles in as-welded and laser peened Alloy 22 closure lids.
Stress intensity factor profiles.	Stress corrosion cracking of the drip shield, the waste package outer barrier and the stainless steel structural material. Submittal date: 03/22/2000.	LL000316205924.142	Input data (see Table 4.1-3) are used in Section 6.4.2.

Table 4.1. Input Data (Contnued)

Data Name	Data Source	DTN	Discussion
YS (yield strength) for Alloy C22	Waste package material properties: corrosion resistant materials.	MO0003RIB00071.000	Input data (see Table 4.1-4) are used in Sections 6.2.1 & 6.4.5.
YS (yield strength) for titanium grade 7	Waste package material properties: corrosion resistant materials.	MO0003RIB00073.000	Input data (see Table 4.1-4) are used in Sections 6.2.1 & 6.3.7.
E (modulus of elasticity) for titanium grade 7	Waste package material properties: corrosion resistant materials.	MO0003RIB00073.000	Input data (see Table 4.1-4) are used in Section 6.3.7.
V_{gc}, general corrosion rates for Alloy 22	Corrosion rate calculations for Alloy C22 after 5+ years exposure.	LL030412512251.57	Input data (see Table 4.1-5) are used in Section 6.3.5.

Table 4.1-1. Measured Crack Growth Rates for Alloy 22 Specimens

Specimen	Tested stress intensity factor, MPa(m)^.5	Measured Crack Growth Rate, mm/s	Source (page # of DTN: L021105312215.023
c153	30	2.50E-10	p. 11
c153	30	5.00E-10	p. 11
c144	30	See note below	p. 7
c152	45	See note below	p. 10
c152	45	4.00E-10	p. 10

Note: Test results indicated that either cracking appeared to cease or growth rate seemed to arrest.

Table 4.1-2. Coefficients of Stress Profiles for the Original and Modified CRM-21 PWR Design from DTN: LL000316205924.142.

Stress coefficient	A_0	A_1	A_2	A_3	Source in DTN
Unit	ksi	ksi/in	ksi/in^2	ksi/in^3	
As-welded 25-mm lid, radial stress Sx	16.871	33.5486	-294.333	264.368	File Skvrbr1, sheet UnAnneal,Sx, cells C9-C12.
As-welded 25-mm lid, hoop stress Sz	55.4242	29.8255	-186.269	143.597	File Skvrbr1, sheet UnAnneal,Sz, cells C9-C12.
As-welded 10-mm lid, Sn on Sec. 1-1	26.344	-427.51	934.32	-596.71	File Thinlid11, sheet UnAnneal,1-1,Sn, cells C9-C12.
As-welded 10-mm lid, Sz on Sec. 2-2	31.895	101.42	-463.23	297.75	File Thinlid11, sheet UnAnneal,2-2,Sz, cells C9-C12.
Laser peened 25-mm lid, radial stress Sx	-38.5684	383.082	-922.377	603.035	File Skvrbr1, sheet Peening,Sx, cells C9-C12.
Laser peened 25-mm lid, hoop stress Sz	-42.4391	656.764	-1322.67	759.752	File Skvrbr1, sheet Peening,Sz, cells C9-C12.

Table 4.1-3. Stress Intensity Factor (SIF) Profiles from DTN: LL000316205924.142.

As-welded outer lid, CRM-21 PWR Design			As-welded 10-mm lid, Modified CRM-21 PWR Design			Outer lid with laser peening, CRM-21 PWR Design		
DTN File Skvrbr1			DTN File Thinlid11			DTN File Skvrbr1		
Sheet UnAnnel,Sx Cells A87-A136	Sheet UnAnnel,Sx Cells C87-C136	Sheet UnAnnel,Sz Cells I87-I136	Sheet UnAnnel,1-1,Sn Cells A89-A138	Sheet UnAnnel,1-1,Sn Cells C89-C138	Sheet UnAnnel,2-2,Sz Cells C89-C138	Sheet Peening,Sx Cells A87-A136	Sheet Peening,Sx Cells C87-C136	Sheet Peening,Sz Cells C87-C136
Crack size, mm	SIF for Sx, MPa √m	SIF for Sz, MPa √m	Crack size, mm	SIF for Sn, MPa √m	SIF for Sz, MPa √m	Crack size, mm	SIF for Sx, MPa √m	SIF for Sz, MPa √m
0.3988	4.5146	9.1593	0.2438	4.9033	7.5754	0.3988	-9.1866	-5.6943
0.8001	6.5821	12.9737	0.4902	6.2685	10.9665	0.8001	-11.7979	-6.4965
1.1989	8.2395	15.9139	0.7341	6.8580	13.7144	1.1989	-13.0189	-6.1528
1.6002	9.6422	18.4031	0.9804	6.9761	16.1330	1.6002	-13.4298	-5.1372
1.9990	10.8381	20.6048	1.2243	6.7631	18.3358	1.9990	-13.2965	-3.6697
2.4003	11.8425	22.6028	1.4681	6.3044	20.3775	2.4003	-12.7780	-1.8824
2.7991	12.8589	24.4741	1.7145	5.8250	22.3816	2.7991	-12.2958	0.1212
3.2004	13.7858	26.2367	1.9583	5.2651	24.3197	3.2004	-11.7214	2.2821
3.5992	14.5688	27.9039	2.2047	4.6000	26.1726	3.5992	-11.0116	4.5533
3.9980	15.2083	29.4912	2.4486	3.8615	27.9459	3.9980	-10.2080	6.8939
4.3993	15.7061	31.0103	2.6924	3.0726	29.6433	4.3993	-9.3437	9.2702
4.7981	16.0778	32.4703	2.9388	2.2534	31.2668	4.7981	-8.4525	11.6543
5.1994	16.4072	33.9004	3.1826	1.4282	32.8922	5.1994	-7.6096	14.0165
5.5982	16.7029	35.3092	3.4290	0.5951	34.5292	5.5982	-6.8298	16.3364
5.9995	16.8783	36.6797	3.6728	-0.2400	36.1060	5.9995	-6.0675	18.6024
6.3983	16.9527	38.0157	3.9167	-1.0656	37.6220	6.3983	-5.3416	20.8003
6.7970	16.9314	39.3202	4.1631	-1.8707	39.0762	6.7970	-4.6612	22.9177
7.1984	16.8188	40.5961	4.4069	-2.6491	40.4676	7.1984	-4.0331	24.9441
7.5971	16.7108	41.8581	4.6533	-3.4047	41.8264	7.5971	-3.4507	26.9023

Table 4.1-3. Stress Intensity Factor (SIF) Profiles from DTN: LL000316205924.142. (Continued)

7.9985	16.7482	43.1357	4.8971	-4.1787	43.2168	7.9985	-2.8535	28.8612
8.3972	16.7231	44.3927	5.1410	-4.9390	44.5479	8.3972	-2.2745	30.7287
8.7986	16.6321	45.6302	5.3873	-5.6775	45.8181	8.7986	-1.7170	32.5008
9.1973	16.4938	46.8495	5.6312	-6.3965	47.0265	9.1973	-1.1860	34.1745
9.5987	16.3042	48.0515	5.8776	-7.0865	48.1718	9.5987	-0.6829	35.7479
9.9974	16.0808	49.2372	6.1214	-7.7528	49.2531	9.9974	-0.2101	37.2200
10.3962	16.0751	50.4839	6.3652	-8.2576	50.3451	10.3962	-0.3513	38.4530
10.7975	15.9957	51.7195	6.6116	-8.7427	51.3729	10.7975	-0.5163	39.5674
11.1963	15.8601	52.9442	6.8555	-9.2143	52.3351	11.1963	-0.7070	40.5636
11.5976	15.6646	54.1589	7.1018	-9.6605	53.2313	11.5976	-0.9242	41.4432
11.9964	15.4259	55.3639	7.3457	-10.0894	54.0602	11.9964	-1.1690	42.2086
12.3977	15.1398	56.5598	7.5895	-10.4950	54.8214	12.3977	-1.4403	42.8627
12.7965	15.0982	57.8007	7.8359	-10.9446	55.4811	12.7965	-1.7949	43.4439
13.1978	15.0836	59.0538	8.0797	-11.4131	56.0586	13.1978	-2.1728	43.9342
13.5966	15.0159	60.3022	8.3261	-11.8636	56.5637	13.5966	-2.5554	44.3269
13.9954	14.8966	61.5462	8.5700	-12.3055	56.9965	13.9954	-2.9438	44.6272
14.3967	14.7274	62.7862	8.8138	-12.7309	57.3567	14.3967	-3.3378	44.8409
14.7955	14.5229	64.0228	9.0602	-13.1320	57.6444	14.7955	-3.7396	44.9743
15.1968	14.6570	65.2900	9.3040	-13.7114	57.7587	15.1968	-4.0160	45.0329
15.5956	15.1057	66.5871	9.5504	-14.4707	57.6946	15.5956	-4.1354	45.0208
15.9969	15.4787	67.8801	9.7942	-15.2333	57.5522	15.9969	-4.2182	44.9464
16.3957	15.7929	69.1690	10.0381	-15.9891	57.3322	16.3957	-4.2696	44.8182
16.7945	16.0516	70.4537	10.2845	-16.7277	57.0353	16.7945	-4.2904	44.6449
17.1958	16.2578	71.7343	10.5283	-17.4611	56.6626	17.1958	-4.2805	44.4361
17.5946	16.6700	73.0349	10.7747	-18.4707	56.1419	17.5946	-4.3087	44.2112
17.9959	17.6878	74.4062	11.0185	-20.3589	55.3276	17.9959	-4.5204	43.9968
18.3947	18.5558	75.7773	11.2624	-22.2128	54.4422	18.3947	-4.7313	43.7750
18.7960	19.2803	77.1483	11.5087	-24.0173	53.4878	18.7960	-4.9400	43.5578
19.1948	19.8861	78.5193	11.7526	-25.7872	54.6294	19.1948	-5.1487	43.3569
19.5961	20.3775	79.8904	11.9990	-27.4989	56.2191	19.5961	-5.3536	43.1853
19.9949	20.7777	81.2616	12.2428	-29.1709	57.7865	19.9949	-5.5551	43.0560

Table 4.1-4. Input Data for Yield Strength, and Modulus of Elasticity

Input Data Name (Input DTN)	Temperature K (^{o}C)	Input Data Value	Input Data Unit
YS (yield strength) for Alloy C22 (MO0003RIB00071.000)	Room Temperature 366 (93) 477 (204)	372 338 283	MPa
YS (yield strength) for titanium grade 7 (MO0003RIB00073.000)	Room Temperature 477 (204)	275-450 138-152	MPa
E (modulus of elasticity) for titanium grade 7 (MO0003RIB00073.000)	294 (21) 366 (93) 422 (149)	106.87 103.42 100.66	GPa

Table 4.1-5. 5-year General Corrosion (GC) Rates (in nanometers/year) from DTN: LL030412512251.057

Sample	GC rate	Sample	GC rate	Sample	GC rate	Sample	GC rate	Sample	GC rate	Sample	GC rate
DCA 019	9.40	DCA 053	8.30	DCA 111	5.77	DCA 175	0.82	DCB 049	16.07	DCB 112	9.05
DCA 020	8.22	DCA 054	6.40	DCA 112	3.11	DCA 176	0.81	DCB 050	14.51	DCB 113	10.86
DCA 021	8.63	DCA 079	3.06	DCA 113	10.56	DCA 177	46.67	DCB 052	4.29	DCB 139	0.00
DCA 022	6.36	DCA 080	3.10	DCA 114	10.91	DCA 178	8.40	DCB 053	5.92	DCB 140	2.85
DCA 023	9.75	DCA 081	4.19	DCA 139	4.71	DCA 179	5.24	DCB 079	2.00	DCB 142	2.03
DCA 024	22.52	DCA 082	9.52	DCA 140	3.54	DCA 180	5.28	DCB 080	7.88	DCB 143	5.69
DCA 049	12.04	DCA 083	7.23	DCA 141	2.74	DCB 019	10.24	DCB 082	19.58	DCB 175	0.41
DCA 050	17.29	DCA 084	14.71	DCA 142	6.27	DCB 020	6.94	DCB 083	13.61	DCB 176	2.08
DCA 051	15.75	DCA 109	5.81	DCA 143	5.89	DCB 022	5.84	DCB 109	4.32	DCB 178	1.25
DCA 052	5.76	DCA 110	11.60	DCA 144	8.27	DCB 023	6.89	DCB 110	2.01	DCB 179	0.41

4.2 CRITERIA

The Waste Package Technical Work Plan (BSC 2002 [161132], Table C5) has identified the following acceptance criteria (AC) based on the requirements mentioned in the Project Requirements Document (Canori and Leitner 2003 [161770]) and the Yucca Mountain Review Plan (NRC 2003 [162418]):

1. System Description and Demonstration of Multiple Barriers (NRC 2003 [162418], Section 4.2.1.1.3; PRD-002/T-014, PRD-002/T-016)

2. Scenario Analysis and Event Probability (NRC 2002 [158449], Section 4.2.1.2.1.3; PRD-002/T-015)

3. Degradation of Engineered Barriers (NRC 2002 [158449], Section 4.2.1.3.1.3; PRD-002/T-015)

A closer examination indicates that only Criteria 3 (Degradation of Engineered Barriers) is applicable to this AMR. Specific requirements include describing deterioration or degradation of engineered barriers and modeling degradation processes using data for performance assessment, including total system performance assessment (TSPA). Consideration of uncertainties and variabilities in model parameters and alternative conceptual models are also required. To fulfill these requirements, the following acceptance criteria are identified in the Waste Package TWP (BSC 2002 [161132], Table C5):

- AC1: System Description and Model Integration are Adequate
- AC2: Data are Sufficient for Model Justification
- AC3: Data Uncertainty is Characterized and Propagated Through the Model Abstraction
- AC4: Model Uncertainty is Characterized and Propagated Through the Model Abstraction
- AC5: Model Abstraction Output is Supported by Objective Comparisons

4.3 CODES AND STANDARDS

No codes and standards were used to develop the model for this AMR.

5. ASSUMPTIONS

No assumption was used to perform the model activity in this AMR.

6. MODEL DISCUSSION

6.1 INTRODUCTION

One of the most common corrosion-related causes for premature fracture of metal structural components is stress corrosion cracking (SCC). SCC is the initiation and propagation of cracks in structural components due to three factors, which must be present simultaneously: metallurgical susceptibility, critical environment, and static (or sustained) tensile stresses.

The discussion on SCC will be restricted to the waste package outer barrier (WPOB) and the drip shield (DS), which are made of Alloy 22 and titanium grade 7, respectively. The stainless steel structural material is not modeled. Performance assessment does not take corrosion credit from the stainless steel inner barrier of the WP.

Alloy 22, the material used for WPOB, is highly corrosion resistant but it will be shown in the rest of this section that its susceptibility to SCC cannot be ignored for the test conditions that simulate the Yucca Mountain environment (Sections 6.2 and 6.3) and the co-existing stress conditions induced by welding in the closure welds of the WP lids (Section 6.4). For the DS, Section 6.3.7 provides a post-cracking analysis, which forms the technical basis for screening out SCC in the DS.

A lifetime modeling scheme is developed to assess the degradation of the WPOB due to SCC. As indicated by the flow diagram shown in Section 1.2, the lifetime modeling considers both crack initiation and pre-existing manufacturing flaws (Section 6.2), the stress conditions that drive the crack initiation and propagation (Section 6.4), the stress threshold that defines the crack initiation (Section 6.2.1), the threshold stress intensity factor (Section 6.3.5) that defines propagation of both initiated incipient cracks and manufacturing flaws, the crack growth model (based on the film rupture/slip dissolution theory) that determines the crack growth rate (Section 3). The SCC model provides all the elements (as summarized in Section 8) needed for the performance of a lifetime prediction of the WPOB subjected to the effects of SCC.

Stress corrosion cracking has historically been separated into “initiation” and “propagation” phases (Jones and Ricker 1987, p. 146). For the purpose of lifetime modeling, it is appropriate that initiation is associated with microscopic crack formation at localized corrosion or mechanical defect sites. In the area of environmentally assisted cracking (such as SCC), coalescence of microscopically small cracks will take place and develop into deeper cracks. Ford and Andresen (1988, p. 798) used a crack size of 0.05 mm to start propagating SCC cracks. Initial cracks can also be flaws (or defects) resulting from manufacturing processes (such as welding). Crack initiation (including the threshold stress for crack initiation) and manufacturing defects are discussed in Section 6.2.

To account for crack propagation, the slip dissolution/film rupture (SDFR) model is adopted in this AMR as the base-case model to provide mathematical formulas for the prediction of crack growth rate. The SDFR model relates the advance (or propagation) of cracks, subsequent to crack initiation from the bare metal surface, to the metal oxidation that occurs when the protective film at the crack tip is ruptured. The SDFR SCC model is described in Section 6.3. A crack, however, may reach an “arrest” state before it enters the "propagation" phase. There exists

a threshold stress intensity factor (SIF), which provides a criterion for determining if an initiated crack or pre-existing flaw will reach the "arrest" state. The threshold SIF is based on the theory that below a threshold value (K_{ISCC}) for the stress intensity factor, K_I, no growth occurs for a given crack. The threshold SIF (K_{ISCC}) will be discussed in Section 6.3.6 and the determination of the weld induced stress and K_I profiles through the WP wall will be described in Section 6.4 of the AMR. The threshold stress, threshold stress intensity factor, and parameters associated with the SDFR crack growth model are determined from experimental data developed for environments relevant to the waste package and drip shield materials used in the Yucca Mountain repository. Therefore, there do not appear to be limitations as they are applied to the performance assessment of waste packages and drip shields.

An alternative conceptual model, the coupled environmental fracture (CEF) model, was developed for the case where the internal and external environments are coupled by the need to conserve charge in the system. The CEF model represents an alternative approach to the base-case SDFR model for the prediction of the crack growth rate. It will not be used to evaluate the total system performance assessment (TSPA) but will be considered in the AMR only for the purpose of validation of the base-case model. The CEF model and the technical basis for screening out this model are discussed in Section 6.3.6.

Both the base-case SDFR model and the alternative CEF model were developed to account for SCC of sensitized Type 304 stainless steel. An evaluation of other SCC models for sensitized Type 304 stainless steel indicates a lack of theoretical basis for these models (Macdonald and Urquidi-Macdonald 1991). Therefore, no additional alternative conceptual models for SCC are considered in this AMR.

Output parameters associated with the base-case crack growth models developed in this AMR will be used as one input to the total system performance assessment. A summary of the various output to be generated by this AMR is presented in Section 8.

6.2 CRACK INITIATION AND MANUFACTURING FLAWS

6.2.1 Threshold Stress for SCC Initiation

For a given alloy, metallurgical condition, set of environmental conditions, and in the absence of cyclic stresses, initiation of SCC will not occur on a 'smooth surface' (without sharp defects such as weld defects that can generate a significant stress intensity factor) if the surface stress is below a threshold value defined as the threshold stress (ASM International 1987, Vol. 13, p. 276). Recently obtained SCC crack initiation measurements under constant load conditions reported in DTN: LL021105312251.023 are summarized in Figure 12 (which is Figure 2-15 in DTN: LL021105312251.023), where the measurements of crack initiation stress are presented as applied stress ratio (the ratio of applied stress to yield strength) vs. time-to-failure (or total exposure time without failure) for specimens subjected to 9,600 hours of exposure in hot concentrated salt solution (pH=10.3 at 105^{o}C), known as Basic Saturated Water (BSC 2001 [155640], Section 6.12), designed to simulate the chemistry of concentrated Yucca Mountain ground water. The reference indicated that Alloy 22 exhibits excellent SCC resistance since failure was not observed for any of the 120 Alloy 22 specimens covering a variety of

metallurgical conditions (including the as-welded condition). The applied stress ratios were up to about 2.1 times the yield strength (YS) of the as-received material and up to 2.0 times the yield strength of the welded material. This stress ratio corresponds to an applied stress of about 89 to 96% of the ultimate tensile strength (UTS). The high degree of SCC initiation resistance for Alloy 22 is corroborated by results of high magnification visual examination of a number of Alloy 22 U-bend specimens exposed to a range of relevant environments at 60 and 90°C (Fix et al. 2003). No evidence of SCC initiation has been observed in these U-bend specimens after five years of exposure.

Titanium grade 7 was apparently more susceptible to SCC initiation as indicated by specimen failures at applied stress ratios of about 1.1 to 1.4 times the yield strength in the constant load tests summarized in Figure 1. Some specimens failed relatively early (≤168 hours) at applied stresses above 110% of yield stress but, at 110% of yield stress, there was a mixture of failure and non-failure runout times from ~200 hours for first failure to greater than 7000 hours without failure. This is consistent with a runout stress somewhat less than 110% of yield stress and is estimated to be at the yield stress value. A threshold value very near the yield stress is also consistent with the observation that no SCC initiation was detected in a number of fixed deflection titanium Grade 7 U-bend test specimens exposed for two years and titanium Grade 16 (an analogous Ti-Pd alloy) specimens exposed for five years to a range of relevant environments at 60 and 90°C (Fix et al. 2003). These U-bend specimens were bent ~180 degrees and then the legs were restrained to give an apex strain (cold work level) of greater than about 10% which resulted in sustained stress levels at or over yield stress.

Since the above SCC initiation test results are for exposures out to five years, an extrapolation scheme is needed in order to derive a defensible threshold stress value associated with the lifetime of waste packages and drip shields from the available experimental results. The ASME Boiler Pressure Vessel code (ASME 1969, p. 80) typically uses a safety factor of 2 on the runout stress (endurance limit) for defining fatigue lifetime cycles. Following this precedent, the threshold stress value (criterion) may be derived from the minimum failure stress (or runout stress without failure) obtained from the constant load tests (i.e., 2.0 (YS) for Alloy 22 and 1.1(YS) for titanium grade 7) by applying an appropriate safety factor. Based on the criterion that the safety factor used should be consistent with or somewhat more conservative than the ASME code precedent and the resulting threshold stress should not exceed 0.9(YS), a stress reduction factor of 2.2 is applied to the estimated runout stress to obtain a threshold stress value. This approach results in threshold stress values of 0.9(YS) for Alloy 22 and 0.5(YS) for titanium Grade 7. The YS values or Alloy 22 and titanium grade 7 are listed in Table 4.1-4. For conservative purpose, it is recommended that the YS value at the maximum temperature is to be used. The estimated temperature is 200°C (with YS approximately 286 MPa) for the waste package (see Section 6.3.4) and 140°C (with YS approximately 221 MPa) for the drip shield (see Section 6.3.7).

The development of threshold stress is based on uniaxial test data. However, assessment of the integrity of components subjected to a multiaxial stress condition using uniaxial information is an acceptable and industry consistent approach. For example, the prediction of stress-strain behavior in sophisticated elastic-plastic analyses typically uses the equivalent (von Mises) stress-strain approach and uniaxial material stress-strain behavior. The American Society of Mechanical Engineers (ASME) Boiler and Pressure Vessel Code uses uniaxial based material

strength data to assess multi-axial stress conditions. In order to apply the uniaxial stress-strain information to multiaxial conditions, principal stresses are used. This approach considers that a combination of stresses can be equivalent to a uniaxial condition. Even in a uniaxial stress-strain test (where failure typically occurs along the 45-degree plane, in pure shear), the cross sections that are not perpendicular to the load line are in a biaxial stress condition that is "equivalent" to the uniaxial condition. These biaxial stress states can be observed using Mohr's circle. Thus, the use of uniaxial stress-strain curves for multiaxial loading conditions is acceptable when used in combination with Von Mises stresses determined from the stress analyses. It is often a good simplification to consider only the principal stress component.

Density of Incipient Cracks–In a commercial metal alloy, there is a relatively high density of potential incipient surface cracks associated with microscopic discontinuities such as precipitates, grain boundaries, passive film rupture sites, etc. The surface of the WP is divided into many subdivisions, referred to as patches, in the performance assessment. Patch size in terms of width and length will be determined by the size of the closure weld as well as the stress distribution in and near the weld since failure can only occur in the closure weld. In any given surface location where the principal tensile stress above the threshold value exists, multiple cracks may initiate and grow together but only one becomes predominant. Therefore, it appears to be sufficient to consider one incipient crack per patch for the WP performance assessment (i.e., the number of incipient cracks is the same as the number of patches along the circumferential weld).

Incipient Crack Size–Environmental cracking has historically been separated into “initiation” and “propagation” phases (Jones and Ricker 1987, p. 146). Although the particular crack depth defining the separation of the two phases is arbitrary, for the purpose of lifetime modeling it is defined here that the initiation is associated with microscopic crack formation at localized corrosion or mechanical defect sites. A crack size of 0.05 mm is developed (Ford and Andresen 1988, p. 798) if the stress exceeds the threshold stress. Thereafter, the crack may either reach the arrest state or the "propagation" phase once the crack tip stress intensity factor exceeds the threshold K_{ISCC} value.

6.2.2 Manufacturing Flaws

6.2.2.1 Flaw Size and Flaw Density Distribution

Flaw size and flaw density distributions are addressed in the *Analysis of Mechanisms for Early Waste Package/Drip Shield Failure* (BSC 2003 [161238], Section 6.2.1).

The current welding process being considered for the WP final closure weld is one of Gas Tungsten Arc Welding (GTAW) processes (CRWMS M&O 1996 [124950], p. 5). This process selection is fully consistent with the recommendations resulting from an expert evaluation of a range of potential closure welding processes (Lundin 2002). This evaluation concluded that the Cold Wire Feed Gas Tungsten Arc Welding (CW-GTAW) process should be selected for the WP final closure weld process to be implemented in a hot cell. This process was chosen primarily for its ability to provide high quality closure weld joints with optimum control of the welding variables. This process produces welds that can be readily inspected by automated and remote methods (Lundin 2002). The choice of the GTAW process also naturally limits and defines the

size and other characteristics of the discontinuities that can be induced during welding. Further, the weld face is optimally contoured for ready inspection by remote visual methodologies. The discontinuities generated by GTAW are well defined and include lack of penetration (LOP), lack of fusion (LOF), porosity and microfissuring. It is also possible to form defects such as tungsten inclusions, caused by the flaking of the tungsten electrode. The extent of any of the discontinuities noted above will be related to a single weld pass and do not have a tendency to propagate between passes during welding. Thus, they are of a nature, which naturally limits their size and orientation within the weld. Since the possible generation of discontinuities during welding is limited to the types indicated above, they are readily amenable to detection by remote and automated inspection using eddy current, ultrasonic and visual methods. With a priori knowledege of the type and orientation of any discontinuities, the non-destructive examination (NDE) processes most capable for detection and sizing of the discontinuities can be defined (Lundin 2002). Since the volumetric ultrasonic (UT) inspection method will be employed as the primary flaw detection method for post-weld inspections, there should be no significant undiscovered subsurface defects for these welds. Additionally, eddy current or surface wave type UT inspections are planned for evaluating the surface of the weld to detect and repair any surface breaking defects. The lack of fusion defect is by definition, oriented in the direction of the weld bead. The tungsten inclusion and porosity defects tend to be smaller, rounded defects that have no effective directionality.

Consistent with the above discussion, the expected type, size and orientation of defects that can result from the GTAW process is supported by a recent weld defect evaluation study in which sixteen full diameter 21 PWR container Alloy 22 closure weld mockup ring specimens were fabricated using a prototypical cold-wire GTAW process under conditions that simulated hot cell type access restrictions (Smith 2003, Sections 1.1 and 2.3). Weld defects present in these rings were examined by various NDE techniques including liquid penetrant and eddy current surface examinations and volumetric radiographic and ultrasonic (UT) examinations (Smith 2003, Section 3). These were followed by metallographic destructive examination (Smith 2003, Section 4). Information gathered from these weld mockup experiments were used to develop a flaw density, orientation and size distribution applicable to the closure welds of the WP (BSC 2003 [161238], Section 6.2.1). The UT inspection defect detection threshold used was 1 mm and this was confirmed by the metallographic examinations that verified the presence of eight defects (BSC 2003 [161238], p.12) that were detected by UT and confirmed by metallography. The UT dimensions were consistent with or slightly overestimated the metallographically measured dimensions (BSC 2003, p.12). Imperfections uncovered by metallographic examinations but not detected by UT inspections were gas bubbles, and the majority of them were less than 0.003 inch (approximately 0.08 mm) in diameter (BSC 2003 [161238], p. 16). Gas bubbles are spherical in shape (BSC 2003 [161238], p. 16) and are not sharp cracks which can propagate due to stress corrosion cracking (Andresen and Ford 1985, p. 20). Crack initiation on the bubble surface due to stress concentration is ruled out since weld induced tensile stress at and near the WP surface will be mitigated. All flaws found in the mockup specimens were in the weld metal and root of the weld. The flaws were characterized as lack of fusion in each case (Smith 2003, Section 5.1). Based on the results of this sixteen weld mockup ring study, the defect size and orientation distributions were determined and reported (BSC 2003 [161238]).

The initial weld flaw size distribution is exponentially distributed with an upper bound truncation due to the weld thickness. The size distribution parameter is uncertain and described by a gamma

distribution (BSC 2003 [161238], Section 6.2.1.1.1, Equation 2). Flaws are uniformly distributed spatially and their frequency of occurrence is represented by a Poisson distribution. The mean flaw density (Poisson distribution parameter) of the closure weld region is uncertain and described by a gamma distribution (BSC 2003 [161238], Section 6.2.1.1.2, Equation 12). These densities were derived from analysis of the defects observed in sixteen welded rings subjected to ultrasonic tests.

These flaw characteristics are representative of those to be expected in the non-inspected weld. An ultrasonic inspection will be performed to detect and repair the flaws that would affect the waste package performance. Consideration of this fact is modeled by use of a probability of non-detection curve to derive post inspection flaw size and density distributions (BSC 2003 [161238], Section 6.2.1.2, Equations 24 and 28).

6.2.2.2 Embedded Flaws

As general corrosion proceeds, embedded flaws can become surface breaking flaws. Consideration of pre-existing surface breaking flaws only may not be conservative. As an alternative conservative approach, the fraction of flaws considered for propagation is increased by adding a fraction of the flaws embedded within the entire thickness region of the weld in the performance assessment. It is recommended that the fraction of surface breaking flaws is increased by adding the fraction of flaws embedded within the 1/4 thickness region of the weld surface. This recommendation appears to be conservative since, based on the mean general corrosion rate of 7.23 nm/year (Section 6.3.5), it will take 864,400 years to remove the 1/4 thickness of the surface of the outer lid or 345,800 years to remove the 1/4 thickness of the surface of the middle lid.

6.2.2.3 Radial Crack Versus Circumferential Crack in WP Closure Welds

The defect description and orientation distribution obtained from the sixteen-ring study (BSC 2003 [161238]) is consistent with Shcherbinskii and Myakishev (1970) that describes a statistical treatment of weld flaw orientations based on analysis of a significant data set of ultrasonic flaw orientation measurement and concludes that planar type weld defects detected ultrasonically tend to be predominately oriented in the direction of the weld center line. More than 98% of the defects fall within ±16 degrees of the weld center line in the case of steam pipe welds, e.g., the tails of the distributions fall to less than 2% probability as the azimuth approaches 90 degrees (Shcherbinskii & Myakishev, 1970, Fig. 1). A similar conclusion, drawn from the data for plate welds (Shcherbinskii & Myakishev 1970, Fig. 2), indicates that the statistical distribution of defects with respect to the orientation angle approximated by a centered normal distribution with a maximum standard deviation of 5 degrees yields a probability of 99% that the defects are located within about ±13 degrees. These data suggest that much less than one percent of these flaws have a potential to undergo SCC as radial cracks. (Note: There appears to be an obvious typographical error in the figures. This reference is an English translation of a Russian publication. The frequencies given as 1.8 and 2.5 Hz should read 1.8 and 2.5 MHz, typical of those used in ultrasonic testing.)

As discussed above, manufacturing defects, especially those due to welding, would would likely be oriented along the weld direction. When initiated, the propagation of cracks tend to follow the

direction perpendicular to the maximum principle stresses whether the cracks are propagating due to fatigue or stress corrosion. In structures where shear stress is not significant (i.e. thin wall pipes or plates), the maximum principle stresses are the same as the three directional component stresses. Thin wall pipes are usually defined by a radius-to-wall-thickness ratio greater than 10. For an axisymmetric structure or model, there is no shear stress in the in-plane direction. The hoop (circumferencial) stress is usually the most dominant stress component and the stress in the through-wall direction (which would drive laminations) is usually the lowest among the three stress components. A typical example is a cylindrical shell subjected internal pressure loading.

Due to the orthogonality effect of stresses, once an oblique oriented crack (measured with respect to the direction of loading) turns into the direction perpendicular to the maximum stress, the stresses in the other directions have little effect in turning the crack from that direction. Thus, oblique oriented flaws turning to become perpendicular to the maximum stress cannot be ruled out. However, once this occurs, the orientation will not change. Likewise, a radial flaw, which is already oriented perpendicular to the maximum (hoop) stress, will remain radially oriented.

In addition, cracks tend to propagate in the direction that offers the least resistance. If a crack initiates at the bottom of the weld, near or in the heat affected zone, it tends to propagate in the heat affected zone, parallel to the fusion line between the weld and base metal instead of turning into the base metal at an oblique angle. Therefore, any crack, initiated and oriented in any direction at its very early stage, would adjust its direction and tend to align and propagate in the hoop or circumferential orientation, whichever results in the largest stress intensity factor.

Based on the flaw orientation measurement data given in Shcherbinskii and Myakshev (1970), there is a strong dependence of the flaw orientation on the direction of welding. This is consistent with the expected behavior that most defects are associated with the application of the weld metal and would tend to be oriented along the interface of deposited beads. Although it is unlikely that flaws will be observed at significant oblique angles to the direction of the weld travel direction, this circumstance cannot be entirely ruled out. Depending on the quality of the welds and welding procedures, a more uniform distribution with regards to angular orientation may be obtained. However, it is expected that a very tightly controlled process will be in place when the waste package closure weld is applied. If flaws are present that make a significant oblique angle with the direction of the weld placement, it would not be surprising to see the flaw direction turn towards the radial direction.

The potential for flaws turning or not turning towards the radial direction can be studied by determining the stress intensity factor for a crack in a plate, with an angle θ to the direction of the load, subjected to a constant stress. As an example, for an arbitrary stress and crack length, the ratio of the stress intensity factor for a flaw at an angle θ with the direction of the load to the stress intensity factor oriented perpendicular to the stress direction (maximum stress intensity factor) can provide some insight to the expected behavior of flaws. Figure 2 shows the ratio ($\sin^2\theta$) with respect to the angle that the flaw makes with the direction of the load. The analyses in the figure are based on the solutions presented in Tada et al. (1973, p. 5.2). The results of this calculation demonstrate that for a circumferentially oriented flaw in the waste package closure welds, subjected to hoop stress, the stress intensity factor would be very low. The ratio of

the stress intensity factor for a circumferential flaw oriented at a small angle to the load direction subjected to hoop stress to a radial flaw oriented perpendicular to the load is very low. The ratio is 0.03 and 0.05 for flaws at 5 and 10 degrees to the load direction, respectively. This demonstrates a very low driving force for the crack to change orientation from circumferentially oriented to radially oriented. This same circumferential flaw would be oriented close to 90 degrees (perpendicular) to the radial stress. The figure shows that the ratio of the stress intensity factors is at least 95% of a flaw perpendicular to the load direction ($\theta = 90$). Thus, there is a significant driving force to keep the flaw in its circumferential direction. Combined with the presence of the heat affected zone, it is unlikely that these flaws would turn radially.

Combining the test results regarding flaw orientation from Shcherbinskii and Myakshev (1970) and the stress intensity factor ratio discussed above, it is concluded that the probability of an expected circumferentially oriented flaw turning radially is very small. Only flaws that are oriented at angles greater than approximately 45 degrees with the load direction may turn in the radial direction and the probability that such flaws exist is very unlikely. Essentially all flaws will be oriented towards the direction of the welding (circumferentially). An investigation of the stress intensity factor for flaws at oblique angles to the load direction supports the conclusion that flaws oriented to within approximately ±15 degrees of the loading direction will not be subjected to sufficient driving force to cause the flaw to turn radially. Supporting this conclusion also is the fact that the flaw would need to turn away from the path of least resistance, the heat affected zone, to grow into the base or weld metal. It should be noted that if a flaw were to occur and be oriented an angle greater than ±15 degrees, the flaw orientation may change such that the flaw will become radially oriented. However, as noted earlier, the probability of such flaws occurring is small relative to flaws orienting within ±15 degrees of the welding direction.

In summary, radially oriented flaws are important to the SCC analysis for waste package lifetime calculations since the hoop stress, which drives the radially oriented cracks, is usually the dominant stress component. However, almost all of the flaws are more or less in the direction of the weld and only flaws that are oriented at angles greater than about 45 degrees with the weld direction may turn in the radial direction. As discussed earlier, about 98% to 99% of the flaws are within about ±13 to ±16 degrees of the weld center line. In accordance with all the discussions given above, it is conservative to recommend that the fraction of flaws that are radially oriented (making an angle of 45 degrees or more with respect to the direction of the weld) is around 0.5% of the flaws.

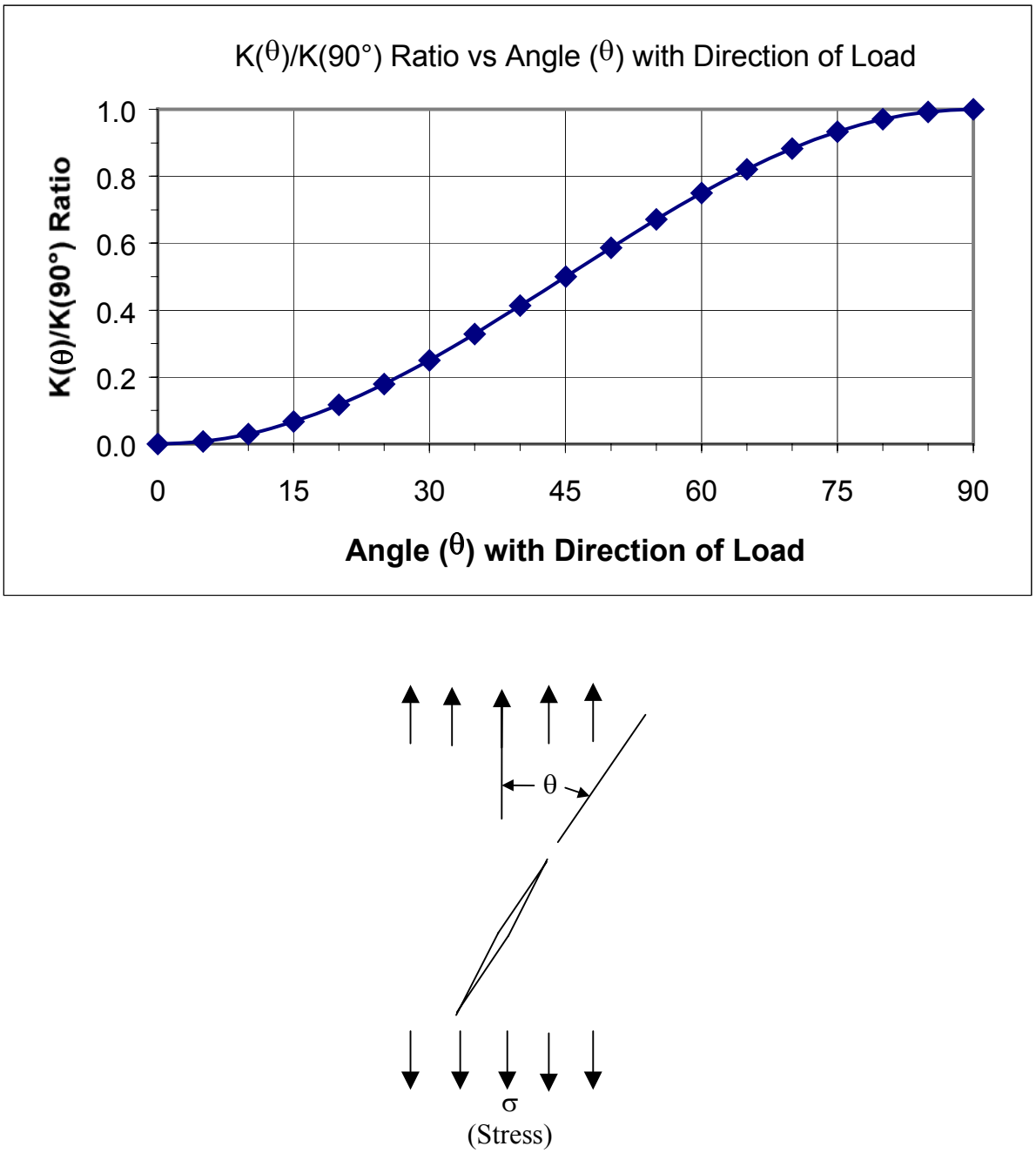

Figure 2. Ratio of the Stress Intensity Factor ($K(\theta)$) of a Crack Making an Angle (θ) with the Stress Direction to the Factor ($K(90°)$) of a Crack Oriented Perpendicular to the Stress Direction as a Function of the Angle (θ), for a Crack with an Arbitrary Stress and Crack Length.

6.2.2.4 Crack Aspect Ratio

Crack size is normally characterized by crack depth but crack length is needed in determination of the crack opening area as the crack becomes a through-wall crack. Determination of the crack length for either a manufacturing crack or an incipient crack is based on the following considerations:

(1) Surface flaws are semi-elliptical in shape with depth "a" and length "2c."

(2) The aspect ratio (γ) is the ratio of one-half of crack length ("c") vs. crack depth ("a"), i.e., γ = c/a. A semi-circular flaw has an aspect ratio of 1 ($\gamma = 1$).

(3) A crack maintains its aspect ratio during its growth until the depth reaches the wall thickness. Then, at this point, the shape instantaneously turns into a rectangular one.

(4) The crack aspect ratio is 1 for radial cracks in the closure weld.

(5) The crack aspect ratio is greater than 1 for circumferential cracks with an exponential distribution based on one of the formulations given in Harris et al. (1981, Equation 2-10, p. 29):

$$P\gamma(>\gamma) = e^{-(\gamma-1)/\lambda} \qquad \text{(Eq. 1)}$$

where λ is the standard deviation of γ and has the value of 0.7. From Equation 1, the mean and median values (γ_{mean} and γ_{50}) and the standard deviation (γ_{sd}) of γ can be obtained by the following formulas.

$\gamma_{mean} = 1 + \lambda = 1.7$
$\gamma_{50} = 1 + \lambda \ln 2 = 1.485$
$\gamma_{sd} = \lambda = 0.7$

It is noted that a gamma or Weibull distribution with a shape factor of one is equivalent to an exponential distribution.

6.3 THE BASE-CASE SLIP DISSOLUTION/FILM RUPTURE (SDFR) MODEL

6.3.1 Introduction

Environmental cracking has historically been separated into “initiation” and “propagation” phases (Jones and Ricker 1987, p. 146). For the purpose of lifetime modeling it is appropriate to assume that initiation is associated with microscopic crack formation at localized corrosion or mechanical defect sites. In the area of environmentally assisted cracking (such as SCC), coalescence of microscopically small cracks will take place and develop into deeper cracks. Thereafter, the crack may either reach an "arrest" state or a "propagation" phase. Ford and Andresen (1988, p. 798) assumed that cracks start propagating from a size of about 0.05 mm. A lifetime crack propagation prediction model can be achieved via a fundamental understanding of the cracking mechanism. The formulation of such a fundamentally based model of crack propagation requires the choice of a working hypothesis for the cracking mechanism and the evaluation of the parameters of importance in the mechanism. For the systems of interest, the slip dissolution/film rupture mechanism has been chosen. This cracking mechanism has been successfully applied to model SCC of stainless steel, low-alloy steel, and nickel-based alloys in light water reactor environments (Ford and Andresen 1988, pp. 798-800; Andresen and Ford 1994, pp. 61-70).

6.3.2 Slip Dissolution/Film Rupture Mechanism

In accordance with the slip dissolution/film rupture theory, crack advance is Faradaically related to the metal oxidation that occurs when the protective film at the crack tip is ruptured. Figure 3 (Ford and Andresen 1988, Figure 2; Andresen and Ford 1994, Figure 1) schematically shows the change in oxidation current and charge densities with time following the rupture of a protective film at the crack tip. In Figure 3, $\overline{V_T}$ is the average crack growth rate at the tip, V_S is the crack growth rate at the crack side, M and ρ are atomic weight and density of the crack tip metal, F is Faraday’s constant, n is the number of electrons involved in the oxidation of a metal atom, Q_f is the oxidation charge density per film rupture, $\dot{\varepsilon}_{ct}$ is the strain rate at the crack tip, and ε_f is the fracture strain of the film. The initial oxidation rate (and, hence, crack advance rate) will be rapid, typically controlled by activation or diffusion kinetics as the exposed metal rapidly dissolves. Availability of the balancing cathodic reduction current is also clearly necessary but is generally not limiting in hot water environments. However, in most (if not all) hot water cracking systems, a protective oxide reforms at the bared surface, and the rate of total oxidation (and crack tip advance) slows with time. Thus, crack advance can only be maintained if the film rupture process is repetitive. Therefore, for a given crack tip environment, corrosion potential, and metallurgical condition, crack growth will be controlled by the change in oxidation charge density with time and the frequency of film rupture at the strained crack tip. The latter parameter is determined by the fracture strain of the film, ε_f, and the strain rate at the crack tip, $\dot{\varepsilon}_{ct}$. By invoking Faraday’s law, the average environmental crack growth rate, V_t, can be related to the strain rate at the crack tip, $\dot{\varepsilon}_{ct}$ ($\dot{\varepsilon}$ in Figure 3) by the following equation (Ford and Andresen 1988, Figure 2, p. 790; Andresen and Ford 1994, Figure 1, p. 62):

$$V_t = \frac{M}{z\rho F}\frac{Q_f}{\varepsilon_f}\dot{\varepsilon}_{ct} \qquad \text{(Eq. 2)}$$

where M, ρ = atomic weight and density of the crack tip metal
F = Faraday's constant
z = number of electrons involved in the oxidation of a metal atom (n in Figure 3)
Q_f = oxidation charge density per film rupture
ε_f = fracture strain of the film

The time, t_f, to reach the fracture strain, ε_f, is:

$$t_f = \varepsilon_f / \dot{\varepsilon}_{ct} \qquad \text{(Eq. 3)}$$

Figure 4 show the schematic of oxidation current density vs. time following repeated oxide rupture events. Repassivation current transients exhibit an initially high bare surface dissolution current density, i_o, at an initial short time, t_o. Thereafter, oxide growth (or thickening) leads to a decay in the oxidation current density, which often follows a power law relationship:

$$i_t = i_o\left[\frac{t}{t_o}\right]^{-n} \qquad \text{(Eq. 4)}$$

Because of this power law relationship, Equation 2 can be reformulated as follows (Andresen and Ford 1994, Equation 1, p. 62):

$$V_t = A(\dot{\varepsilon}_{ct})^n \qquad \text{(Eq. 5)}$$

where, for a given environment, "A" and "n" are material constants, which can be measured from the repassivation response. The repassivation slope, n, is the slope on a log-log plot of (i_t/i_o) vs (t/t_o) from Equation 4.

If a bare surface condition is maintained at the crack tip (i.e., $\varepsilon_f/\dot{\varepsilon}_{ct} < t_o$, or $t_f < t_o$, hence, $i_t=i_o$), a "maximum" crack growth rate should result. Integration of Equation 4 leads to:

$$Q_f = \int_0^{t_f} i_t\,dt = i_o\left(t_f\right) = i_o\left(\varepsilon_f \Big/ \dot{\varepsilon}_{ct}\right) \qquad \text{(Eq. 6)}$$

Substitution of Equation 6 into Equation 2 yields the predicted maximum environmental crack growth rate:

$$V_{max} = \frac{M}{z\rho F} i_o \qquad \text{(Eq. 7)}$$

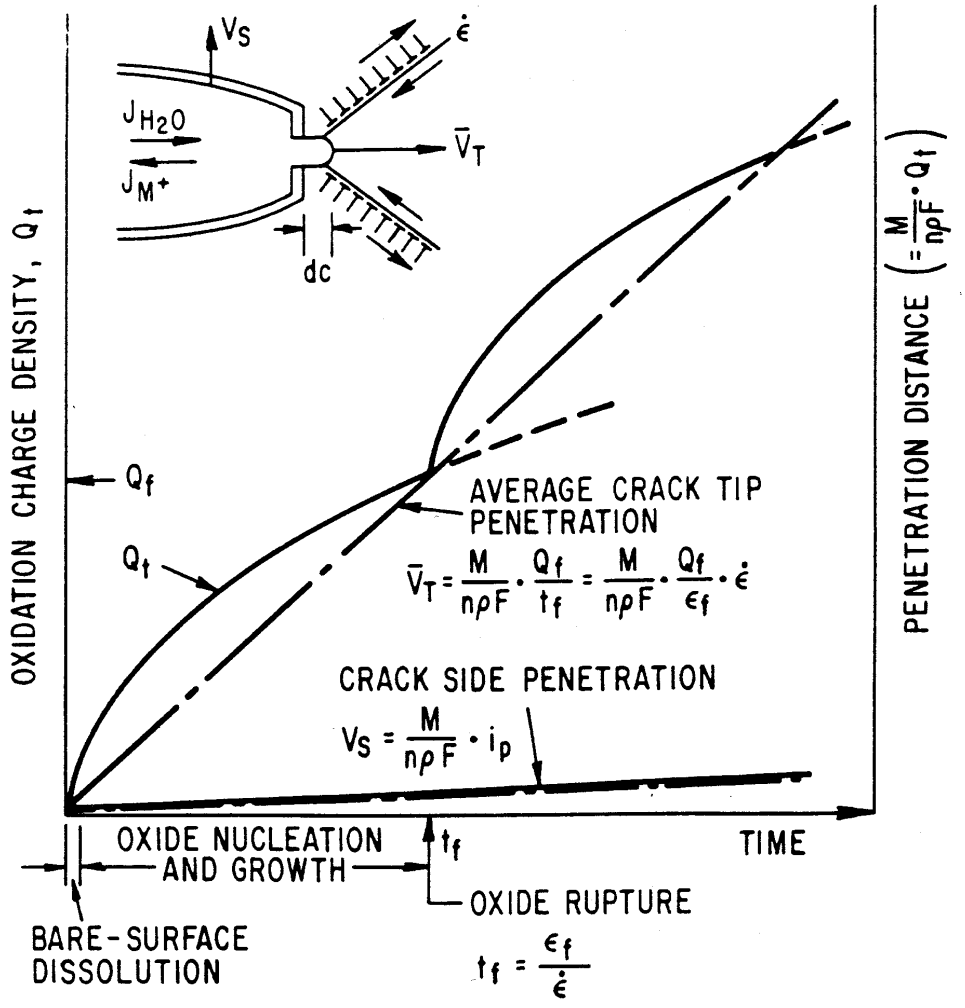

Figure 3. Schematic Oxidation Charge Density Versus Time for a Strained Crack Tip and Unstrained Crack Sides in the Slip Dissolution Mechanism

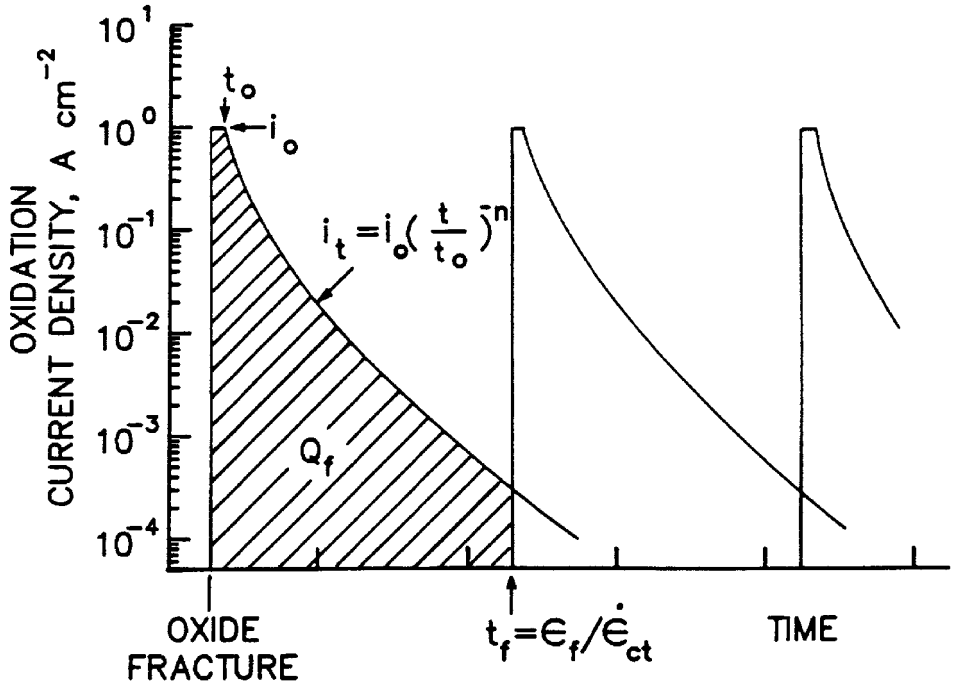

$$V = \frac{da}{dt} \; ; \; \bar{V}_{av} = \frac{M}{z\zeta F} \cdot \frac{Q_f}{t_f}$$

FOR HIGH $\dot{\epsilon}_{ct}$ AND/OR LONG t_o :

$$\bar{V}_{av} = \frac{M}{z\zeta F} \cdot i_o$$

FOR LOW $\dot{\epsilon}_{ct}$ AND/OR SHORT t_o :

$$\bar{V}_{av} = \frac{M}{z\zeta F} \frac{i_o t_o^n}{(1-n)\epsilon_f^n} \dot{\epsilon}_{ct}^n = f(n)\, \dot{\epsilon}_{ct}^n$$

Figure 4. Schematic of Oxidation Current Density Versus Time Following Repeated Oxide Rupture Events

This expression for the maximum environmental crack growth rate is the quantitative basis for the early observations relating the maximum oxidation current density on a straining surface to the maximum crack growth rate. However, these early correlations were obtained primarily for alloys in concentrated environments (boiling $MgCl_2$, 9M NaOH solutions, etc.) under dynamic straining conditions. By comparison, in relatively dilute environments it is expected that (a) the passivation rate will be high (e.g., in unaggressive chemistries or for lower-susceptibility materials) and thus "n" (in Equation 4) will be high; (b) the onset of repassivation is rapid, and thus t_o will be short; and (c) under constant load or displacement conditions, the periodicity of oxide rupture, $\varepsilon_f/\dot{\varepsilon}_{ct}$, will be much greater than t_o. Consequently, the oxidation charge rate Q is given by the following equation:

$$Q_f = \int_0^{t_f} i_t dt = \frac{i_o t_o^n}{(1-n)\left(\varepsilon_f \Big/ \dot{\varepsilon}_{ct}\right)^{n-1}} \qquad \text{(Eq. 8)}$$

Under these circumstances, a bare surface will not be maintained at the crack tip, and the crack propagation rate will be given by the substitution of Equation 8 into Equation 2:

$$V_t = \frac{M}{z\rho F}\frac{i_O t_O^n}{(1-n)\varepsilon_f^n}(\dot{\varepsilon}_{ct})^n \qquad \text{(Eq. 9)}$$

This is an expanded version of Equation 5 and relates the parameters "A" and "n" to the specific oxidation rates (e.g., Equation 4) and the fracture strain of the oxide at the crack tip:

$$A = \frac{M}{z\rho F}\frac{i_o t_o^n}{(1-n)\varepsilon_f^n} \qquad \text{(Eq. 10)}$$

6.3.3 Model Quantification

Since the repassivation current follows a power law response (i.e., Equation 4), the Faradaic relationship between the oxidation rate following oxide rupture and crack advance increment per time (growth rate, V_t), coupled with the relationship between crack tip strain rate, $\dot{\varepsilon}_{ct}$ and periodicity of oxide rupture, distills to the expression shown in Equation 9.

Evaluation of the crack advance mechanism leads to the conclusion that the film rupture/slip oxidation mechanism represents a justifiable model for hot water systems that is capable of being quantitatively evaluated. The mechanism is justifiable because almost all engineering alloys depend on the presence of a stable oxide film to act as a kinetic barrier to rapid dissolution/oxidation, especially in hot water. It is quantifiable, because predictions result directly from measurements of repassivation kinetics, typically obtained by rapidly straining wires of base alloy or synthetic (e.g., representative of the grain boundary) composition (see Figure 4).

In accordance with Andresen and Ford (1994, p. 62), the model can be quantified by evaluating the following processes: (1) the steady-state and transient compositions of the environment at the crack tip as a function of the conditions in the bulk (external) solution; (2) the oxidation rates for the material/environmental system expected at a strained crack tip; and (3) the oxide fracture strain and the crack tip strain rate, defined in terms of engineering parameters such as the stress intensity factor. For practical application, empirical approaches have been used for the model quantification processes.

The initial application of the slip dissolution/film rupture model was on the quantitative prediction of cracking in austenitic type 304/316 stainless steels in 288°C high-purity BWR water (Ford and Andresen 1988). The model quantification processes can be summarized by the following steps:

Step 1 - Measurements of n can be obtained from repassivation tests as the repassivation current follows a power law response (Equation 4). Those tests typically involve rapidly straining wires to increase the anodic passive current density, and subsequently measuring the decay of the passive current density with time.

Step 2 - Once n is known, the value of A can be determined from Equation 10 which relates the parameters "A" and "n" to the specific oxidation rates and the fracture strain of the oxide at the crack tip.

An alternative procedure, however, is used to quantify the model parameters. Based on this procedure , "A" can be directly determined from "n" empirically. The empirical determination of A is based on SCC crack growth tests that measure the crack growth rate V_t at specific crack tip strain rate $\dot{\varepsilon}_{ct}$. The value of A is calculated in accordance with Equation 5 for each set of n, V_t and $\dot{\varepsilon}_{ct}$. Curve fitting is then used to develop the empirical relationship between A and n.

An empirical relationship between A and n (with A in cm-$s^{(n-1)}$ and n being dimensionless),

$$A = 7.8 \times 10^{-3}\, n^{3.6} \qquad \text{(Eq. 11)}$$

has been given by Ford and Andresen (1988, p. 791) for 304 stainless steel in 288°C water. For Alloy 22 and Ti-7, independent experimental measurement of A and n is preferred but, due to lack of experimental data, the expression above will be used for the slip dissolution mechanism of Alloy 22 for present purposes. The resulting model is validated experimentally as indicated in Section 7.

Substitution of Equation 11 into Equation 5 leads to:

$$V_t = 7.8 \times 10^{-3}\, n^{3.6}\, (\dot{\varepsilon}_{ct})^n \qquad \text{(Eq. 12)}$$

where V_t has the unit of cm/s and $\dot{\varepsilon}_{ct}$ has the unit of s^{-1}.

For 304 stainless steel in 288°C water, Figure 5 (Ford and Andresen. 1988, Figure 7, p. 791) indicates that Equation 12 with n = 0.54 (i.e., A = 8.5 x 10^{-4}) is a good prediction model for observed crack growth rate versus crack tip strain rate relationships. Further, this slip dissolution/film rupture model (using the 304 stainless steel A vs n relationship in 288 °C water) has been statistically validated for the chromium containing, nickel base Alloys 600 and 182 over a range of anionic impurity concentrations (Ford and Andresen 1988, Figure 10).

The crack tip strain rate, $\dot{\varepsilon}_{ct}$ in Equation 12 is related to the engineering stress parameters (such as the stress intensity factor) via the formulations in Table 1 of Ford and Andresen (1988). According to Ford and Andresen (1988), p. 791, the formulations given in the table are semi-empirical relationships to normalize the effects of a wide range of stressing conditions on the environmentally assisted crack propagation rates. For constant load, the relationship is:

$$\dot{\varepsilon}_{ct} = 4.1 \times 10^{-14} K_I^4 \qquad \text{(Eq. 13)}$$

where the stress intensity factor K_I is in MPa $(m)^{1/2}$.

For constant load, substituting Equation 13 in Equation 5 leads to the following alternative crack growth rate equation:

$$V_t = \overline{A}(K_I)^{\overline{n}} \qquad \text{(Eq. 14)}$$

where

$$\overline{A} = A\left(4.1 \times 10^{-14}\right)^n \qquad \text{(Eq. 15)}$$

$$\overline{n} = 4n \qquad \text{(Eq. 16)}$$

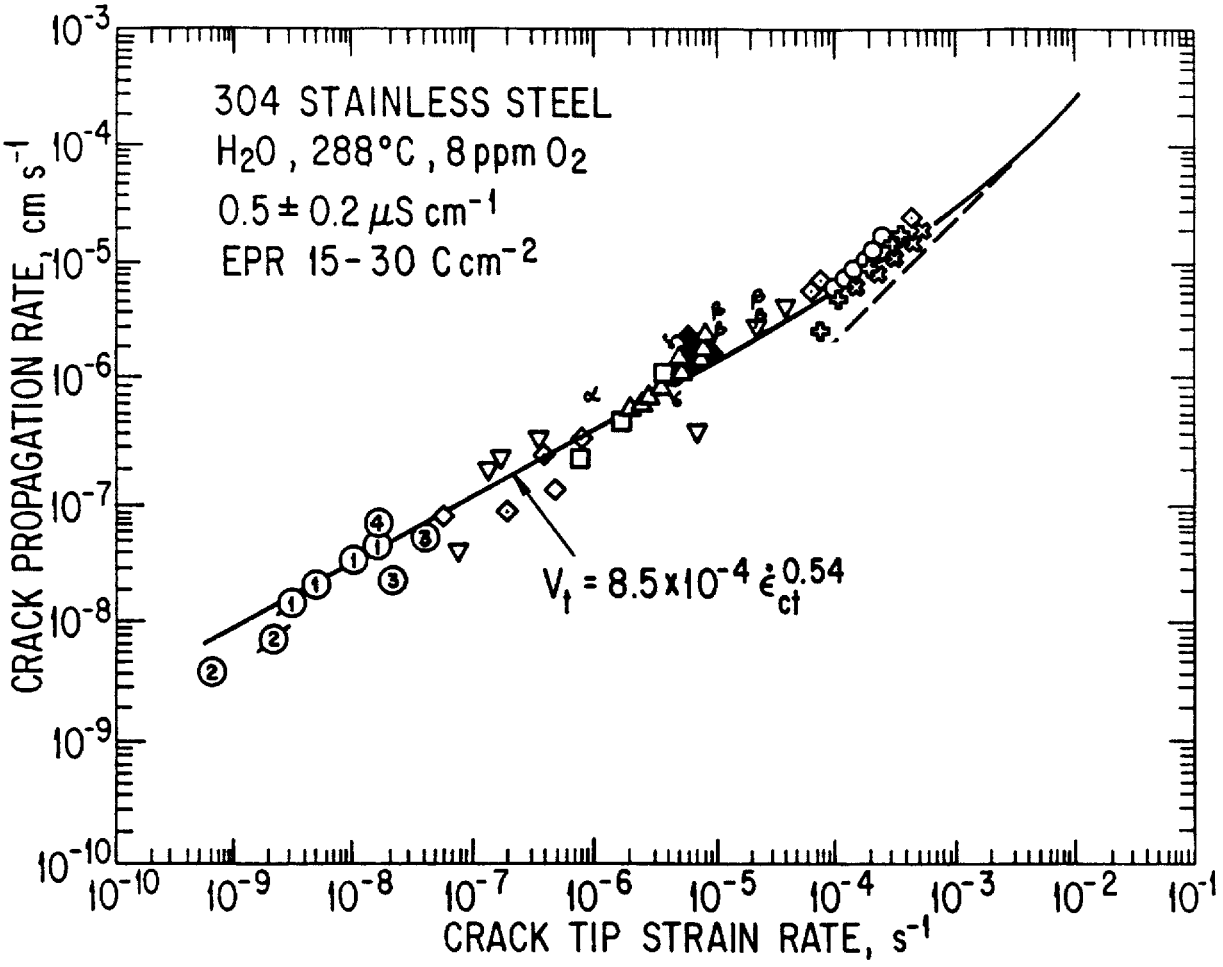

Figure 5. Crack Growth Rate (Presented by Observed Data Points and Predicted Curve) vs. Crack Tip Strain Rate for Sensitized Type 304 Stainless Steel in Oxygenated 288°C Water

6.3.4 Adaptation of Slip Dissolution Model To Alloy 22

Andresen and Ford (1994), p. 62, indicated that the SDFR model has been applied to stainless steels, low alloy and carbon steels, ductile nickel alloys, and irradiated stainless steels. Ford and Andresen (1988, p. 789), also used the SDFR model for, in addition to 304/316L stainless steel, A533B/A508 low alloy steel and Inconel 600/182 nickel-based alloys. Therefore, there is ample reason to hypothesize that SCC of nickel-based Alloy 22 occurs by the same fundamental mechanism characterized by the slip dissolution SCC model, i.e., Equation 5:

$$V_t = A\,(\dot{\varepsilon}_{ct})^n \qquad \text{(Eq. 5)}$$

The model quantification process is also used for Alloy 22. The resulting model is validated experimentally using data generated by the Yucca Mountain Program.

The relationship between A and n described by Equation 11 (with A in cm-$s^{(n-1)}$ and n being dimensionless) becomes the following equation (with A in mm-$s^{(n-1)}$ and n being dimensionless):

$$A = 7.8 \times 10^{-2}\, n^{3.6} \qquad \text{(Eq. 17)}$$

For constant load condition, with V_t in mm/s and K_I in MPa $(m)^{1/2}$ in Equation 14, Equation 15 becomes:

$$\overline{A} = 7.8 \times 10^{-2}\, n^{3.6} \left(4.1 \times 10^{-14}\right)^n \qquad \text{(Eq. 18)}$$

Substitution of Equations 17 and 18 in Equation 5 leads to:

$$V_t = 7.8 x 10^{-2} n^{3.6} \left(4.1 x 10^{-14}\right)^n (K_I)^{4n} \qquad \text{(Eq. 19)}$$

For Alloy 22 under constant load condition, the parameter "n" can be determined from Equation 19 based on crack growth rates measured at various levels of applied stress intensity factor, K_I. Recent SCC crack growth rate measurements from the General Electric Global Research Center (GEGRC) (DTN: LL021105312251.023) have been made available for the quantification of parameters for the SDFR SCC model to be used for Alloy 22. The test data were developed from four Alloy 22 specimens (c144. c152, c153, and c200) tested at 110°C in a concentrated mixed salt environment know as Basic Saturated Water (BSW) with a target composition and solution pH (pH = 13.4 at room temperature) listed in DTN: LL021105312251.023, p 3, 6. The specimens were subjected to cyclic loading in order to initiate crack growth and then followed by constant loading conditions with various hold times. The set of data from DTN: LL021105312251.023 to be used as input for establishing value of n for Alloy 22 are summarized in Table 6-1 of which the measured crack growth rates are derived from Table 4.1-1. These data were selected based on the following criteria. Firstly, the minimum hold time is 24 hours (or 85,400 seconds) because Equation 19 is applicable only to constant loading condition. It is unrealistic to determine the parameters $\overline{A}$ and $\overline{n}$ (or A and n) in this equation based on test

data at relative short hold times. The only exception is the data point associated with specimen c144 for which the hold time is relatively short (3,000 seconds or approximately one hour) but, according to DTN: LL021105312251.023, p. 7, cracking appeared to cease, i.e., reaching the constant load state. Secondly, data associated with specimen c200 were not included because this specimen was aged at 700°C for 175 hours. This aging condition is ultra-severe relative to the expected WP closure weld thermal exposure. According to the conclusion of BSC (2001) [151550]), material aging does not appear to be a problem for the waste package at temperature below about 260°C. It is noted in Table 6-1 that a crack growth rate of 10^{-11} mm/s is used to represent the test results that indicated either cracking appeared to cease or the growth rate seemed to arrest. The choice of 10^{-11} mm/s is judged to be the limit of measurement base on the observation that the lowest growth rate measured in the test program appeared to be 1.4×10^{-10} mm/s. (DTN: LL021105312251.023, p. 9)

Crack growth rate measurements reported in DTN: LL021105312251.023, p 10-11, were also obtained for Specimen c152 after the addition of 1000 ppm of Pb added as $PbNO_3$ was made to the autoclave BSW test solution. The Pb addition was made following 8670 hours of testing in just the 110°C BSW solution (composition given in DTN: LL021105312251.023, p 3 and solution pH, p 6 (pH = 13.4 at room temperature)). Because of the relatively high pH of this solution, most of the Pb becomes insoluble in the test solution because of lead carbonate, lead sulfate and possibly lead oxide precipitation. Based on a detailed comparison of crack growth rates made before and after the Pb addition, in all cases, the growth rate after the Pb addition was the same or somewhat slower. The test conditions varied over a significant range in loading conditions and growth rates. In addition to these higher pH brine SCC crack growth rate results, there are also SCC initiation test results obtained using Slow Strain Rate Tests (SSRT), at 76-95°C in low pH, SAW brine solution (pH ~3) with and without 0.005% lead nitrate additions DTN:LL020603612251.015. These results also show no effect of Pb on SCC susceptibility, Thus, there appears to be no basis for concern that Pb will affect SCC susceptibility in these relevant concentrated brine environments over a broad range of pH values.

Table 6-1. Summary of source data for Alloy 22 SDFR model quantification.

Specimen	Hold time, hours	Tested stress intensity factor, MPa(m)^.5	Measured Crack Growth Rate, mm/s	Source (page # of DTN: LL021105312251.023	Calculated "n" value (see Note 3)
c153	CL[Note 1]	30	2.50E-10	p. 11	1.168
c153	CL[Note 1]	30	5.00E-10	p. 11	1.119
c144	1	30	1.00E-11 [Note 2]	p. 7	1.391
c152	24	45	1.00E-11 [Note 2]	p. 10	1.563
c152	24	45	4.00E-10	p. 10	1.281

Notes:
1. CL = Constant Load
2. Crack growth rate of 1.0E-11 is used to represent test results where either cracking appeared to cease or the growth rate seemed to arrest.
3. Each of the values in the column "Calculated "n" value" is calculated from Equation 19.

To characterize the uncertainty for n, it can be determined from the n values in the last column of Table 6-1 that the mean value of n, n_{MEAN}, is 1.304 and the standard deviation (SD), n_{SD}, is 0.160, using "Excel" functions AVERAGE and STDEVP, respectively. Based on these mean and standard deviation, a normal distribution for "n" can be constructed. The n values at various percentiles, up to ±2(SD), are listed in Table 6-2, where the percentile value is obtained by the Excel function NORMDIST for each set of given values of n, n_{MEAN}, and n_{SD}. For TSPA applications, it is recommended that “n” is to be sampled from a truncated normal distribution with a mean of 1.304, a standard deviation of 0.16, and an upper bound and a lower bound of 1.624 and 0.984, the ±2(SD) of the normal distribution, respectively.

The base case slip dissolution/film rupture SCC model developed for Alloy 22, represented by Equation 19, is graphically illustrated in Figure 6 for n values at 0.984 (the lower bound), 1.304 (mean), and 1.624 (the upper bound), along with test data presented in Table 6-1, as well as the graphical representation of Equation 19 for stainless steel (with n=0.54). Excellent resistance to SCC for Alloy 22 is clearly illustrated in Figure 6 where even the higher crack growth rates exhibited by the top curve of Alloy 22 with n=0.984 are about 2 orders of magnitude lower than the crack growth rates associated with stainless steel curve.

Table 6-2. Distribution of the parameter "n"

n-value	Percentile
0.984 (-2 SD)	2.28
1.041	5.00
1.099	10.00
1.139	15.00
1.145 (-1 SD)	15.87
1.170	20.00
1.221	30.00
1.264	40.00
1.304 (Mean)	50.00
1.345	60.00
1.388	70.00
1.439	80.00
1.464 (+1 SD)	84.13
1.470	85.00
1.509	90.00
1.568	95.00
1.624 (+2 SD)	97.72

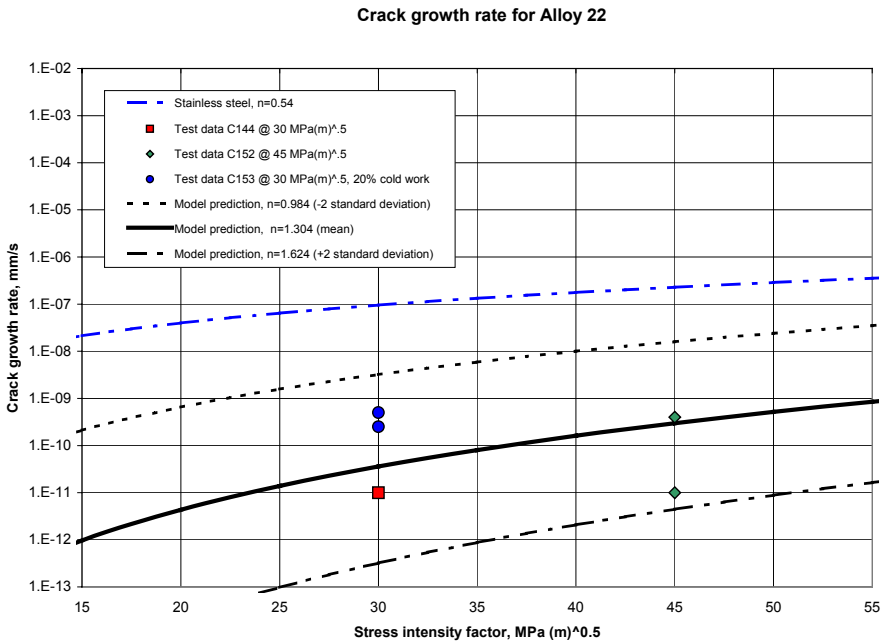

Figure 6. Crack growth rate vs. stress intensity factor for Alloy 22 based on the SDFR model.

6.3.5 Threshold Stress Intensity Factor

The threshold stress intensity factor (K_{ISCC}) is a critical value of stress intensity factor (K_I) such that any pre-existing crack will not grow or is in an arrest state if K_I corresponding to the crack size and the applied stress does not exceed K_{ISCC}. Pre-existing cracks are usually caused by manufacturing processes (especially welding) or crack initiation (see Section 6.2).

The concept of threshold stress intensity factor (K_{ISCC}) has been commonly used to assess the susceptibility of material to SCC. The description of this concept can be found in Jones and Ricker (1987, pp. 145-163) and Sprowls (1987, pp. 245-292). To apply the method, it is necessary to obtain values of (1) stress intensity factor K_I as a function of crack size correspondent to the stress state at and near the crack site and (2) the threshold stress intensity factor K_{ISCC}. The calculations of stress intensity factor for the closure welds in the inner and outer lids of the WP are described in Section 6.4. The threshold stress intensity factor is normally determined experimentally. Such experiments, which require very long test times and extremely high measurement accuracy, are impractical for Yucca Mountain Project applications. As an alternative approach, a crack blunting criterion is used to define the threshold stress intensity factor. Based on the crack blunting criterion (Andresen and Ford 1994, p. 62), crack blunting occurs when the corrosion rate of the crack sides approaches the oxidation rate at the crack tip, i.e., the sharp crack will degenerate to a blunt pit. It follows that an SCC crack will not grow if the general corrosion rate at the crack sides exceeds the crack tip growth rate. If V_{gc} is the general corrosion (GC) rate, the threshold stress intensity factor K_{ISCC} can be calculated from Equation 19, or the following equation:

$$K_{ISCC} = (V_{gc} / \overline{A})^{1/\overline{n}} \qquad \text{(Eq. 20)}$$

The mean general corrosion rate, which can be calculated from Table 4.1-5, will be used in Equation 20. Observation of Table 4.1-5 indicated that the GC rate associated with sample DCA 177 appears to be an outlier. The mean GC rate is 7.23 nm/y if this outlier is removed from the data set. Values for $\overline{A}$ and $\overline{n}$ can be determined from Equations 18 and 16 for a given value of 'n'. The threshold stress intensity factor for Alloy 22, accordingly, can be expressed in Table 6-3, based on the "n" values shown in Table 6-2.

The threshold stress intensity factor will be applied to both incipient flaws (once the threshold stress for initiation is exceeded) and for weld flaws. At each time step, the stress intensity factor, K_I, at a growing crack tip or defect tip will be compared with the K_{ISCC} value. At the point that the K_I value drops below K_{ISCC}, the crack will arrest.

Table 6-3. Distribution of the Threshold Stress Intensity Factor, K_{ISCC}, for Alloy 22

n-value	K_{ISCC} –value (MPa√m)
0.984 (-2 SD)	2.65
1.041	3.65
1.099	4.90
1.139	5.90
1.145 (-1 SD)	6.06
1.170	6.76
1.221	8.35
1.264	9.85
1.304 (Mean)	11.38
1.345	13.10
1.388	15.04
1.439	17.56
1.464 (+1 SD)	18.87
1.470	19.19
1.509	21.36
1.568	24.89
1.624 (+2 SD)	28.50

6.3.6 Alternative Model: The Coupled Environment Fracture (CEF) Model

Alternative conceptual models (ACMs) are based on assumptions and simplifications that are different from those employed, or not used, in the base model. An important reason for considering ACMs is to help build confidence that changes in modeling assumptions or simplifications will not change conclusions regarding subsystem and total system performance. Conceptual model uncertainty results from sparse observational data and a lack of available information to corroborate or refute plausible alternative interpretations of the subsystem and the processes occurring within the subsystem.

In addition to the base-case slip dissolution/film rupture Model, which provides formula for prediction of the crack growth rate, an alternative conceptual model, the coupled environmental fracture (CEF) model (Macdonald and Urquidi-Macdonald 1991, Macdonald et al. 1994), was developed on the basic assumption that the internal and external environments are coupled by the need to conserve charge in the system. Thus the solution of Laplace's equation for the external environment, as oxygen reduction on the external surface consumes the positive current emanating from the crack mouth, yields a boundary condition for solving Laplace's equation for the internal crack environment. Metal dissolution at the crack tip is described by the slip dissolution model, with the frequency of rupture of the passive film being a strong function of the stress intensity factor. The reduction of oxygen on the external surfaces is described in terms of a general Butler-Volmer equation that incorporates mass transport and charge transport phenomena. In this way, the model incorporates the effects of oxygen concentration, flow rate, and the conductivity of the external environment as well as accounting for effect of stress on crack growth. The CEF model represents an alternative approach for the prediction of the crack growth rate. It will be considered in the AMR only for the purpose of validation of the base-case model.

The CEF model is a physico-electrochemical model developed for intergranular stress corrosion cracking in sensitized Type 304 stainless steel in simulated light water reactor environments to explain and explore the effects of various environmental and mechanical variables on the kinetics of crack propagation. The goals were: (1) to derive a physically realistic model that unifies the electrochemical, chemical and mechanical aspects of the propagation of cracks through sensitized Type 304 SS in pure water under BWR recirculation piping conditions, and (2) to use this model to explore how the rate of crack propagation depends on various environmental variables, including oxygen concentration, conductivity and mechanical (stress intensity) parameters. The mathematical development of the model can be found in Macdonald and Urquidi-Macdonald (1991) and Macdonald et al. (1994).

The slip dissolution/film rupture model and the CEF model are similar in several ways. Both were developed for intergranular stress corrosion cracking in sensitized Type 304 stainless steel in simulated light water reactor environments. Both use Faraday's law to develop the equation for the crack growth rate. The departure point starts as the slip dissolution/film rupture model takes an empirical approach to develop a functional form to express the crack growth rate in terms of, explicitly, the crack tip strain rate and a couple of parameters (i.e., "A" and "n") while the CEF

model stays with an implicit approach. It can be said that the CEF model is more a theoretical model and the slip dissolution/film rupture model is a mixed theoretical and empirical model.

Both the slip dissolution/film rupture model and the CEF model are capable of predicting the crack growth rate for stress corrosion cracking. However, it was discovered that the CEF model appears to have the tendency of underestimating the crack growth rate as compared to the slip dissolution/film rupture model when both models were applied to predict the crack growth rate for Type 304 stainless steel in the light boiling water reactor (BWR) environment. This nonconservatism is evidenced by Figure 7. Comparison with experimental data summarized by Ford and Andresen (1988), Figure 22, for crack propagation rate versus stress intensity factor for sensitized Type 304 stainless steel in fully aerated, high purity water at elevated temperature indicated that the crack growth rate predicted by the CEF model (i.e., 3.2×10^{-9} cm/s at 20 MPa $m^{0.5}$) (Macdonald and Urquidi-Macdonald 1991, p. 78) tends to be at the lower end of the range cited by Andresen and Ford (1988). For this reason, the CEF model was not included for further evaluation but only used to validate the base case slip dissolution/film rupture model.

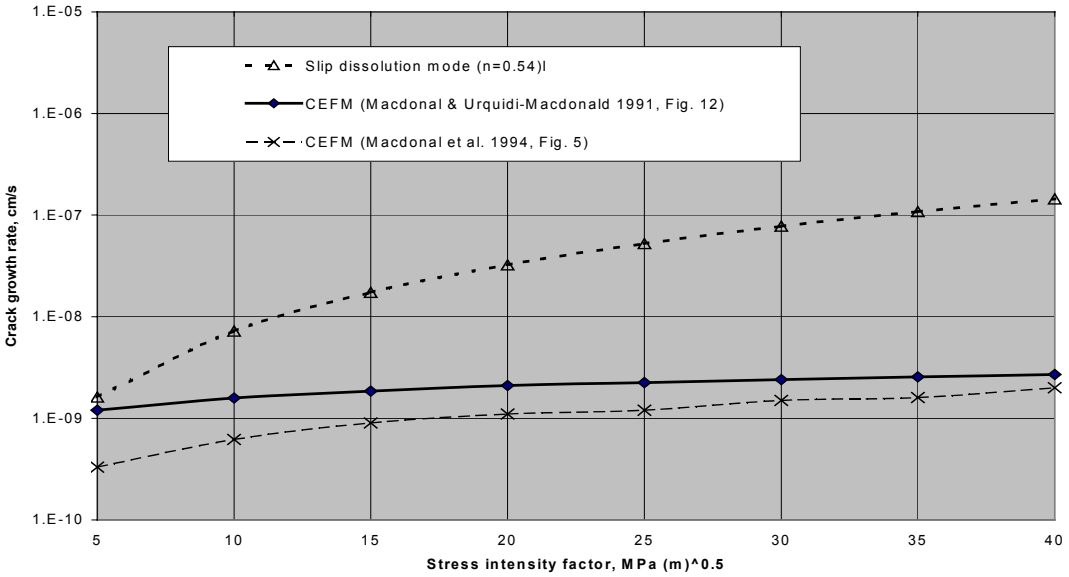

Figure 7. Comparison of predicted crack growth rates for 304 stainless steel.

6.3.7 Stress Corrosion Cracking for the Drip Shield Material Titanium Grade 7

The sources of stress corrosion cracking in the titanium grade 7 DS are (1) weld induced residual stress; (2) plasticity induced residual stress caused by seismic events; and (3) residual stress produced by rock falls. The weld induced residual stress will be mitigated by annealing. The threshold stress for crack initiation developed in Section 6.2.1 will be used as the failure criterion for seismic induced stress and, if the seismic induced residual stress exceeds the threshold, the affected areas of the waste package or drip shield are conservatively defined as having failed as a barrier to flow and transport. An analysis of the consequence of residual stress produced by rock falls is presented in this section.

Stress corrosion cracks in passive alloys such as Ti Grade 7 tend to be very tight (small crack opening displacement) by nature because the crack tip stress induced passive film rupture, repassivation and re-rupture repetitive process (or the analogous crack tip hydride precipitation, hydride fracture and reprecipitation of crack tip hydrides repetitive process) results in a relatively high effective crack tip corrosion rate as compared to the unstressed sides of the crack. As the crack grows through-wall, the tensile stresses normal to the crack walls are relieved, and the resulting crack faces continue to corrode by general corrosion at the very low passive corrosion rate with a median value of 0.03 microns/year (CRWMS M&O 2000 [144971], Section 6.5.4).

According to Section 6.2.1, residual stress resulting from rock falls can cause SCC crack initiation in the drip shield if the stress exceeds the threshold stress for the DS material (titanium grade 7). The maximum temperature in the drip shield wall, according to CRWMS M&O 2001 [154594], Figure 48, is 140^{o}C. The average yield strength (YS) for titanium grade 7 at 140^{o}C, using a straight-line interpolation between the room temperature (20^{o}C) and 204^{o}C from Table 4.1-4, is 220.7 MPa. The threshold stress for crack initiation, according to Section 6.2.1, is 0.5(YS), i.e., 110.4 MPa. The size (depth) of the initiated crack, based on Section 6.2.1, is 0.05mm. It will take about 40 years for the crack to grow through the 15-mm DS wall (BSC 2001 [156807], Table 5-13) based on an SCC crack growth rate of 1.25 x 10^{-8} mm/s estimated by DTN: LL021105312251.023, Section 1.3, p. 13.

Once the SCC initiated crack develops into a through-wall crack, the crack length "2c" and the crack gap (or width) "δ", according to BSC 2001 [156807], *Plugging of Stress Corrosion Cracks by Precipitation*, Table 5-13, are 130 mm and 157 microns, respectively. Thus, the dense passive corrosion oxide film growing normal to each opposing crack face would need to grow until it fills the 157-micron gap. This is equivalent to ~103 microns of metal loss/crack side and results in a total per side oxide thickness of ~182 microns based on a TiO_2 oxide/metal volume ratio of 1.76 (Bradford 1987, Table 2, p. 64). At a passive growth rate of .03 microns metal loss/year it will take ~3400 years for the crack to fill with corrosion product. In the interim, while the crack faces are corroding passively but before the corrosion film grows to a thickness where it will completely fill the crack, there could be a small amount of water transport by surface diffusion (film flow) into the crack and through the drip shield. However, the small heat flux present across the drip shield wall will result in evaporation of the slowly flowing water and a resultant scale deposit (principally calcium carbonate - [calcite]) will form over the crack where it intersect the upper drip shield surface as well as within the crack. This formation of calciferous deposits is well documented in seawater environments and in heat exchangers through which natural brines are forced to flow; e.g. in desalination plants (carrying ~6% NaCl solutions) and in

potash plants (carrying >12% brine (NaCl/KCl mixtures)). In both these cases, Ti surfaces are heat sources at operating temperatures of ~100°C. Such deposits form rapidly under flowing conditions, and have to be regularly removed to avoid loss of heat exchanger efficiency. In the case of concentrating pore water or J-13 water, calcite precipitation is the first stage of the concentration process (BSC 2001 [155640], Section 6.7.1). Other minerals such as amorphous silica will also precipitate.

A detailed calculation of the expected rate of SCC plugging due to calcite precipitation resulting from evaporation of a pore water of typical composition dripping onto a drip shield at the crack location has been performed (BSC 2001 [156807]). The calculation conservatively assumes (BSC 2001 [156807], Section 5.3) corrosion products generated on the crack faces as well as colloids, particulates and any precipitated silica minerals do not help in plugging the crack opening and that there is a uniform water seepage flow in space and time. It was concluded that (BSC 2001 [156807], Section 6.3) SCC cracks are sealed in a few hundred years at most when water is allowed to flow through the cracks at the expected very low film flow rate. When the cracks are bridged by water, the sealing process may take thousands of years, but no flow occurs since the water is held by capillary forces. In a more realistic case of a non-uniform flow onto the drip shield, more precipitation and faster plugging will occur.

Following plugging of such a drip shield crack, any solution flow through the crack would be dominated by an efficiency factor determined by the ratio of solution run-off on the drip shield surface compared to through crack flow which in turn is determined by scale porosity/permeability. Because of the expected high density of the calcite deposits BSC 2001 [156807] and lack of a pressure gradient to drive water through the crack, the probability of solution flow through the plugged crack would approach zero.

Finally, multiple rock falls on the same spot of the waste package is ruled out because of the small probability. Drip shield structural response to rock falls induced by seismic events is addressed in BSC 2003 [162598], where the damaged area of the drip shield is calculated for each of the given rock masses. The damaged area is defined as a region of the drip shield where the calculated stress exceeds the threshold stress. Seismic effects are being treated in the Seismic Consequences Abstraction AMR, MDL-WIS-PA-000003 REV 00.

6.4 EVALUATION OF STRESS INTENSITY FACTOR

6.4.1 Introduction

The stress intensity factor K_I is usually defined as a function of stress (σ) and crack depth size (a):

$$K_I(a, \sigma) = \beta \sigma (\pi a)^{1/2} \quad \text{(Eq. 21)}$$

where,

β is a geometry factor dependent on the size and shape of the crack and the configuration of the structural component

σ is the tensile stress distribution through the wall thickness of the structural component.

Closed-form solutions are possible only in some simple cases of uniform tensile stress and simple geometry. For example, in considering the classical problem of a single edge cracked plate with thickness "h," it has been shown that β can be expressed by the following approximate formula (Ewalds and Wanhill 1984, p. 49):

$$\beta = 1.12 - 0.231\left(\frac{a}{h}\right) + 10.55\left(\frac{a}{h}\right)^2 - 21.72\left(\frac{a}{h}\right)^3 + 30.95\left(\frac{a}{h}\right)^4$$

In most practical cases where stresses are non-uniformly distributed across the thickness, the stress intensity factor has to be calculated by some numerical algorithms, such as the finite element method. Rice (1968, p. 381) has shown that path independent J-Integral taken over an arbitrary contour surrounding the crack tip is proportional to the square of the crack tip stress intensity factor K_I. In accordance with Chan et al. (1970, p. 8), by numerically evaluating the J-Integral for the finite element solution over a path surrounding the crack tip, an estimate of the crack tip stress intensity factor can be obtained.

Although finite element programs can be used to evaluate the stress intensity factor, the effort is usually quite time consuming because a series of elaborate finite element analyses must be completed for numerous crack sizes starting from 0 through the thickness of the containment wall. A simplified solution has been developed by using fracture mechanics to evaluate the parameter $(K_I)_{PCCRACK}$ (more detail in Section 6.4.2.3). Then a geometry correction factor, G, which is usually a function of the crack size "a," is evaluated from the results of finite element analysis. Finally, the true stress intensity factor K_I is derived from $(K_I)_{PCCRACK}$ and G. This section of the AMR summarizes the methodology, calculation procedures, and selected results, which are discussed is detailed in SI (2003).

6.4.2 Calculations of Stress Intensity Factors for Waste Package Closure Welds

6.4.2.1 Introduction

Only weld induced residual stress in the final closure welds of the waste package outer barrier will be considered for performance assessment, based on the following reasons:

1. SCC of the DS will be excluded from the performance assessment. According to Section 6.3.7, the sources of stress corrosion cracking in the titanium grade 7 DS are (1) weld induced residual stress; (2) plastic residual stress caused by seismic events; and (3) residual stress produced by rock falls. The weld induced residual stress will be eliminated by annealing. The threshold stress for crack initiation developed in Section 6.2.1 will be used as the failure criterion for seismic induced stress and, if the seismic induced residual stress exceeds the threshold, the effected area of the waste package or drip shield are assumed to have failed as a barrier to flow and transport. An analysis of the consequence of residual stress produced by rock falls presented in Section 6.3.7 indicated that SCC resulting from rock fall will result in very tight crack openings and will not degrade the water diversion or function of the DS. The Type 316 stainless steel inner barrier of the WP will also be excluded from the SCC evaluation because the performance assessment will not take credit from the inner barrier.

2. Welds are the most susceptible to SCC because (1) welding can produce high tensile residual stress in the weld; (2) pre-existing flaws due to fabrication and welding have much higher concentration in the weld than in the base metal; and (3) welding could result in segregation and non-equilibrium brittle phases, which could enhance material susceptibility to SCC. All the welds with the exception of the final closure welds will be subjected to heat treatment to relieve the residual stress when the entire WP is heat treated before the loading of spent fuel elements. It is recognized that plastic deformation resulting from lower probability seismic events has the potential of leading to plastic upsets and resultant sustained residual stresses that may initiate cracks and drive them through the wall. Failure criteria governing seismic initiated residual stress will be developed for the WP material, i.e., Alloy 22. The failure criteria are based on a threshold stress which was discussed in Section 6.2.1 of this AMR. Therefore, weld residual stress is the only type of stress of SCC concern for the waste package.

Since by definition, embedded flaws are not exposed to the external waste package aqueous surface environment, they will not be subjected to SCC and only outer surface-breaking flaws are of concern for performance.

According to Arthur (2003), Attachment 1, Figure 1, the currently recommended waste package design for the license application (LA) consists of the following changes from the Site Recommendation (SR) design:

(a) replacing the full penetration stainless steel lid weld with a spread ring and seal weld;

(b) eliminating the outer lid extension;

(c) changing the outer lid mitigation method from induction annealing to laser peening;

(d) changing the inner lid weld configuration from a full penetration weld to a seal weld; and

(e) eliminating laser peening of the inner lid.

Sketches of the Site Recommendation design and the current recommended LA design of the waste package are shown in Figure 8 (Arthur 2003, Attachment 1, Figure 1).

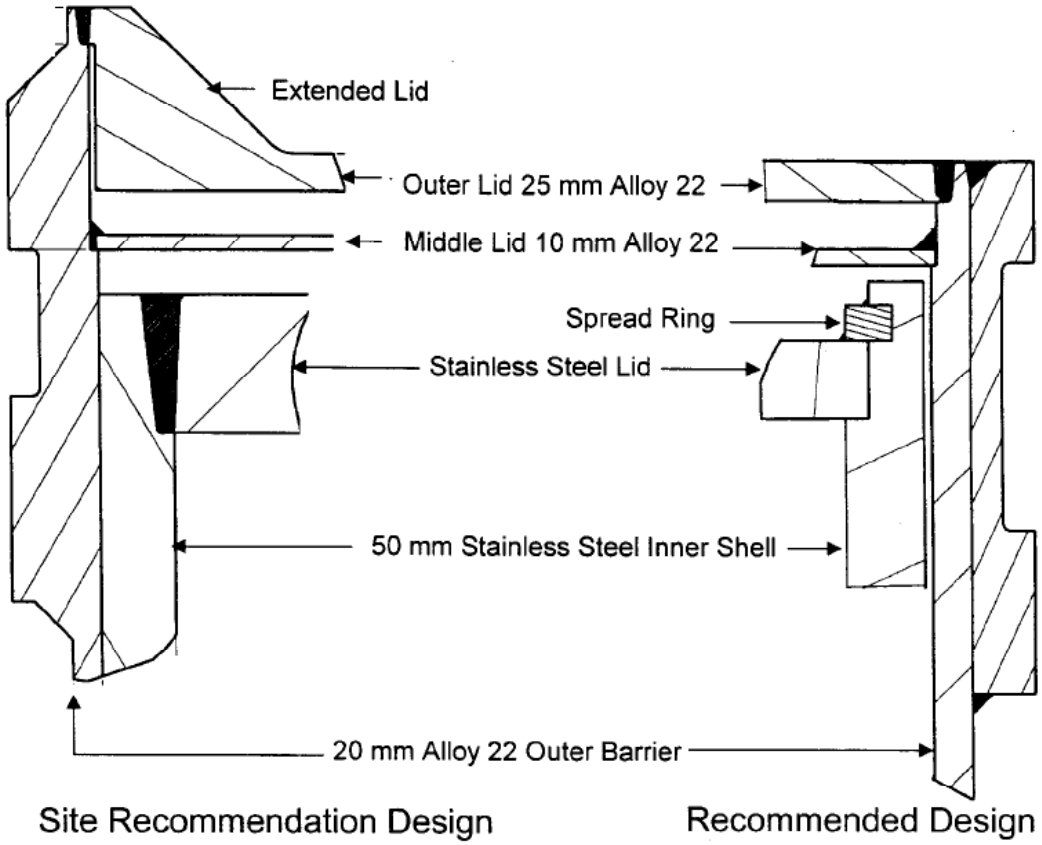

Figure 8. Site Recommendation Design and Recommended LA Design of Waste Package

For the performance assessment of the waste package subjected to stress corrosion cracking, stress and stress intensity factor profiles due to weld residual stress in the closure welds are needed for the 25-mm Alloy 22 outer lid subjected to laser peening and the as-welded 10-mm Alloy 22 middle lid. Calculated stress and stress intensity factor profiles due to weld residual stresses for the currently recommended waste package design are not available. However, stress and stress intensity factor profiles have been calculated and saved in DTN: LL000316205924.142 for two different WP designs: the CRM-21 PWR design (which has a single 25-mm Alloy 22 outer lid), as shown in Figure 9 (SI 2003, Figure 1-4), and the modified CRM-21 PWR design (which is similar to the CRM-21 PRW design but the thickness of the outer lid is reduced from 25 mm to 10 mm). It can be seen that the flat-head outer lid of the currently recommended WP design is similar to the outer lid of the CRM-21 PWR design not only in their geometrical configurations but also in the welding processes. It is indicated in Section 6.2.2.1 that the current welding process being considered for the WP final weld is a GTAW process. It will be shown in Section 6.4.2.2 that the heat generation rate used as the input

for the thermal analysis of the CRM-21 PWR design is equivalent to that of a GTAW welding procedure. Therefore, it is recommended that calculated stress and stress intensity factor profiles for the 25-mm outer Alloy 22 lid of the CRM-21 PWR design are used for the as-welded and laser peened Alloy 22 waste package outer lid (WPOL) of the current design and calculated stress and stress intensity factor profiles for the as-welded 10-mm Alloy 22 lid of the modified CRM-21 PWR design are used for the Alloy 22 waste package middle lid (WPML) of the current design.

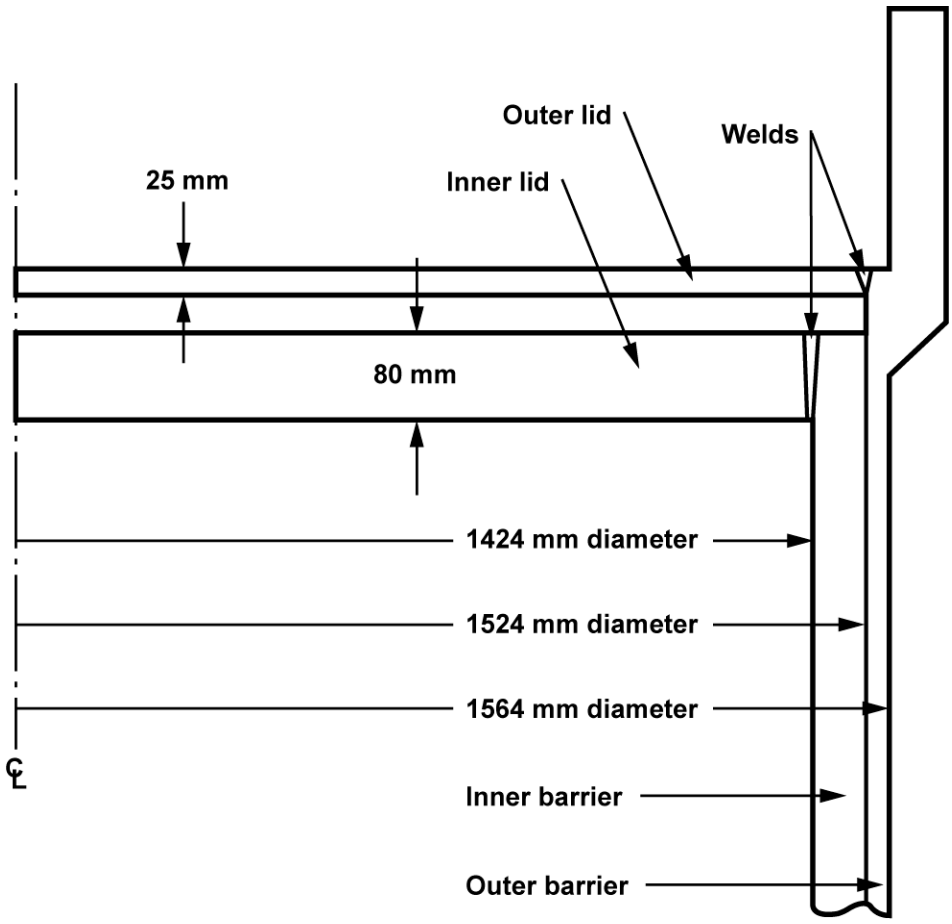

Figure 9. Schematic and Dimensions for the CRM-21 PWR WP Design

6.4.2.2 Stress Analysis

Finite Element Model–Determining the weld residual stress requires a thermal analysis to determine the temperature history caused by the welding process and a subsequent weld residual stress analysis. This problem has been solved using finite element analysis methods. Although the determination of weld residual stress for the WP welds is a three-dimensional problem, it has been found that the use of two-dimensional axisymmetric modeling of the problem provides a reasonable estimate of the behavior (Chan et al. 1970, p. 3). Thus, the WP closure weld models were assumed to be two-dimensionally axisymmetric about the WP axial centerline.

The finite element model for the CRM-21 PWR design of the WP (Figure 9) is shown in Figure 10. The weld geometry and immediate neighboring material are modeled in detail with sufficiently small elements to capture the large thermal and strain gradients associated with the weld pass application. The element sizes become larger with distance from the weld since the field variable gradients are significantly lower.

Figure 10 shows the finite element model with all weld passes deposited and both lids in place. Material making up the individual weld passes is added to the model as each weld pass is simulated. This process continues until all weld beads (or groups of weld beads) are applied.

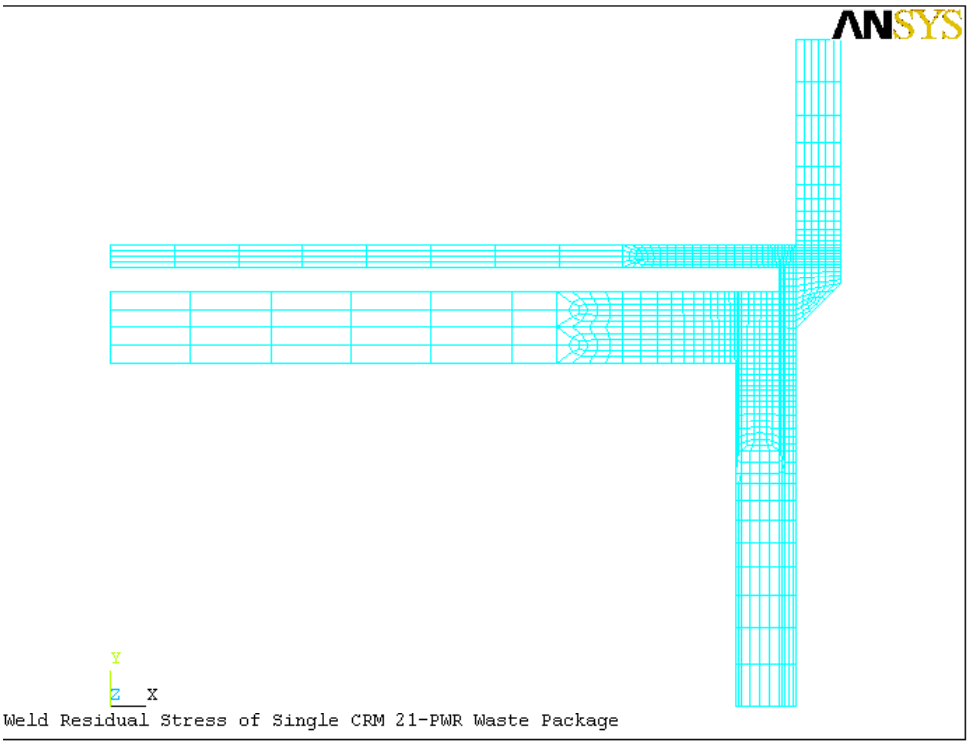

DTN: LL000319805924.143

Figure 10. Finite Element Model for the CRM-21 PWR WP Design

Figure 11 shows a close-up view of the finite element model (Figure 10) where axisymmetrical cross sections selected for stress output are identified. The radial stress, Sx, in the x-direction, is normal to the section while the hoop stress, Sz, in the z-direction, is tangential to the section. Similarly, Figure 12 is the close-up view of the modified CRM-21 PWR design which shows the cross sections for stress output. Section 1-1 is selected such that the stress Sn normal to the section is maximized. The stress component Sn will be conservatively used as the radial stress, Sx, in the weld. Section 2-2, likewise, is selected such that the stress Sz, the hoop stress, is maximized and this stress component will be conservatively used as the hoop stress in the weld. The distance (or crack depth) measured from the outer surface of the closure lid on section 1-1 or 2-2 will be projected to a vertical cross section which is normal to the plane of the closure lid.

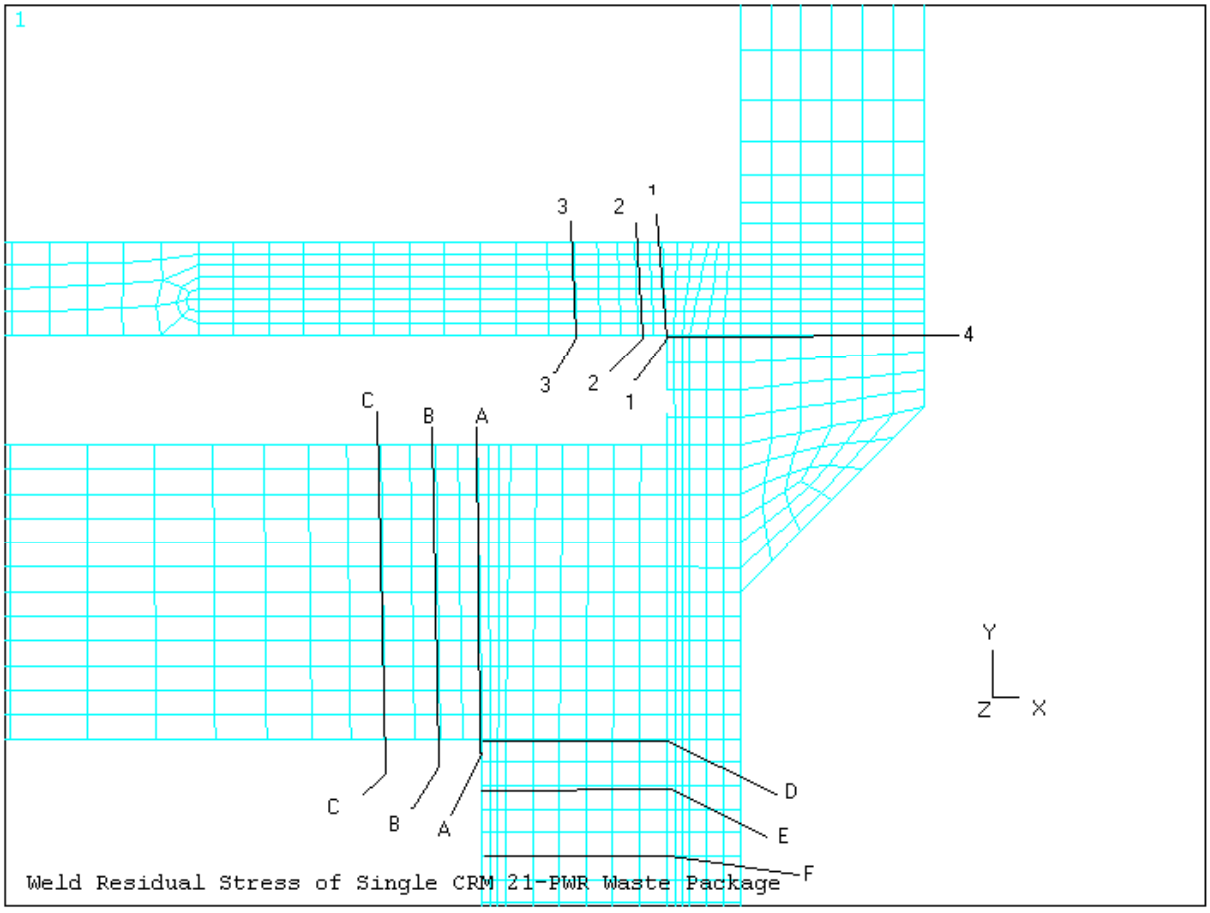

DTN: LL000319805924.143

Figure 11. Selected Cross-Sections for CRM-21 PWR WP Design

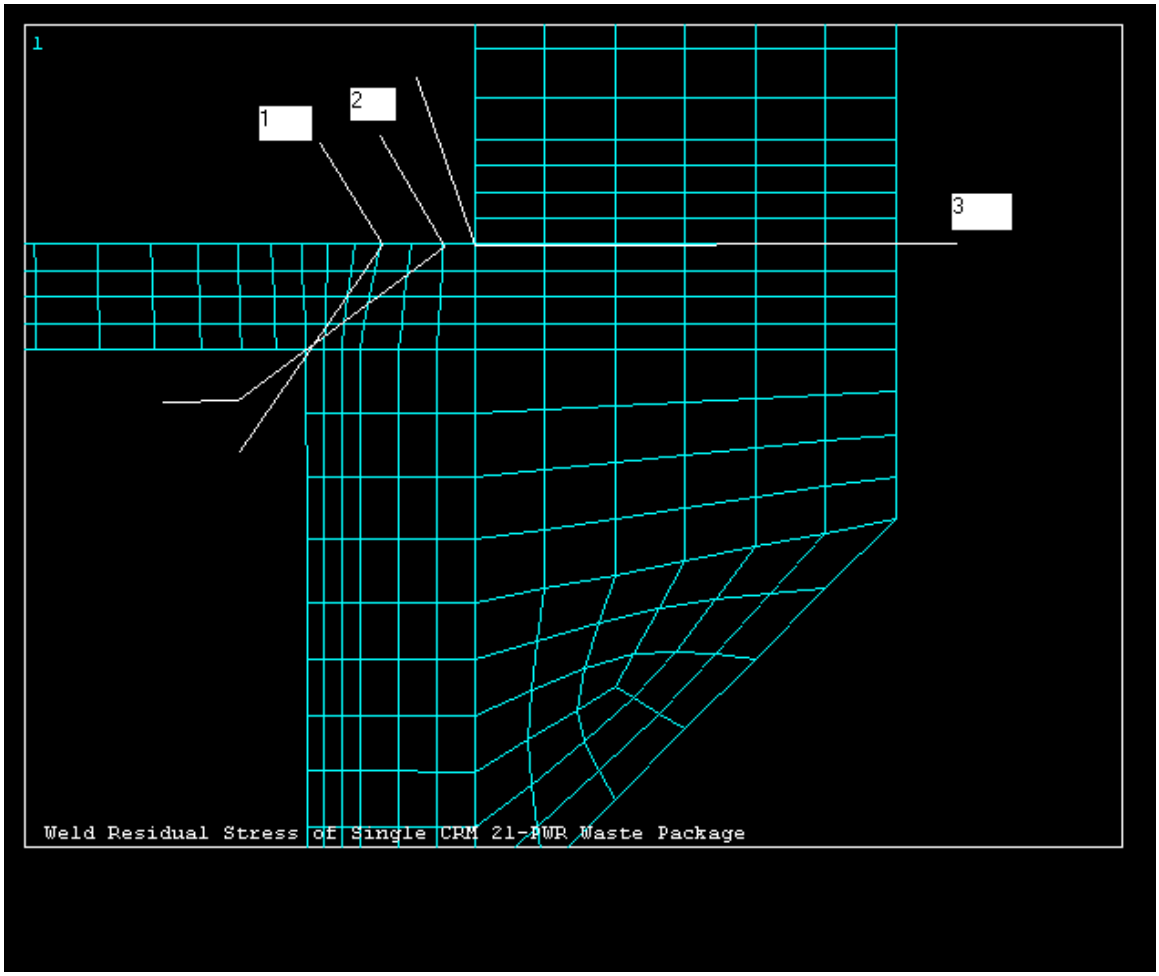

DTN: LL000319805924.143

Figure 12. Selected Cross-Sections for the Modified CRM-21 PWR WP Design

Material Properties–The material properties are important to the determination of the final weld residual stress. The material properties used in this evaluation for Alloy 22 are discussed in detail in SI (2003). For the thermal analysis, the material properties used are thermal conductivity, specific heat, and density. For the stress analysis, the material properties used are coefficient of thermal expansion, Young's modulus, Poisson ratio, density, and yield strength. Non-linear properties, such as the elastic-plastic behavior, and temperature dependency are properly considered.

Thermal Analysis–A thermal analysis of the WP closure was performed to simulate the temperature history caused by each weld pass. Each weld pass will result in a different temperature field since as passes are applied, more material is added, residual stress from

previous passes are being incorporated, and the relative location of the weld heat input is changing with respect to the lid thickness.

The effect of each weld pass was simulated through heat generated in the finite elements, which represent the weld pass, and then the heat is transferred to the adjoining parts of the WP. The heat generated in the weld pass, represented by the net heat input (H_{net} in joules/in.) of the welding process can be calculated according to Equation (2.3), p. 33, of DTN: LL000312705924.132, $H_{net} = f_1 EI/v$, for given welding parameters including voltage (E), amperage (I) and travel velocity of the heat source (v in in./sec.) and heat transfer efficiency (f_1). Based on a Gas Tungsten Arc Welding (GTAW) process, the amperage, voltage and average travel speed are, respectively, 330-335 A, 12.1-13.0 V and 8.0 in./min. (0.133 in./sec.) (CRWMS M&O 1998, Table 7-1, p. 12). The heat transfer efficiency (f_1) for gas tungsten arc welding, according to DTN: LL000312705924.132, Figure 3.1A, p. 69, is 21-48%. Using the average values for E (12.55 V), I (332.5 A), v (0.133 in./sec.) and f_1 (0.345) and adding 15% to the final result (to represent heat contributed by the filler material), the net heat input is found to be 12,400 Joules/in, which is very close to the heat generation rate 12268 Joules/in used in the finite element thermal analysis (SI 2003, p. 1-8).

For the axisymmetric representation of the three-dimensional problem, it is desired to convert the non-axisymmetric heat input into an equivalent axisymmetric heat input, which would be representative of what a typical point on the circumference of the weld would experience. Since a typical point on the circumference would experience essentially an impulse heat input (i.e., a large amount of heat input over a short amount of time) the heat input is represented by a triangular-shaped pulse over a two-second time interval (ramp up in one second and ramp down in one second) followed by a cooling period. The length of cooling period after the deposit of weld beads is determined by the time required for the weld torch to travel around the circumference of the closure weld.

Weld Residual Stress Analysis–The stress analysis is performed for all individually modeled weld passes. For example, if six weld passes are being modeled, then six thermal stress analyses are performed. The analysis of Weld Pass 1 uses the temperature history for Weld Pass 1 thermal analysis. The analysis of Weld Pass 2 uses the Weld Pass 2 thermal analysis and the residual stress due to Weld Pass 1 as the initial condition. This process continues until all weld passes are analyzed. The final solution (at ambient conditions) is the room temperature weld residual stress.

6.4.2.3 Stress Intensity Factor Calculations

For the WP closure welds, the flaw orientations most likely susceptible to crack propagation are those of a circumferential flaw (parallel to weld) and a radially oriented flaw (perpendicular to weld). Figure 13 shows the flaw orientations with respect to the weld. A radially oriented flaw would be potentially driven by hoop stress. A circumferentially oriented flaw would be driven by radial stress.

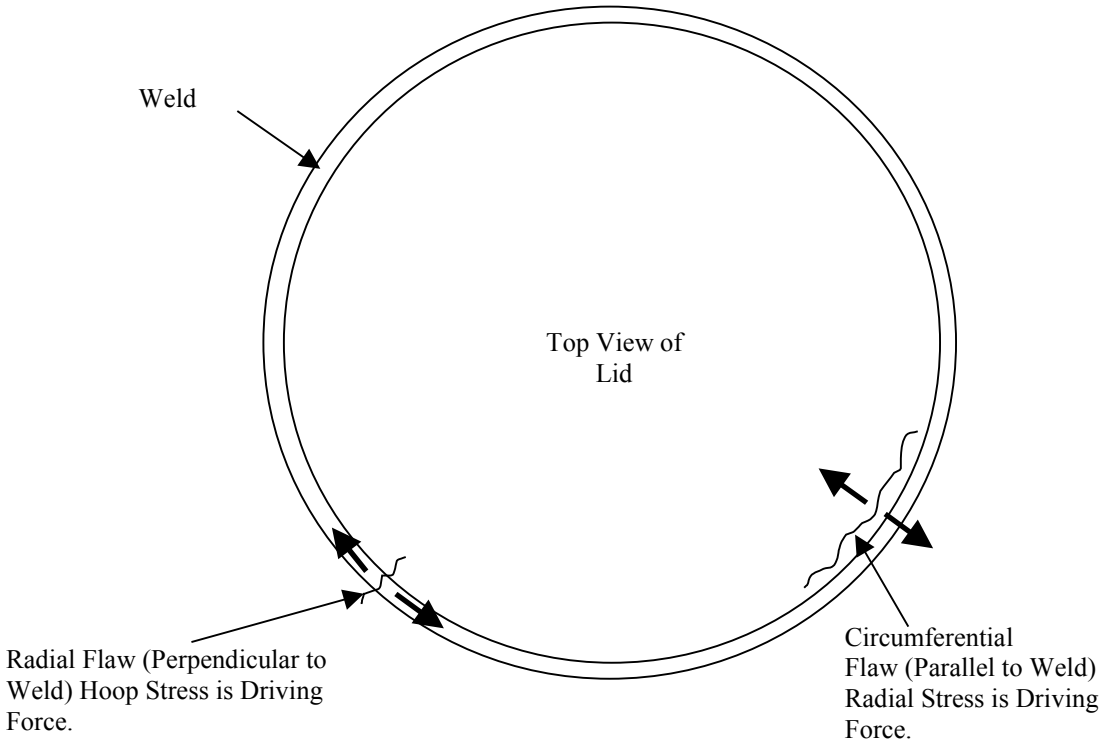

Figure 13. Flaw Orientation for Lid Welds

A general form of the stress intensity factor can be expressed by Equation 21, i.e.,

$$K_I = \beta \sigma (\pi a)^{1/2}$$

As indicated in Section 6.4.1, β is a geometry factor dependent on the size and shape of the crack and the configuration of the structural component, and σ is the stress distribution through the wall thickness of the structural component. Closed-form solutions of Equation 21 are possible only in some simple cases of uniform tensile stress and simple geometry.

Although finite element analyses can be used to evaluate the stress intensity factor (see Section 6.4.1.1), the effort is usually quite time consuming because a series of elaborate finite element analyses must be completed for numerous crack sizes starting from 0 through the thickness of the containment wall.

A simplified solution procedure was developed by using fracture mechanics to evaluate the parameter $(K_I)_{PCCRACK}$ for a given stress distribution. Then a geometry correction factor, G, as a function of the crack size "a," was developed by curve fitting from comparing the simplified solutions with the results of finite element analysis for only a limited number of crack sizes. Given the geometry correction factor, the true stress intensity factor K_I for any crack size can be

derived from $(K_I)_{PCCRACK}$ and G, without going through the finite element analysis using the following relationship:

$$K_I = G\left(K_I\right)_{PCCRACK} \quad \text{(Eq. 22)}$$

For a circumferential flaw, $(K_I)_{PCCRACK}$ was derived from an infinite single edge cracked plate (SECP) with an infinitely long flaw. For a radial flaw, $(K_I)_{PCCRACK}$ was derived from an elliptical surface crack in an infinite plate with a crack aspect ratio of 0.5 (a semi-circular crack). In either case, the stress distribution was calculated by using a third order polynomial of the type represented by the following equation:

$$\sigma = A_0 + A_1x + A_2x^2 + A_3x^3 \quad \text{(Eq. 23)}$$

where x is the distance from the outer surface of the closure lid and A_0, A_1, A_2, A_3 are coefficients of the third-order polynomial fit of the through-wall stress distribution (or profile).

The model of a circular crack in an infinite plate is a better representation of a radial crack in the closure weld than an infinite edge crack in an infinite SECP. It is judged that a radial crack in the closure weld would not grow into a long semi-elliptical crack due to the rapid decay of hoop stress in the radial distance away from the weld and base metal interface (Figure 14, where "1-1", "2-2", etc. are section identifications as indicated in Figure 11).

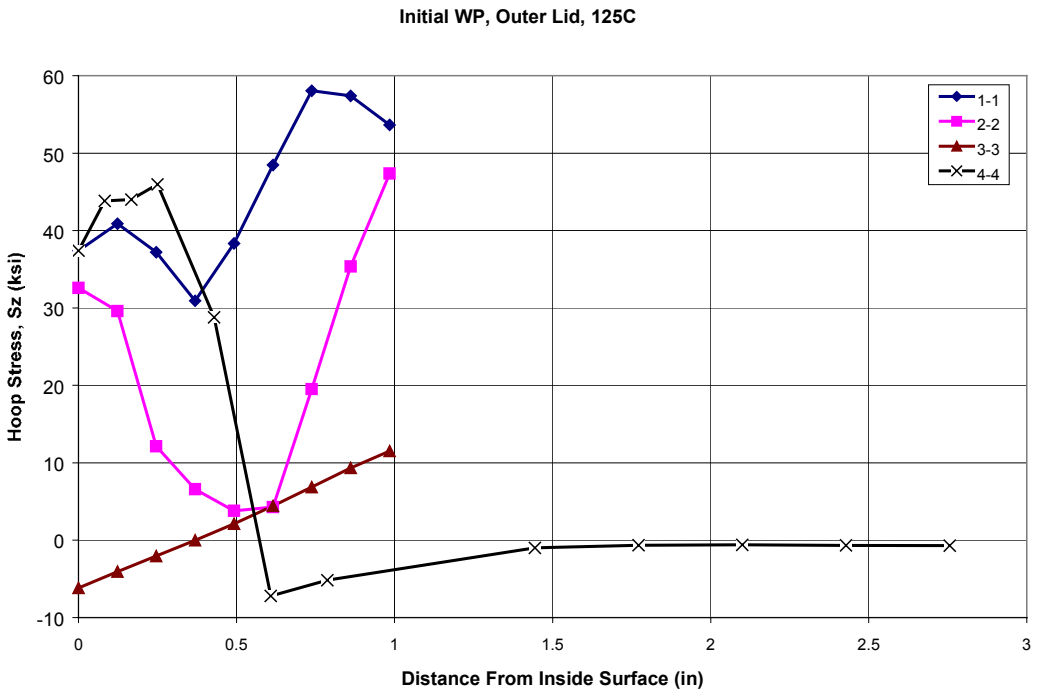

DTN: LL000316205924.144

Figure 14. Hoop Stresses in Outer Lid of CRM-21 PWR Design

The stress intensity factor for an infinite SECP with an infinitely long flaw is (Buchalet and Bamford 1976, Equation 2, p. 388):

$$(K_I)_{SECP} = \sqrt{(\pi a)}\left[A_0F_1 + \left(\frac{2a}{\pi}\right)A_1F_2 + \left(\frac{a^2}{2}\right)A_2F_3 + \frac{4a^3}{3\pi}A_3F_4\right] \qquad \text{(Eq. 24)}$$

where F_0, F_1, F_2, and F_3 are magnification factors and A_0, A_1, A_2, A_3 are coefficients of the third-order polynomial fit of the through-wall stress distribution (or profile) as indicated in Equation 23.

The magnification factors F_0, F_1, F_2, and F_3 are functions of the crack depth ("a") versus thickness ("h") ratio (a/h) and are graphically presented in Buchalet and Bamford (1976), Figure 6, which are used to calculate the stress intensity factor.

The SECP stress intensity factor is for the ideal geometry and must be modified by the geometry correction factor G to consider the actual geometry. Figure 15 shows, for a circumferential flaw, the G factor distribution in the closure weld of the outer lid of the CRM-21 PWR WP as a result of curve fit based on the exact G values calculated at four discrete points corresponding to crack-versus-thickness ratios of 0.2, 0.3, 0.4 and 0.6. Figure 15 indicates that, for shallow flaws, the correction factor is near 1. For deeper flaws, the correction becomes significant, and using the SECP solution would be very conservative. For a radial flaw, the simplified solution obtained from a fracture mechanics crack model which contains a semi-circular surface flaw in a flat plate and is judged to be close to the final solution. Therefore, the geometrical correction factor is assumed to be equal to unity for the case of radial cracks.

6.4.2.4 Numerical Results

According to Section 6.4.2.1, calculated stress and stress intensity factor profiles for the 25-mm outer Alloy 22 lid of the CRM-21 PWR design will be used for the as-welded and laser peened outer Alloy 22 lid of the current design and calculated stress and stress intensity factor profiles for the as-welded 10-mm Alloy 22 lid of the modified CRM-21 PWR design will be used for the middle Alloy 22 lid of the current design.

The values of the coefficients in Equation 23 for the closure-lid welds of both WP designs are documented in DTN: LL000316205924.142. For radial and hoop stresses in ksi in the 25-mm outer closure-lid weld of the CRM-21 PWR design, the coefficients, A_0, A_1, A_2, and A_3 with stress in ksi and distance x in inches are obtained from DTN: LL000316205924.142, file name: Skvrbr1, sheet "UnAnneal, Sx", cells C9 - C12 for radial stress and sheet "UnAnneal, Sz", cells C9-C12 for hoop stress. The coefficients are listed in the third and fourth rows of Table 4.1-2. Table 6-4 shows the converted stress coefficients, A_0, A_1, A_2, and A_3, in the metric unit system. The unit conversions used are: 1 in. = 25.4 mm; and 1 ksi = 6.8947568 MPa.

Similarly, for radial and hoop stresses in ksi in the 10-mm lid of the modified CRM-21 PWR design, the stress coefficients with stress in ksi and distance x in inches are obtained from DTN: LL000316205924.142, file name: Thinlid11, sheet "UnAnneal,1-1.Sn", cells C9 - C12 for radial stress and sheet "UnAnneal,2-2,Sz", cells C9-C12 for hoop stress. The coefficients are listed in

the fifth and sixth rows of Table 4.1-2. Table 6-5 shows the converted stress coefficients, A_0, A_1, A_2, and A_3, in the metric unit system.

Tables 6-6 and 6-7 show calculated stress profiles (using Equation 23 and the stress coefficients in Tables 6-4 and 6-5) and stress intensity profiles (obtained directly from Table 4.1-3) for the outer and middle lids of the WP design. The values of x's to be used in Equation 23 to calculate the radial and hoop stress profiles are listed in the first column of Table 6-6 or Table 6-7. Note that, for the 10-mm middle lid, the projected distance should be used as the value of 'x' in Equation 23 to calculate the stress profiles (see Section 6.4.2.2 and Figure 12).

Table 6-4. Stress coefficients for the As-Welded WP Outer Lid.

Stress Coefficient	Unit	Radial Stress	Hoop Stress
A_0	MPa	116.321	382.136
A_1	MPa/mm	9.107	8.096
A_2	MPa/mm^2	-3.146	-1.991
A_3	Mpa/mm^3	0.111	0.060

Table 6-5. Stress coefficients for the As-Welded WP Middle Lid.

Stress Coefficient	Unit	Radial Stress	Hoop Stress
A_0	MPa	181.636	219.908
A_1	MPa/mm	-177.592	56.494
A_2	MPa/mm^2	23.385	-20.848
A_3	Mpa/mm^3	-0.900	1.083

Table 6-6. Stress Intensity Factor (SIF) Profiles for As-Welded WP Outer Lid

Depth, mm	Radial stress (Sx), MPa	SIF due to Sx, MPa-$m^{0.5}$	Hoop stress (Sz), MPa	SIF due to Sz, MPa-$m^{0.5}$
0.3988	119.4598	4.5146	385.0522	9.1593
0.8001	121.6510	6.5821	387.3707	12.9737
1.1989	122.9098	8.2395	389.0855	15.9139
1.6002	123.2952	9.6422	390.2419	18.4031
1.9990	122.8448	10.8381	390.8484	20.6048
2.4003	121.5958	11.8425	390.9359	22.6028
2.7991	119.6065	12.8589	390.5265	24.4741
3.2004	116.8946	13.7858	389.6383	26.2367
3.5992	113.5369	14.5688	388.3055	27.9039
3.9980	109.5607	15.2083	386.5472	29.4912
4.3993	104.9776	15.7061	384.3711	31.0103
4.7981	99.8883	16.0778	381.8281	32.4703
5.1994	94.2707	16.4072	378.9090	33.9004
5.5982	88.2385	16.7029	375.6738	35.3092
5.9995	81.7579	16.8783	372.1047	36.6797
6.3983	74.9532	16.9527	368.2700	38.0157
6.7970	67.8273	16.9314	364.1710	39.3202
7.1984	60.3743	16.8188	359.8023	40.5961
7.5971	52.7311	16.7108	355.2424	41.8581
7.9985	44.8434	16.7482	350.4565	43.1357
8.3972	36.8535	16.7231	345.5282	44.3927
8.7986	28.7025	16.6321	340.4181	45.6302
9.1973	20.5362	16.4938	335.2140	46.8495
9.5987	12.2935	16.3042	329.8729	48.0515
9.9974	4.1211	16.0808	324.4855	49.2372
10.3962	-3.9906	16.0751	319.0413	50.4839
10.7975	-12.0500	15.9957	313.5283	51.7195
11.1963	-19.9125	15.8601	308.0395	52.9442
11.5976	-27.6353	15.6646	302.5282	54.1589
11.9964	-35.0781	15.4259	297.0873	55.3639
12.3977	-42.2929	15.1398	291.6709	56.5598
12.7965	-49.1458	15.0982	286.3704	57.8007
13.1978	-55.6811	15.0836	281.1418	59.0538
13.5966	-61.7735	15.0159	276.0744	60.3022
13.9954	-67.4234	14.8966	271.1577	61.5462
14.3967	-72.6196	14.7274	266.3850	62.7862
14.7955	-77.2538	14.5229	261.8399	64.0228
15.1968	-81.3421	14.6570	257.4879	65.2900
15.5956	-84.7903	15.1057	253.4070	66.5871
15.9969	-87.5993	15.4787	249.5687	67.8801
16.3957	-89.6911	15.7929	246.0446	69.1690
16.7945	-91.0432	16.0516	242.8325	70.4537
17.1958	-91.6143	16.2578	239.9383	71.7343
17.5946	-91.3547	16.6700	237.4217	73.0349
17.9959	-90.2182	17.6878	235.2739	74.4062
18.3947	-88.1765	18.5558	233.5452	75.7773
18.7960	-85.1608	19.2803	232.2369	77.1483
19.1948	-81.1667	19.8861	231.3887	78.5193
19.5961	-76.1004	20.3775	231.0131	79.8904
19.9949	-69.9834	20.7777	231.1380	81.2616

Table 6-7. Stresses and Stress Intensity Factors for the As-Welded WP Middle Lid (Output DTN: LL030607012251.065)

Depth, mm	Radial stress (Sx), MPa	SIF due to Sx, MPa-$m^{0.5}$	Hoop stress (Sz), MPa	SIF due to Sz, MPa-$m^{0.5}$
0.1593	153.9288	4.9033	228.3849	7.5754
0.3203	127.1172	6.2685	235.9015	10.9665
0.4797	101.7315	6.8580	242.3296	13.7144
0.6407	77.2206	6.9761	247.8300	16.1330
0.8000	54.0676	6.7631	252.3158	18.3358
0.9593	31.9924	6.3044	255.8750	20.3775
1.1203	10.7596	5.8250	258.5570	22.3816
1.2797	-9.2150	5.2651	260.3330	24.3197
1.4407	-28.3699	4.6000	261.2667	26.1726
1.6000	-46.3322	3.8615	261.3655	27.9459
1.7593	-63.3265	3.0726	260.6697	29.6433
1.9203	-79.5368	2.2534	259.1863	31.2668
2.0797	-94.6509	1.4282	256.9724	32.8922
2.2407	-109.0061	0.5951	254.0088	34.5292
2.4000	-122.3284	-0.2400	250.3830	36.1060
2.5593	-134.7922	-1.0656	246.0945	37.6220
2.7203	-146.5363	-1.8707	241.1150	39.0762
2.8797	-157.3405	-2.6491	235.5736	40.4676
3.0407	-167.4522	-3.4047	229.3818	41.8264
3.2000	-176.6850	-4.1787	222.6938	43.2168
3.3593	-185.1690	-4.9390	215.4749	44.5479
3.5203	-193.0032	-5.6775	207.6685	45.8181
3.6797	-200.0480	-6.3965	199.4620	47.0265
3.8407	-206.4725	-7.0865	190.7114	48.1718
4.0000	-212.1664	-7.7528	181.6234	49.2531
4.1593	-217.2211	-8.2576	172.1366	50.3451
4.3203	-221.7016	-8.7427	162.1726	51.3729
4.4797	-225.5376	-9.2143	151.9633	52.3351
4.6407	-228.8312	-9.6605	141.3230	53.2313
4.8000	-231.5367	-10.0894	130.4975	54.0602
4.9593	-233.7127	-10.4950	119.4050	54.8214
5.1203	-235.3959	-10.9446	107.9526	55.4811
5.2797	-236.5735	-11.4131	96.4029	56.0586
5.4407	-237.2926	-11.8636	84.5422	56.5637
5.6000	-237.5602	-12.3055	72.6415	56.9965
5.7593	-237.4080	-12.7309	60.6057	57.3567
5.9203	-236.8501	-13.1320	48.3342	57.6444
6.0797	-235.9201	-13.7114	36.1065	57.7587
6.2407	-234.6208	-14.4707	23.6946	57.6946
6.4000	-233.0011	-15.2333	11.3811	57.5522
6.5593	-231.0713	-15.9891	-0.9356	57.3322
6.7203	-228.8287	-16.7277	-13.3570	57.0353
6.8797	-226.3414	-17.4611	-25.6005	56.6626
7.0407	-223.5802	-18.4707	-37.8942	56.1419
7.2000	-220.6238	-20.3589	-49.9583	55.3276
7.3593	-217.4669	-22.2128	-61.8935	54.4422
7.5203	-214.0957	-24.0173	-73.7955	53.4878
7.6797	-210.6019	-25.7872	-85.3924	54.6294
7.8407	-206.9348	-27.4989	-96.8987	56.2191
8.0000	-203.1923	-29.1709	-108.0509	57.7865

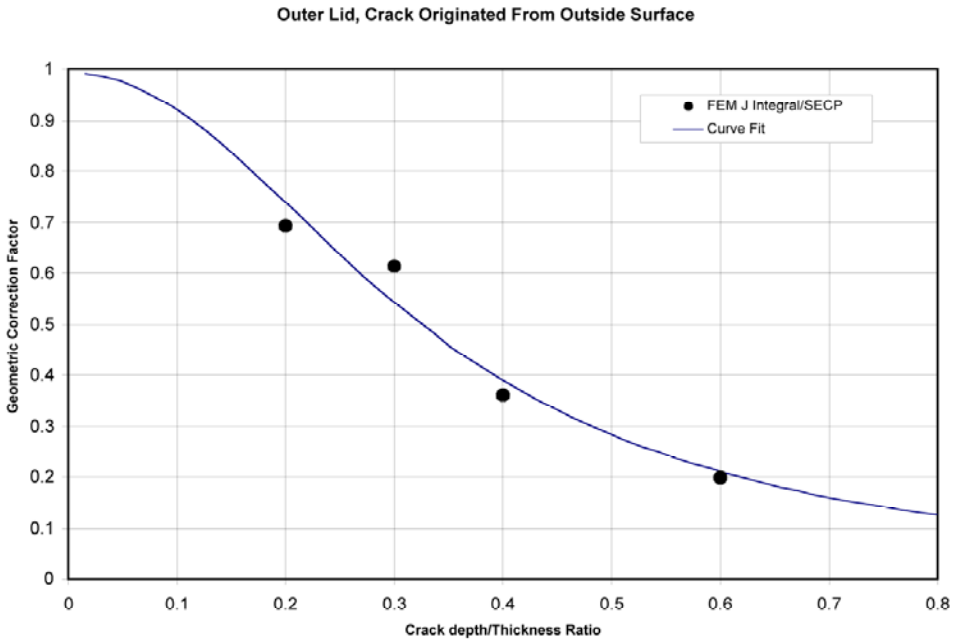

DTN: LL000319905924.144

Figure 15. Outer Lid Circumferential Flaw Geometric Correction Factor

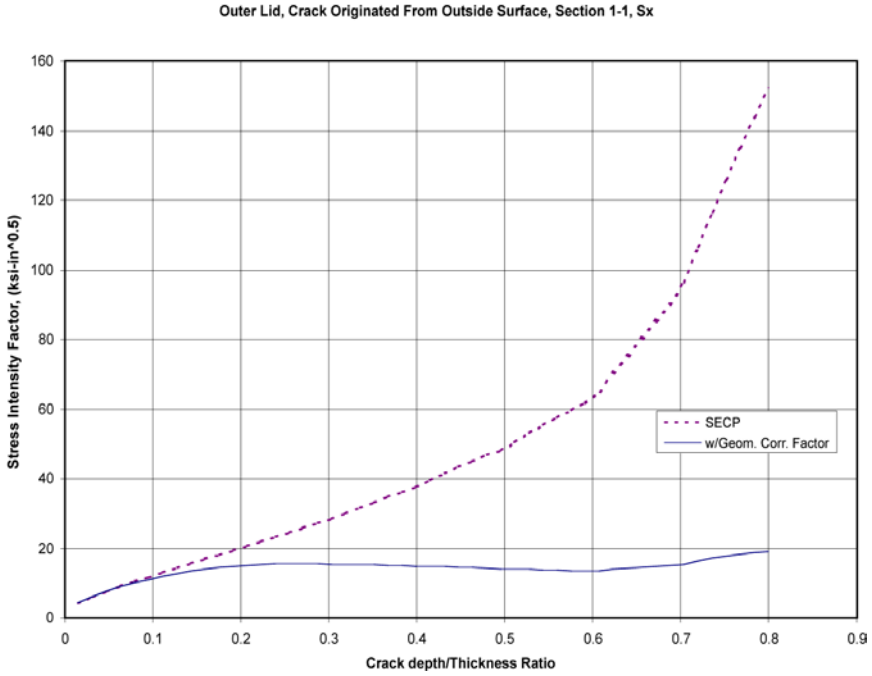

DTN: LL000319905924.144

Figure 16. Stress Intensity Factors for Circumferential Flaw in Outer Lid

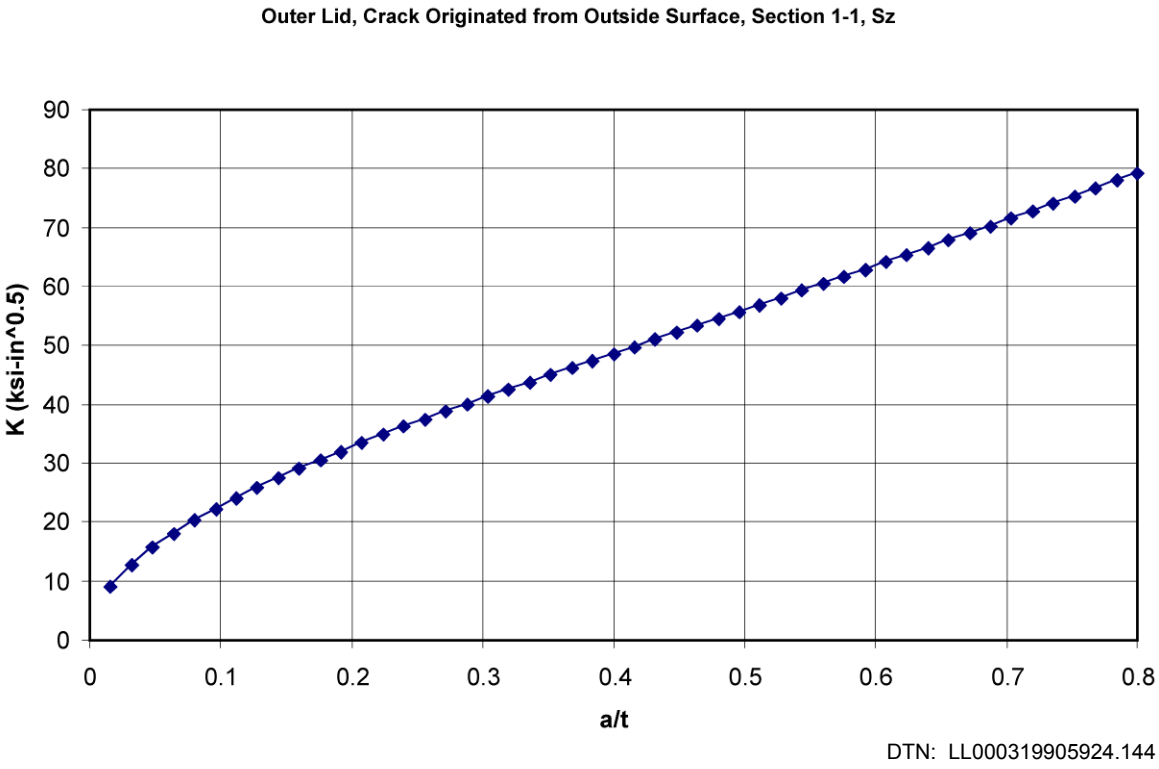

Figure 17. Stress Intensity Factor for Radial Flaw in Outer Lid

6.4.3 Impact of Corrosion

The results presented in Section 6.4.2.3 were performed for the as-built condition. Thus, the full thickness for all the waste package components was used. In order to simulate the effect of wall thinning caused by general corrosion, a layer of elements from the outside surface of the outer lid was removed. The thickness of this layer is 0.125 inch, which is equivalent to the removal of 12.7% of the wall of the outer lid. The general corrosion rates are very low for the Alloy 22 material. Based on the mean general corrosion rate of 7.23 nm/year (Section 6.3.5), the 0.125-inch removal is the amount of material subject to general corrosion in 439,140 years. Removal of these elements causes a redistribution of the stress pattern.

Figure 18 shows the row of elements removed to simulate the general corrosion of the outer lid surface. Figures 19 and 20 show, respectively, the through-wall radial stress profiles (with and without corrosion effects) and hoop stress profiles at Section 1-1 in Figure 18. These results demonstrate the redistribution of the residual stress. In general, stress appears to be not very sensitive to the effects of corrosion.

Figures 21 and 22 show the stress intensity factor distribution for Section 1-1 in Figure 18 for circumferential and radial cracks. These figures show the stress intensity factor as a function of distance from the outside surface and normalized distance from the outside surface. These figures demonstrate that the overall effect of general corrosion is small.

(a)

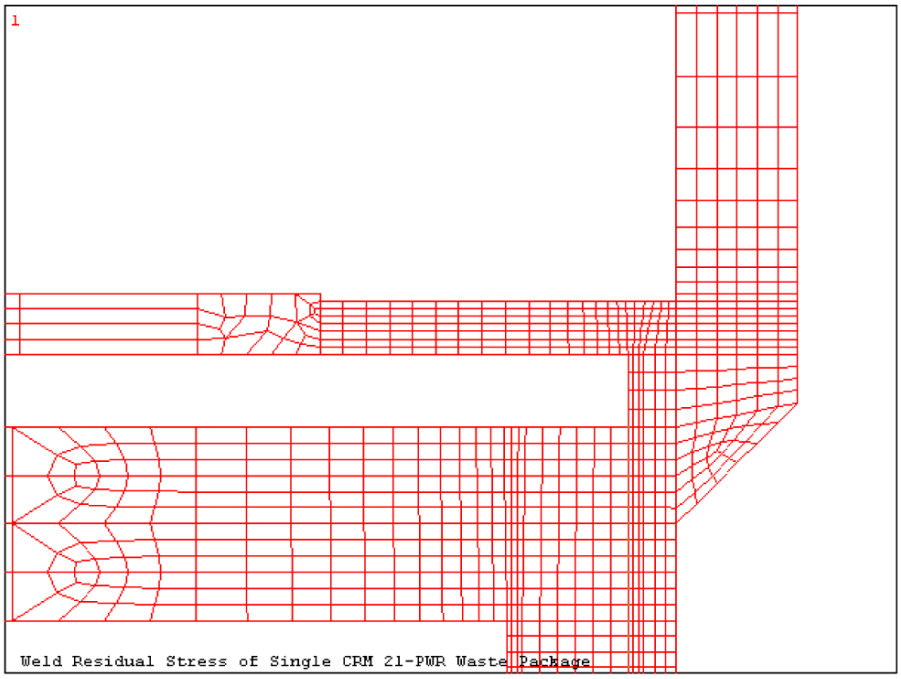

(b)

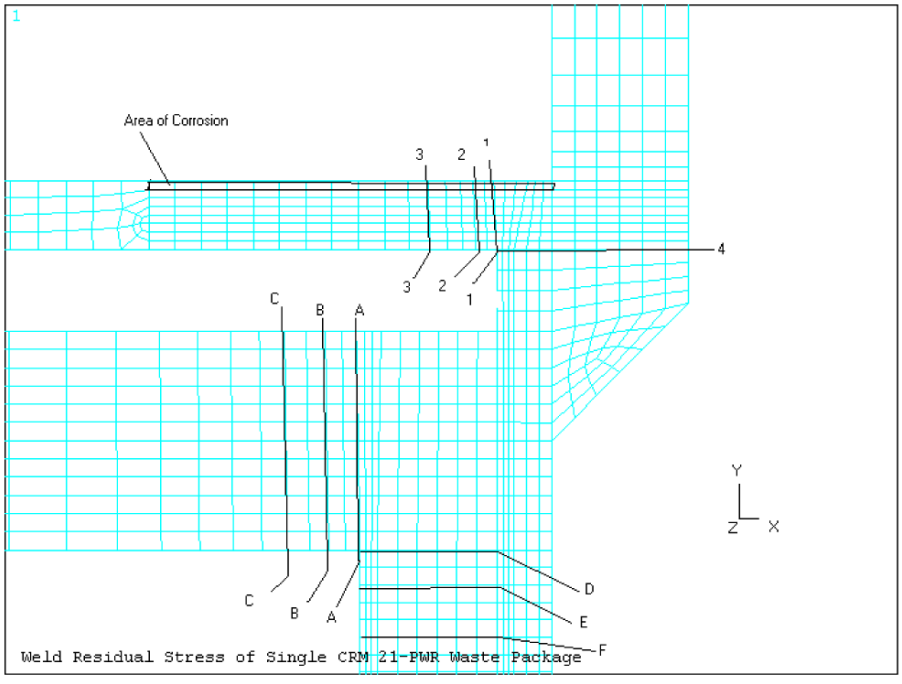

DTN: LL000319805924.143

NOTE: (a) Finite element model
(b) Sections for stress profile

Figure 18. Finite Element Model Used for Study of Corrosion

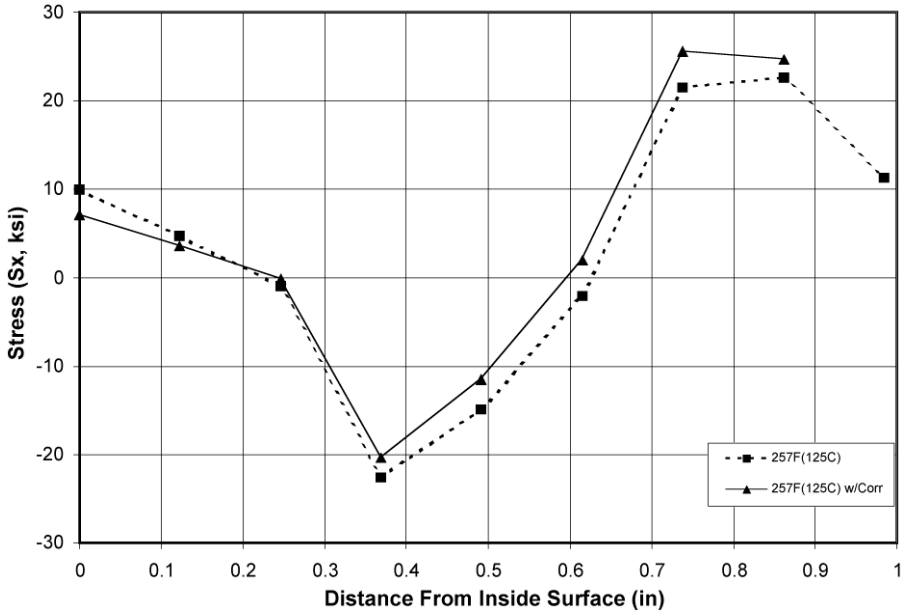

DTN: LL000319905924.144

Figure 19. Effect of Corrosion on Radial Stress in Outer Lid

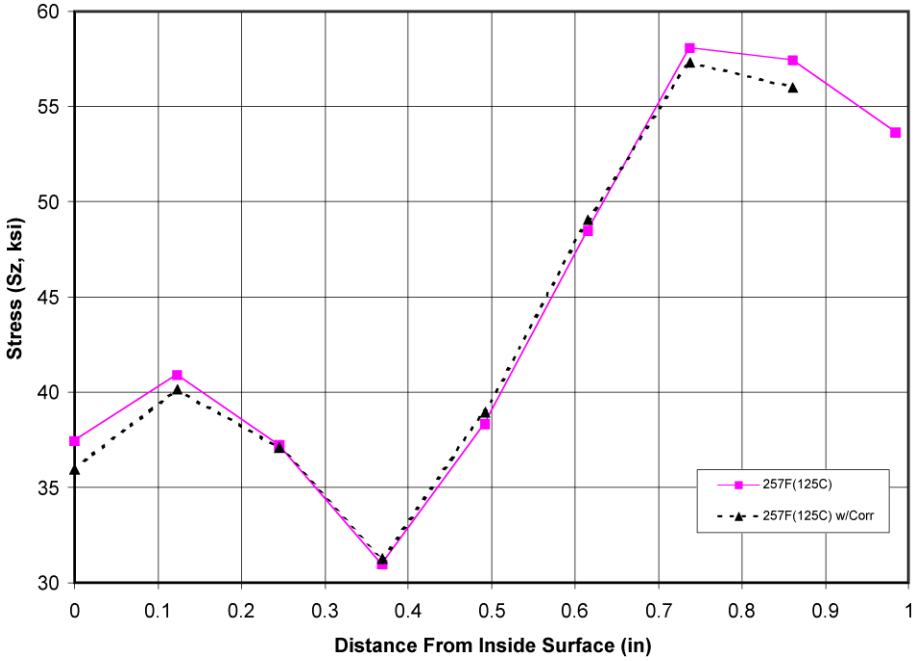

DTN: LL000319905924.144

Figure 20. Effect of Corrosion on Hoop Stress in Outer Lid

(a)

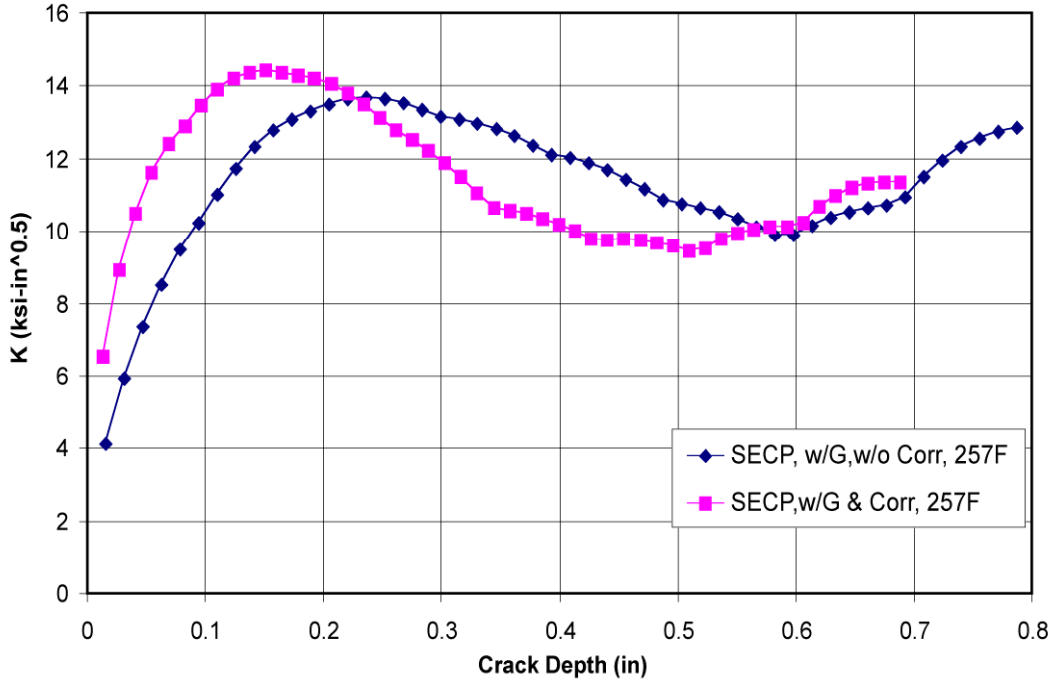

(b)

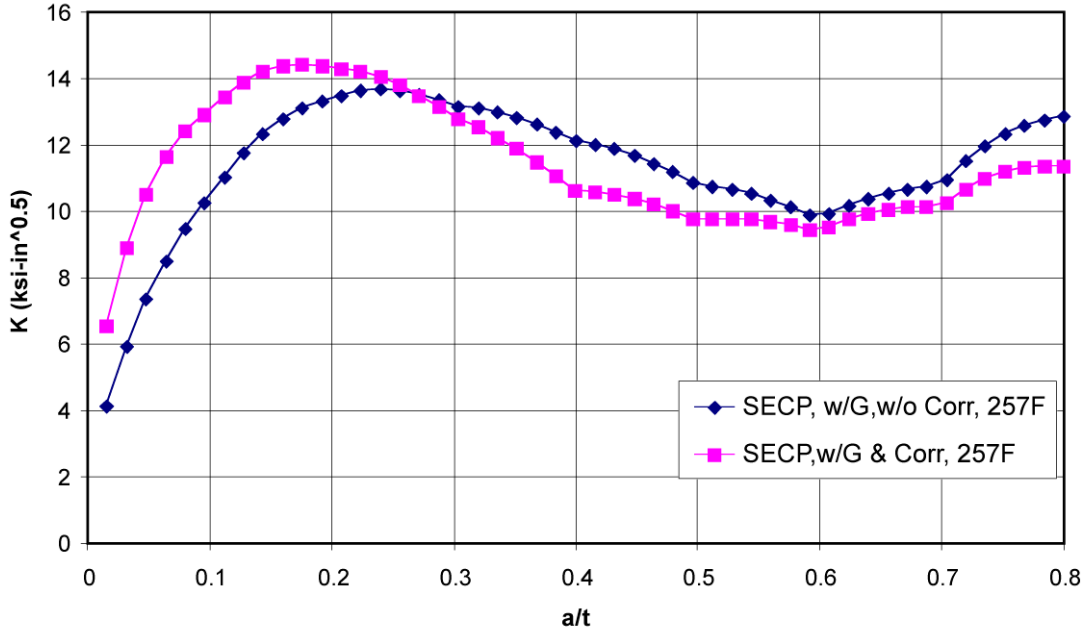

DTN: LL000319905924.144

NOTE: (a) X-axis is crack depth in inches.
(b) X-axis is shown as the ratio of crack depth (a) vs. thickness (t).

Figure 21. Stress Intensity Factor for Full-Circumference Flaw in Outer Lid

(a)

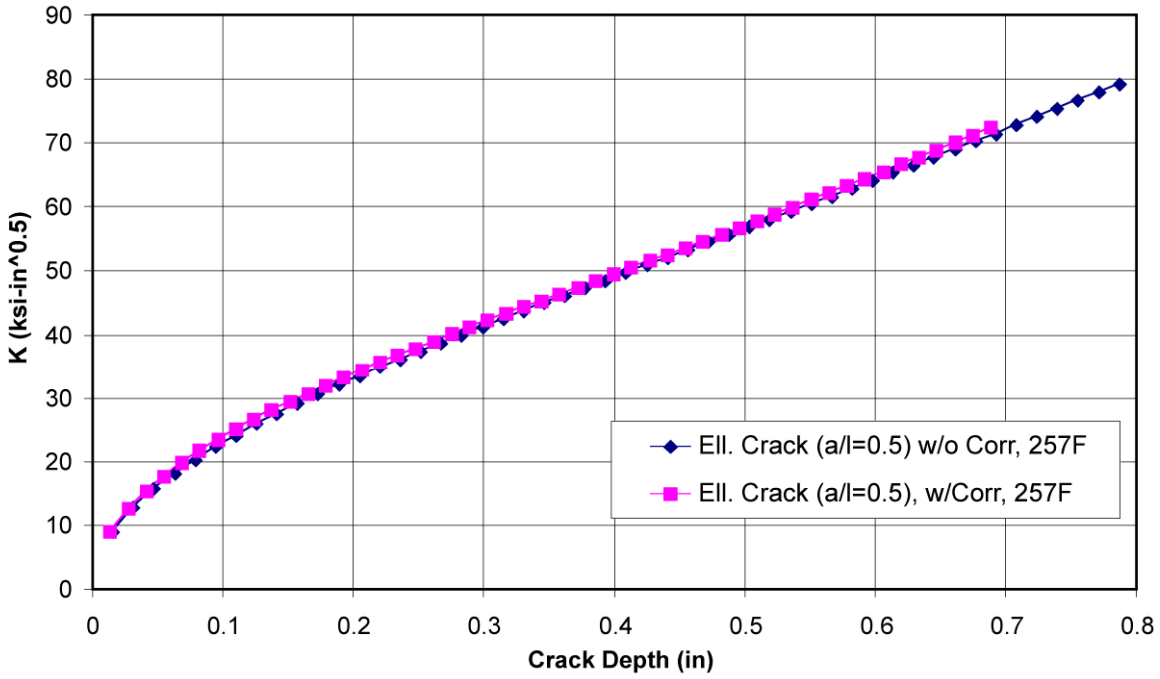

(b)

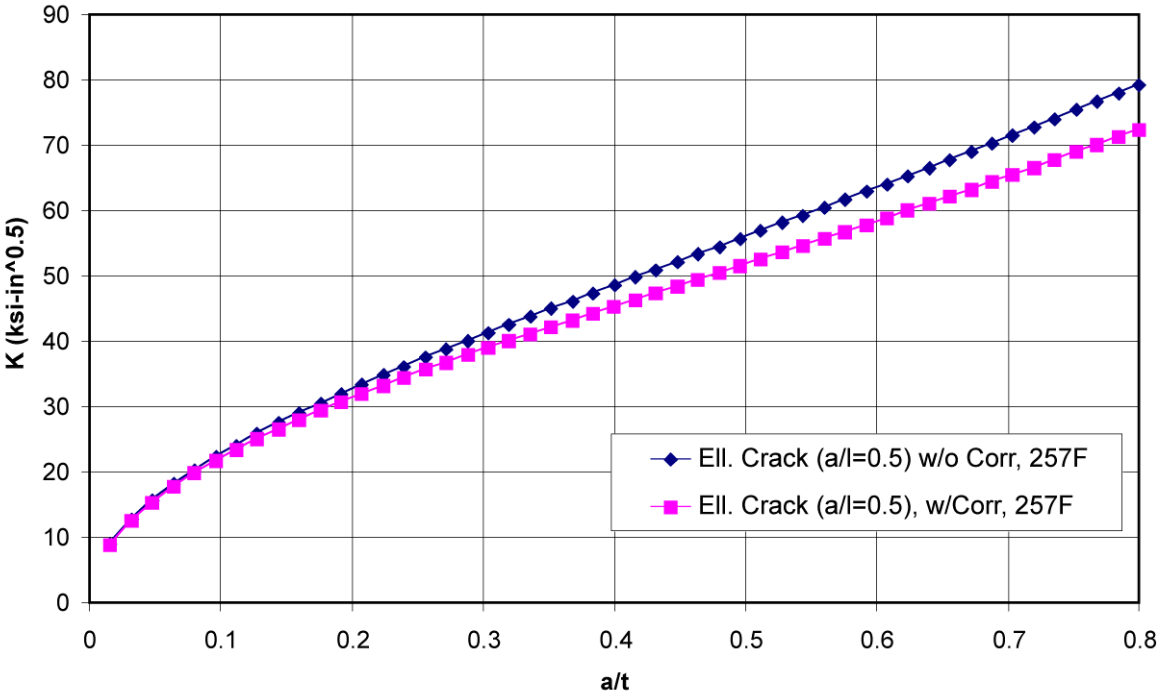

DTN: LL000319905924.144

NOTE: (a) X-axis is crack depth in inches.
(b) X-axis is shown as the ratio of crack depth (a) vs. thickness (t).

Figure 22. Stress Intensity Factor for Radial Elliptical Crack in Outer Lid

6.4.4 Mitigation of Weld Residual Stress

Stress is one of the three basic factors that cause initiation and propagation of cracks in structural components due to stress corrosion cracking. The other two factors are metallurgical susceptibility and environment. SCC can be reduced to a manageable state if the weld residual stress in the WP can be effectively mitigated.

Weld residual stress can be mitigated by optimizing the geometrical configuration of the WP design. Residual stress can also be mitigated through specially designed weld processes, such as "narrow-groove" and other low heat input welding processes as well as spray cooling of final weld passes to produce compressive outer surface stress.

For the final closure welds of the WP, in accordance with Arthur 2003, Attachment 1, p. 6, non-thermal mitigation (laser peening or low-plasticity burnishing) can be applied without heating the spent fuel elements within the WP but, for the purpose of license application (LA), Arthor 2003 indicated that laser peening is the non-thermal mitigation method. The laser peening treatment, which will be used for the 25-mm outer lid of the outer barrier, involves use of the laser peening process, where a high powered laser beam introduces shock pulses on the material surface. Laser peening is similar to the traditional shot-peening procedure but is a much-improved technology. For laser peening, the intense stream of tiny metal or ceramic balls used in the traditional shot peening is replaced by high-energy lasers with pulse lengths in the tens of nanoseconds, short enough to generate a rapid yet energetic shock. This process can produce a uniform layer of highly shocked and compressed material that is extremely resistant to cracks and corrosion.

According to measured data reported in Hornbach (1999), laser peening is capable of producing a compressive surface layer of about 60 mils (1.5 mm) with compressive stress in the range of 20 to 60 ksi for a one inch thick Alloy 22 plate. The depth of stress reduction may be increased by repeated application of laser peening (Hornbach 1999). A typical example is shown in Figure 23 for stress profiles at the weld center line for stress component 1 (S1, parallel to the weld center line) and stress component 3 (S3, perpendicular to the weld center line) before and after laser peening.

To demonstrate the effect of laser peening on the stress intensity factor, the weld induced residual stress in the 25-mm outer lid of the CRM-21 PWR design was reduced from tensile stress to 40 ksi compressive stress for a depth of 0.06 in at the outside surface (see Figure 24). The residual stress then varies linearly from 0.06 in. to 0.12 in. From this point on, the stress remains undisturbed. The stress intensity factor was calculated for the reduced stress profile and compared to the stress intensity factor previously calculated for the original stress profile as shown in Figure 25.

For radial and hoop stresses in ksi in the laser peened 25-mm outer lid of the WP design, the stress coefficients with stress in ksi and distance x in inches are obtained from DTN: LL000316205924.142, file name: Skvrbr1, sheet "Peening,Sx", cells C9 - C12 for radial stress and sheet "Peening,Sz", cells C9-C12 for hoop stress. The coefficients are listed in the seventh and eighth rows of Table 4.1-2. Table 6-8 shows the converted stress coefficients, A_0, A_1, A_2, and A_3, in the metric unit system. Table 6-9 shows the calculated stress and stress intensity profiles for the outer WP lid subjected laser peening.

Table 6-8. Stress coefficients for the Laser Peened WP Outer Lid.

Stress Coefficient	Unit	Radial Stress	Hoop Stress
A_0	MPa	-265.920	-292.607
A_1	MPa/mm	103.987	178.277
A_2	MPa/mm^2	-9.857	-14.135
A_3	Mpa/mm^3	0.254	0.320

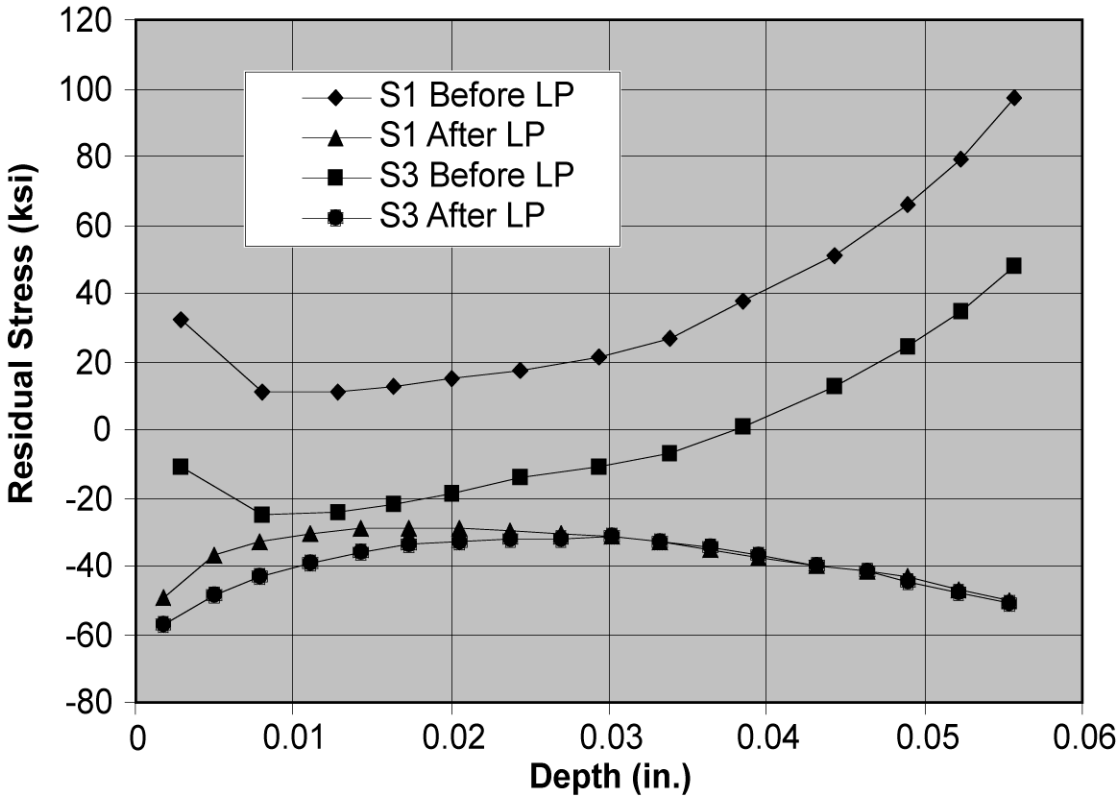

DTN: LL000320005924.145

Figure 23. Mitigation of Weld Stress in Alloy 22 with Laser Peening

Table 6-9. Stresses and Stress Intensity Factors for Laser Peened WP Outer Lid (Output DTN: LL030607012251.065)

Depth, mm	Radial stress (Sx), MPa	SIF due to Sx, MPa-$m^{0.5}$	Hoop stress (Sz), MPa	SIF due to Sz, MPa-$m^{0.5}$
0.3988	-226.0035	-9.1866	-223.7417	-5.6943
0.8001	-188.9005	-11.7979	-158.8532	-6.4965
1.1989	-154.9833	-13.0189	-98.6408	-6.1528
1.6002	-123.7220	-13.4298	-42.2143	-5.1372
1.9990	-95.4153	-13.2965	9.8344	-3.6697
2.4003	-69.6047	-12.7780	58.2916	-1.8824
2.7991	-46.5198	-12.2958	102.6663	0.1212
3.2004	-25.7687	-11.7214	143.6471	2.2821
3.5992	-7.5170	-11.0116	180.8374	4.5533
3.9980	8.4709	-10.2080	214.6297	6.8939
4.3993	22.3728	-9.3437	245.3299	9.2702
4.7981	34.1098	-8.4525	272.6715	11.6543
5.1994	43.9293	-7.6096	297.1262	14.0165
5.5982	51.8041	-6.8298	318.5068	16.3364
5.9995	57.9323	-6.0675	337.2088	18.6024
6.3983	62.3334	-5.3416	353.1178	20.8003
6.7970	65.1483	-4.6612	366.4827	22.9177
7.1984	66.4775	-4.0331	377.4871	24.9441
7.5971	66.4012	-3.4507	386.1141	26.9023
7.9985	65.0162	-2.8535	392.5969	28.8612
8.3972	62.4372	-2.2745	396.9757	30.7287
8.7986	58.7292	-1.7170	399.4297	32.5008
9.1973	54.0361	-1.1860	400.0499	34.1745
9.5987	48.3961	-0.6829	398.9677	35.7479
9.9974	41.9777	-0.2101	396.3190	37.2200
10.3962	34.8443	-0.3513	392.2239	38.4530
10.7975	27.0415	-0.5163	386.7654	39.5674
11.1963	18.7651	-0.7070	380.1350	40.5636
11.5976	10.0075	-0.9242	372.3715	41.4432
11.9964	0.9766	-1.1690	363.6954	42.2086
12.3977	-8.3447	-1.4403	354.1195	42.8627
12.7965	-17.7414	-1.7949	343.8874	43.4439
13.1978	-27.2353	-2.1728	332.9919	43.9342
13.5966	-36.6092	-2.5554	321.6934	44.3269
13.9954	-45.8267	-2.9438	310.0462	44.6272
14.3967	-54.8472	-3.3378	298.0958	44.8409
14.7955	-63.4595	-3.7396	286.1158	44.9743
15.1968	-71.6755	-4.0160	274.0769	45.0329
15.5956	-79.2941	-4.1354	262.2538	45.0208
15.9969	-86.3145	-4.2182	250.6192	44.9464
16.3957	-92.5507	-4.2696	239.4426	44.8182
16.7945	-97.9528	-4.2904	228.7710	44.6449
17.1958	-102.4495	-4.2805	218.6644	44.4361
17.5946	-105.8869	-4.3087	209.3730	44.2112
17.9959	-108.2109	-4.5204	200.9017	43.9968
18.3947	-109.2950	-4.7313	193.4801	43.7750
18.7960	-109.0551	-4.9400	187.1369	43.5578
19.1948	-107.3973	-5.1487	182.0747	43.3569
19.5961	-104.2024	-5.3536	178.3522	43.1853
19.9949	-99.4140	-5.5551	176.1390	43.0560

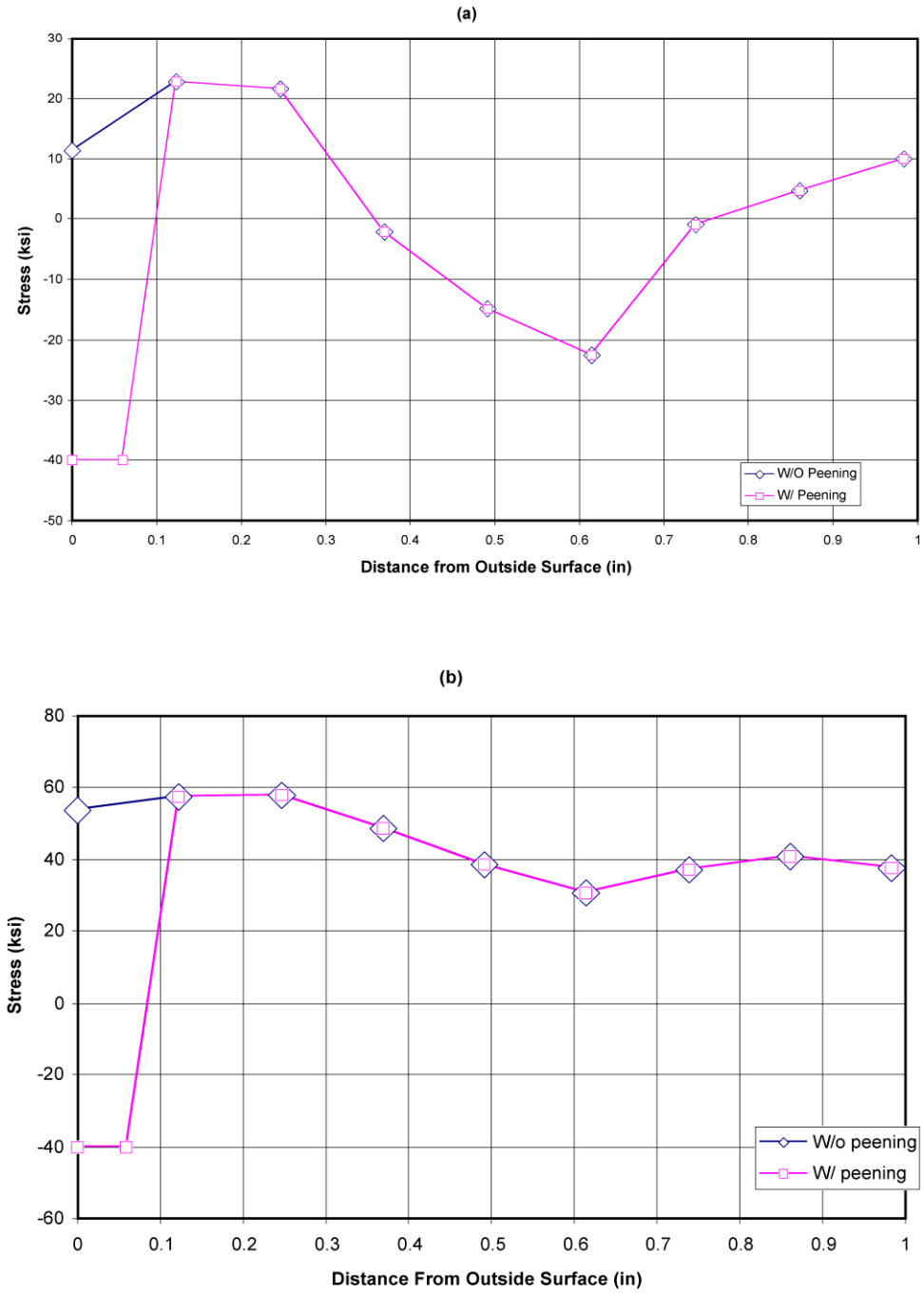

DTN: LL000319905924.144

NOTE: (a) Radial Stress, Sx
(b) Hoop Stress, Sz

Figure 24. Stress in Outer Lid with and without Laser Peening

(a)

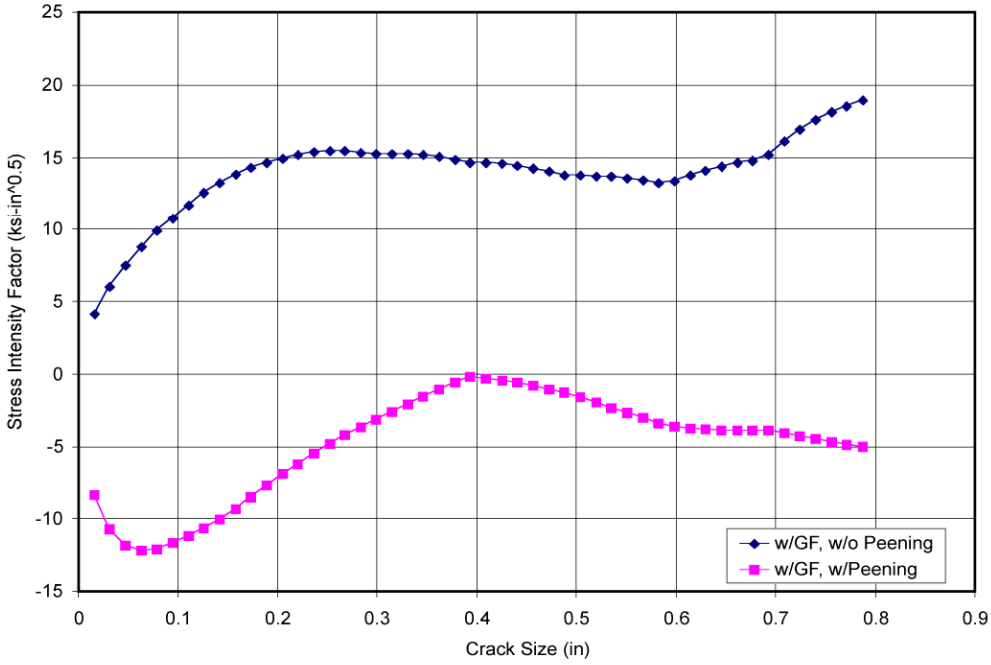

(b)

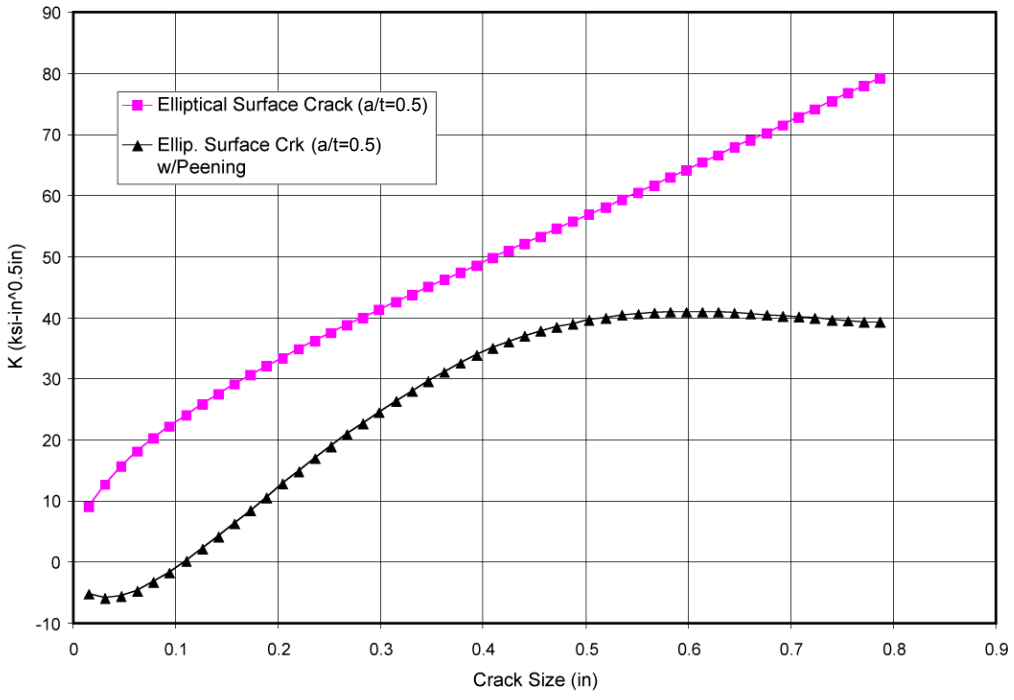

DTN: LL000319905924.144

NOTE: (a) Stress Intensity Factor Plots due to Radial Stress
(b) Stress Intensity Factor Plots due to Hoop Stress

Figure 25. Stress Intensity Factors with and without Laser Peening

6.4.5 Uncertainty and Variability of Residual Stress and Stress Intensity Factor in WP

It was stated in Section 6.4.2.2 that, although the determination of weld residual stress for the WP welds is a three-dimensional problem, a two-dimensional axisymmetric modeling approach has been used for the finite element analyses of the weld residual stresses. The result of this assumption is that the stress distribution is axisymmetrical about the WP axial centerline, i.e., constant along the circumference. An investigation of cause of cracking in austenitic stainless steel piping (Klepfer 1975, Figure 9-95, pp. 9-119) indicated that the residual stress for a 26 inch pipe inside surface shows a sinusoidal distribution around the circumference with a range of about 5 ksi about the mean stress. Based on this conclusion, the variability of the mean stress along the circumference (∇S) can be represented by the following equation:

$$S_\theta(x)= S_0(x) - \nabla S(1 - \cos(\theta)) \qquad \text{(Eq. 25a)}$$

where,

θ is the angle measured from a reference location ($\theta = 0^o$) on the circumference,

$S_\theta(x)$ is the weld residual stress profiles at an angle θ,

$S_0(x)$ is calculated weld residual stress profile at $\theta = 0^o$,

∇S is taken to be 2.5 ksi or 17.236893 MPa.

Variability in stress intensity factor is treated similarly to that for stress because stress intensity factor is a linear function of stress, i.e.,

$$K_\theta(x)= K_0(x) (S_\theta(h) / S_0(h)) \qquad \text{(Eq. 25b)}$$

where h is the thickness of the closure lid.

The uncertainty of the weld residual stress calculated by the simplified finite element analysis can be adequately represented by a normal distribution with the calculated residual stress as the mean ($S_\theta(x)$) and a 3-sigma bound to be defined.

Mohr (1996, p. 39) indicated that the uncertainty range of the residual stress is a function of the yield strength of the material and varies about the mean by ±35% of the yield strength. The high degree of uncertainty associated with Mohr's data was empirically developed by bounding the measured residual stress scatter developed for a large number of different carbon steel welded pipes covering a range of thicknesses, welding processes, weld joint configurations, weld heat inputs, yield strengths, etc. In the case of the final closure welds of the dual-lid improved WP design, the various parameters contributing to residual stress variation will be closely controlled. This includes close, automated control on the welding process parameters, the allowable material and weld wire yield strength range, the weld joint configuration and spacing, etc.

In contrast to the high degree of scatter noted in Mohr (1996), data available on shot peened (analogous to laser peened) nickel alloy Incoloy 908 (Pasupathi 2000) indicate a narrow residual stress scatter range for as-welded and as-welded plus shot peened nickel alloy material with one sigma values of ±3% of the measured stress value for shot peened surfaces (Pasupathi 2000, Table II and Table VI) or an uncertainty range of about ±9% at the 3 sigma level. In comparison, the residual stresses measured on a peened surface by the X-ray diffraction technique (Lu 1996, Table 5-4, p. 103) showed an average measurement uncertainty of about ±15 MPa, which is about ±5% of the Alloy 22 yield strength. Values of yield strength, YS, of Alloy 22 are listed in Table 4-1-4. For conservative purpose, the higher YS value at the room temperature may be used.

The data listed in Pasupathi (2000) are for both welded and non-welded samples (peened and unpeened), many of which also contain some cold work due to tube reduction drawing. Thus, they represent a good sampling of the entire range of material conditions the YMP WP may encounter.

Further, in the case of the final closure welds of the dual-lid WP design, very tight process control plus periodic quality control measurements of weld surface residual stresses will be made in the hot-cell on the final post-processed Alloy 22 material in the near-surface region of the weld and heat affected zone. The quality control meaurement process(es) to be used will depend on the finally selected stress mitigation process. For the laser peening process, the so-called Almen Strips, which are commonly used to control shot peening processing and laser peening processing, may be used. If stresses are found to deviate from the specified range, the weld can be reprocessed, repaired or scrapped.

Thus, based on the above discussion, a 3-sigma stress uncertainty range of ±15% of the material mean yield strength appears to be a conservative representation of the realistic case that is achievable through appropriate levels of process controls.

The minimum and maximum stresses at the 3-sigma level, $S_\theta(x)\min$ and $S_\theta(x)\max$, in the weld can be obtained from the mean stress, $S_\theta(x)$, by the following equations:

$$S_\theta(x)\min = S_\theta(x)\left(\frac{S_\theta(h)-\Delta S}{S_\theta(h)}\right) \quad \text{(Eq. 26a)}$$

$$S_\theta(x)\max = S_\theta(x)\left(\frac{S_\theta(h)+\Delta S}{S_\theta(h)}\right) \quad \text{(Eq. 26b)}$$

where $S_\theta(h)$ is the mean residual stress on inside surface (x=h, where h is the thickness of the closure lid) and ΔS is the amplitude of variation between the maximum and minimum stresses at the inner surface of the WP lid. The stress intensity factor calculated from the mean stress as described in Section 6.4.2.2 is assumed to be the mean stress intensity factor $K_\theta(x)$. The minimum and maximum stress intensity factors are calculated similarly to those for stress because stress intensity factor is a linear function of stress.

$$K_\theta(x)\min = K_\theta(x)\left(\frac{S_\theta(h)-\Delta S}{S_\theta(h)}\right) \quad \text{Eq. 26c)}$$

$$K_\theta(x)\max = K_\theta(x)\left(\frac{S_\theta(h)+\Delta S}{S_\theta(h)}\right) \quad \text{(Eq. 26d)}$$

where θ is the angle measured from a reference location ($\theta = 0^\circ$) on the circumference and ΔS = 0.15 YS (YS is the mean yield strength given in Table 4.1-4).

6.5 ESTIMATE OF LENGTH AND INTERCRACK SPACING OF RADIAL THROUGH-WALL CRACKING AND CRACK OPENING

The information provided in Section 6.5 is not used directly in the SDFR Model. Rather, it is provided as information that can be used by PA in calculating radionuclide release rates through stress corrosion cracks.

6.5.1 Estimated Length and Intercrack Spacing of Radial Through-Wall Cracking

As discussed in Section 6.2.2.3, radially oriented flaws are important to SCC of waste packages since the hoop stress, which drives the radially oriented cracks, is usually the dominant stress component. The stress intensity factor resulting from the through-wall hoop stress gradient (or profile) can result in propagation of through-wall SCC for cracks in the radial direction. Based on stress distributions shown in Figure 14, rapid weld residual stress decay is observed with increasing distance normal to the weld/metal interface, i.e. in the radial direction. As the tensile stress decays, the driving force for crack extension in the radial direction also decreases rapidly and appears to fully attenuate at distances from the weld center line on the order of the welded plate thickness. Thus, the expected maximum length of these radial cracks will be approximately two times the plate thickness.

With respect to the expected minimum spacing between parallel through-wall radial cracks, detailed analysis *Structural Integrity Associates Support of Waste Package Design for 2001* (Structural Integrity Associates 2002, Section I), indicated because of stress field interactions between closely spaced parallel cracks that for a one inch thick plate, the distance between two neighboring through-wall cracks would need to be greater than the plate thickness for the stress (and resultant stress intensity) to be sufficient to drive a flaw through-wall.

6.5.2 Estimate of Crack Opening

Leak through a crack can occur if the crack grows into a through-thickness crack. Leak rate depends on the size of crack opening, among other factors. A comprehensive finite element analysis may be attempted in order to estimate the crack opening. A simplified approach, however, is described below.

1. A crack is either circumferential (perpendicular to the radial stress) or radial (perpendicular to the hoop stress) in the outer surface of the closure weld of the WP.

2. A circumferential crack is assumed to have a semi-elliptical shape with depth “a” and length “2c.” The aspect ratio “c/a” for a radial crack is assumed to be “1,” i.e., a semi-circular crack (c = a).

3. The crack length “2c” of a circumferential crack remains unchanged but the final length of a through-wall crack is at least twice the wall thickness. Under this assumption, most cracks will grow in both directions of the minor (depth “a”) and major (length “2c”) axes and assume the semi-circular shape (i.e., a = c) when they become through-wall cracks. According to fracture mechanics (Ewalds and Wanhill 1984, Section 2.5, p. 43), “a” tends to grow faster than “c” because the stress intensity factor tends to have a maximum value at the end of the minor axis and a minimum value at the end of the major axis. So

eventually a semi-elliptical crack will become a semi-circular crack. The crack length "2c" will remain unchanged only for very long cracks with initial crack length greater than twice the wall thickness. For such long cracks, the occurrence rate is usually very low. The length of a semi-circular crack will always be equal to twice the crack depth.

4. The crack opening has an elliptical shape with length "2c" and a gap "δ."

Tada et al. (1973, p. B.5), showed that the opening of a crack, δ, with length 2c in an infinite sheet is given for plane stress condition as:

$$\delta = \frac{(4c)\sigma}{E} \qquad \text{(Eq. 28)}$$

where σ = stress
E = Young's modulus

The opening area, A_{cr}, for an elliptical crack, therefore, can be estimated by:

$$A_{cr} = \frac{\pi}{4}\delta(2c) = \frac{(2\pi c^2)\sigma}{E} \qquad \text{(Eq. 29)}$$

When Equations 28 and 29 are used to estimate the crack opening and opening area, σ is the maximum stress across the thickness of either the radial stress (for a circumferential crack) or the hoop stress (for a radial crack).

7. MODEL VALIDATION

7.1. INTENDED PURPOSE OF THE MODEL

Stress corrosion cracking (SCC) is a potential corrosion mode that can result in penetration of the drip shield, waste package outer barrier and the stainless steel structural materials. Since no lifetime credit is taken for the stainless steel structural material it is not currently modeled. Therefore, in accordance with the Technical Work Plan for Waste Package Materials Data Analyses and Modeling (BSC 2002 [161132]), the intended purpose of the SCC model is to evaluate the potential for SCC of the drip shield (titanium grade 7) and the waste package outer barrier (Alloy 22) and to develop models for inclusion in abstracted form into the Integrated Waste Package Degradation (IWPD) model. This latter model provides the Performance Assessment Science and Analysis Project realistic waste package and drip shield SCC estimates as a function of time under the exposure conditions anticipated in the proposed repository.

This SCC model, based on BSC 2002 [161132], directly supports the following principal factors:

- Performance of the drip shield/drift invert system
- Performance of the waste package
- Probability of criticality event
- Radionuclide delay through the unsaturated zone

and the following TSPA components:

- Drip Shield Stress Corrosion Cracking and Other Corrosion Modes
- Waste Package Stress Corrosion Cracking and Other Corrosion Modes

7.2. DETERMINATION OF THE LEVEL OF CONFIDENCE REQUIRED

Laboratory test results indicate that the waste package outer barrier material, Alloy 22, is highly resistant to SCC initiation and growth on both smooth surfaces and at defects such as those that might exist in the region of the closure welds. Thus, although SCC is unlikely to initiate and/or grow under waste package highly static loading conditions where the only significant stresses are tensile residual fabrication and welding related stresses, the Project has conservatively chosen to mitigate the SCC potential by residual stress reversal processes that result in a compressive layer over the outer waste package surfaces. Under compression, SCC cannot initiate or grow. However, once the surface compressive layers are removed by general corrosion, SCC will initiate and can grow in the through-thickness direction. The time required for corrosion to remove the compressive layers is calculated to be greater than the 10,000 year regulatory period. Further, finite element model calculations of the expected residual tensile stress patterns present at the Alloy 22 final closure welds (as well as for the residual stresses generated in the deformed region of a drip shield that was impacted by a rock drop) indicate that if SCC were to initiate and grow through-wall, the cracks would be extremely tight and very limited in length and any water transport through the drip shield or waste package or radionuclide egress through these tight

waste package outer barrier cracks would be extremely limited and would not significantly contribute to the dose rate at the regulatory site boundary (BSC 2001 [156807], Table 5.14).

In establishing the required level of confidence for the SCC Model, the following criteria were considered:

Is the model extrapolated over large distances, spaces, or time frames?
Yes. The Stress Corrosion Cracking Model is extrapolated over the entire repository footprint and over the entire regulatory compliance period.

Does the model have large uncertainties?
No. While there is uncertainty in the parameters used in the SCC Model, these uncertainties are not large.

Will the model be used to demonstrate compliance or licensing positions?
Yes. The SCC Model is used as an input to IWPD which provides the Performance Assessment Science and Analysis Project realistic waste package and drip shield SCC degradation estimates as a function of time under the exposure conditions anticipated in the potential repository. The SCC Model inputs to IWPD support several primary factors and TSPA components.

Will the output of the model have impacts (positive or negative) on TSPA dose calculation results?
Yes. Although the effect of SCC penetrations in the drip shield and waste package outer barrier are estimated to have relatively small impacts on TSPA dose calculations, the SCC Model is used as an input to WAPDEG which is used to provide the Performance Assessment Science and Analysis Project realistic waste package and drip shield degradation estimates as a function of time under the exposure conditions anticipated in the proposed repository. The Integrated Waste Package Degradation Model supports several primary factors and TSPA components.

Based on the current Project conservative SCC mitigation approach, it is reasonable to limit the SCC Model level of confidence to moderate.

7.3. CRITERIA USED TO DETERMINE THAT THE REQUIRED LEVEL OF CONFIDENCE HAS BEEN OBTAINED

The SCC Model involves the slip dissolution/film rupture crack growth model and the threshold stress intensity factor (K_{ISCC}) parameter; both are described in peer reviewed scientific journals. Validation of the stress corrosion cracking model(s) is done through quantitative comparisons of input parameters and model predictions to calculated data available in the peer-reviewed published literature as well as "Q" data generated by the Project. The criteria to be used to determine that the required level of confidence has been obtained are discussed in this section.

Criterion One: This criterion deals with the validity of the model predictions of crack growth rate versus stress intensity. This criterion includes two parts:

> Criterion 1A**:** Are crack growth rates for stainless steel predicted by the slip dissolution/film rupture crack growth model for several applied stress intensity factors in

reasonable agreement with observed rates published in the peer reviewed literature for stainless steel using the slip dissolution/film rupture model documented in this AMR?

Criterion 1B: Are crack growth rates predicted for Alloy 22 by the slip dissolution/film rupture crack growth model in reasonable agreement with (or representing conservative upper bounds of) growth rates to be determined under a Project sponsored and OQA accepted Q test program at General Electric Corporate Research and Development Laboratory?

Criterion Two: Does the establishment of the threshold stress intensity K_{ISCC} satisfy an acceptable approach for Alloy 22 under environmental conditions relevant to the waste package? The acceptable approach is that the K_{ISCC} will be determined by using crack growth rate versus applied stress intensity measurements obtained under Q conditions. The measured values will be extrapolated to a conservative threshold value using the K dependence of crack growth rate described in the validated slip dissolution/film rupture model described in Criterion One.

Criterion Three: Does the establishment of threshold stress satisfy an acceptable approach for Alloy 22 under environmental conditions relevant to the waste package? The approach taken is to experimentally establish the material specific threshold stress value based on ongoing qualified experimental testing at General Electric Corporate Research and Development Laboratory and utilizing an accepted precedent in establishing a conservative threshold value.

7.4. ACTIVITIES PERFORMED TO GENERATE CONFIDENCE IN THE MODEL DURING MODEL DEVELOPMENT

For Criterion 1A, input parameter (exponent 'n') obtained for stainless steel is 0.54 as documented in section 6.3.3 of this AMR. Figure 5 indicated that crack growth rates predicted by the slip dissolution/film rupture crack growth model are in reasonable agreement with observed rates published in the peer reviewed literature for stainless steel using the slip dissolution/film rupture model (Ford and Andresen. 1988). This has assured that the model details and calculational methods yield results fully consistent with the peer reviewed journal published values.

For Criterion 1B, validity and predictive capacity of the model being used for Alloy 22 is established because crack growth rates predicted for Alloy 22 by the slip dissolution/film rupture crack growth model are in reasonable agreement with growth rates determined by direct measurements under a Project sponsored and OQA accepted Q test program at General Electric Global Research Center (GEGRC). Essentially, recent SCC crack growth rate measurements from GEGRC (DTN: LL021105312251.023) were made available for the assessment of model uncertainties as well as validation of the assumptions and parameter values developed for the base-case SCC model to be used for Alloy 22 (see Figure 6 in section 6.3.4). It was determined in section 6.3.4 that the mean value of n is 1.304 and the standard deviation is 0.16 with a truncated normal distribution with upper and lower bounds of 1.624 and 0.984, respectively. (see Table 6-2 in Section 6.3.4).

Criterion Two is related to the threshold stress intensity factor. Stress corrosion crack growth can

occur at a rate, such as that predicted by the slip dissolution/film rupture model, only if the calculated stress intensity at any flaw of given dimensions of length and depth exceeds a threshold value known as $K_{ISCC.}$ This criterion specifies an acceptable approach for the establishment of K_{ISCC} for Alloy 22 under environmental conditions relevant to the waste package. Since there is no accepted theoretical basis for a priori or deterministic calculation of K_{ISCC} this parameter is determined by using crack growth rate versus applied stress intensity measurements obtained under Q conditions. The measured values are then extrapolated to a conservative threshold value using the K dependence of crack growth rate described in the validated slip dissolution/film rupture model described in the first criterion. A defensible, conservative K_{ISCC} value was obtained by extrapolating crack growth rate versus K to a crack growth rate equal to the mean general corrosion rate at the alloy surface. The theoretical basis for this approach is that if the crack growth rate equals the rate at which the surface recedes due to general corrosion, then it is not possible to maintain a sharp crack (the crack tip will blunt) and SCC will effectively arrest.

Based on the crack blunting theory, it follows that an SCC crack will not grow if the general corrosion rate exceeds the mean crack growth rate. If V_{gc} is the mean general corrosion rate, the threshold stress intensity factor K_{ISCC} can be calculated from Equation 20 of Section 6.3.5:

$$K_{ISCC} = (V_{gc} / \overline{A})^{1/\overline{n}} \qquad \text{(Eq. 20)}$$

The mean general corrosion rate, V_{gc}, based on Section 6.3.5, is 7.23 nm/y. The threshold stress intensity factor for Alloy 22, accordingly, can be expressed in Table 6-3 of Section 6.3.5, based on the "n" values shown in Table 6-2.

Criterion Three specifies an acceptable approach for the establishment of a defensible threshold stress model. The threshold stress is that value below which stress corrosion cracking will not initiate on a “smooth” metal surface. The threshold stress conceptual model is published in peer reviewed journal papers and is described in Section 6.2.1. However, there is no firm accepted basis for calculating a threshold stress value for a given material/environment combination. Therefore, it is necessary to experimentally establish the threshold stress value.

Recently obtained SCC crack initiation stress measurements reported in DTN: LL021105312251.023 are summarized in Figure 1 in section 6.2.1, where the measurements of crack initiation stress is presented as failure stress vs. time-to-failure for specimens subjected to 9,600 hours of exposure in hot concentrated salt solution (pH=10.3 at 105^{o}C) designed to simulate the chemistry of concentrated Yucca Mountain ground water. The report indicated that Alloy 22 exhibits excellent SCC resistance since failure was not observed for any of the 120 Alloy 22 specimens under applied stress up to about 2.0 times the yield strength (YS) of the material. Titanium grade 7, although still faily resistant to SCC, did see some failures at applied stress levels of about 1.1 times the yield strength. An extrapolation scheme is needed in order to derive the threshold stress associated with the lifetime of waste packages from the available experimental results. The ASME Boiler Pressure Vessel code (ASME 1969, p. 80) typically uses a safety factor of 2 on stress when discussing fatigue lifetime cycles. Following this practice, the threshold stress may be derived from the stress levels from the test (i.e., 2.0(YS) for Alloy 22 and 1.1(YS) for titanium grade 7) by applying an appropriate safety factor. It is recommended a

threshold stress of 0.5(YS) for titanium grade 7 (with a safety factor of about 2.2). The same safety factor will result in a threshold stress of 0.9(YS) for Alloy 22.

Additionally, corroboration with available alternative conceptual models such as the coupled environment fracture model for stress corrosion cracking was considered for the validation of the base-case model. It was concluded in Section 6.3.6 that both the slip dissolution/film rupture model and the CEF model are capable of predicting the crack growth rate for stress corrosion cracking. However, it was discovered that the CEF model appears to have the tendency of underestimating the crack growth rate as compared to the slip dissolution/film rupture model when both models were applied to predict the crack growth rate for Type 304 stainless steel in the light boiling water reactor (BWR) environment. This is evidenced by Figure 7. Comparison with experimental data summarized by Ford and Andresen (1988) for crack propagation rate versus stress intensity factor for sensitized Type 304 stainless steel in fully aerated, high purity water at elevated temperature indicated that the crack growth rate predicted by the CEF model (i.e., 3.2×10^{-9} cm/s at 20 MPa-$m^{0.5}$) tends to be at the lower end of the range cited by Ford and Andresen (1988) (Macdonald and Urquidi-Macdonald 1991). For this reason, the CEF model was not included for further evaluation but only used to validate the base case slip dissolution/film rupture model.

In summary, the slip dissolution/film rupture SCC Model was validated by comparing Type 304 Stainless Steel measured crack growth rates reported in peer reviewed literature with SDFR Model predictions as well as with a less conservative alternate conceptual model and by comparing Alloy 22 SDFR Model predicted rates with subsequently developed experimentally measured Alloy 22 rates and demonstrating good agreement. For the empirical threshold stress intensity factor described in peer reviewed literature, a conservative approach was used to establish a threshold K_{ISCC} value by extrapolating qualified Alloy 22 crack growth rate results experimentally obtained at higher K_I values down to rates representative of the mean general corrosion rate where crack blunting occurs.

Finally with respect to the threshold stress used to describe crack initiation on ‘smooth’ surfaces, establishment of an acceptable conservative threshold SCC initiation stress was based on the ASME Boiler Pressure Vessel Code fatigue lifetime precedent of utilizing a factor of 2.2 reduction in stress below the fatigue runout failure stress. As a result of the above model validation approaches and the selection of conservative threshold values, the required level of confidence has been obtained.

7.5. POST-DEVELOPMENT VALIDATION ACTIVITIES.

Post-development validation activities per Section 5.4.1(C) of AP-SIII.10Q [162696] to be considered were identified in Technical Work Plan for Waste Package Materials Data Analyses and Modeling (BSC 2002 [161132]). Judged from the satisfactory results of the model validation, extended activities specifically for the purpose of validating the current SCC model do not appear to be necessary.

8. CONCLUSIONS

8.1 CONCLUSION

This AMR is a complete document which provides a detailed description of the process-level models and the associated input that have been developed for the performance assessment of the Alloy 22 waste package outer barrier subjected to stress corrosion cracking due to weld induced stress in the final closure welds. All the welds with the exception of the final closure welds will be subjected to heat treatment to relieve the residual stress when the entire WP is heat treated before the loading of spent fuel elements. It is recognized that plastic deformation resulting from lower probability seismic events has the potential of leading to plastic upsets and resultant sustained residual stresses that may initiate cracks and drive them through the wall. Failure criteria governing seismic initiated residual stress have been developed for the WP material, i.e., Alloy 22. The failure criteria are based on a stress threshold which is discussed in Section 6.2.1 of this AMR. If the seismic induced residual stress exceeds the threshold, then the affected areas of the waste package or drip shield are assumed to have failed as a barrier to flow and transport.

The drip shield is excluded from the SCC evaluation because the drip shield will be annealed to relieve the weld residual stress and SCC resulting from rock fall will result in very tight crack openings and will not degrade the water diversion or function of the DS (see section 6.3.7). The only remaining issue of concern for SCC associated with the DS is the potential for crack initiation due to plastic residual stress caused by seismic events. Failure criteria governing seismic initiated residual stress for the DS material, i.e., Titanium Grade 7, are based on a stress threshold which is discussed in Section 6.2.1 of this AMR. The Type 316 stainless steel inner barrier of the WP is excluded from the SCC evaluation because the performance assessment will not take credit from the inner barrier.

The base-case slip dissolution/film rupture model relates crack initiation and the subsequent advance to the metal oxidation that occurs when the protective film at the crack tip is ruptured. The slip dissolution/ film rupture model can be applied to assess the failure (or the lack of it) of the waste package due to the SCC crack propagation for given manufacturing cracks and/or cracks initiated by the combined effects of stress and environment. The threshold stress intensity factor (SIF) is based on the theory that there exists a threshold value (K_{ISCC}) for the stress intensity factor such that there is no growth of a pre-existing crack or flaw having a stress intensity factor less than the threshold value. The threshold SIF provides a criterion for determining if an SCC crack will reach an arrest state or enter a propagation phase.

The model validation was accomplished by comparing experimental measurements of key model parameters to data measurements directly sponsored by the project and corroborative data available from the open scientific literature and by comparing with another alternative conceptual model. Uncertainty and variability associated with model parameters have been assessed.

The application of the SCC models to the WP and DS also requires input of weld residual stress profiles and stress intensity factor profiles along with uncertainty and variability. These input data have been developed for the 25-mm outer lid (subjected to laser peening) and the as-welded

10-mm middle lid. This AMR also provides other needed input for a complete TSPA for the degradation of the waste package due to SCC effects in the following areas: threshold stress for crack initiation and an estimate of crack opening size. In addition, a summary of size, density and orientation distributions for manufacturing flaws or defects (which are technical product output (TPO) of the calculation "Analysis of Mechanisms for Early Failure" [161238]]) is given in Section 6.2.2, but is not part of the TPO of this AMR.

8.2 ACCEPTANCE CRITERIA

As indicated in Section 4.2, the Waste Package Technical Work Plan identifies the following acceptance criteria for this AMR:

1. System Description and Demonstration of Multiple Barriers
2. Scenario Analysis and Event Probability
3. Degradation of Engineered Barriers

A closer examination indicates that only Criteria 3 (Degradation of Engineered Barriers) is applicable to this AMR. Criteria 3 (including AC1, AC2, AC3, AC4, and AC5) are addressed as follows:

AC1 (System Description and Model Integration are Adequate) is addressed in Sections 1.1, 6.3.4, 6.3.7, 6.4.2 and 6.4.3.

AC2 (Data are Sufficient for Model Justification) is addressed in Section 7

AC3 (Data Uncertainty is Characterized and Propagated Through the Model Abstraction) is addressed in Section 6.4.5 and Tables 8-1, 8-2 and 8-3.

AC4 (Model Uncertainty is Characterized and Propagated Through the Model Abstraction) is addressed in Tables 8-1, 8-2, and 8-3.

AC5 (Model Abstraction Output is Supported by Objective Comparisons) is addressed in Tables 8-1, 8-2, and 8-3.

AC3, AC4 and AC5 will also be addressed by the Integrated Waste Package Degradation Model (IWPDM) AMR which describes the abstracted SCC models and the propagation of uncertainties in those models.

8.3 SUMMARY OF OUTPUT

The output of this AMR (DTN: LL030607012251.065) is summarized in Tables 8-1, 8-2, and 8-3 and can be used as input for the IWPDM AMR with no restrictions if the WP design, material, and environment are consistent with those considered in the modeling activities of this AMR. The model uses 25 mm and 10 mm (see Figure 8 in Section 6.4.2.1 and Table 8-1) for the outer and middle lids of the waste packages. The model is also applicable to thicker lids as the use of

smaller thicknesses makes the model more conservative. Weld induced residual stress in the waste package cylinder will be eliminated by an annealing process.

Stress profiles for both radial stress and hoop stress vs. depth are presented in look-up Tables 8.2 and 8.3. For the laser peened WP outer lid, it is clear from Table 8-3 that the hoop stress is the predominant stress component. Based on the hoop stress profile and yield stress of 286 MPa for Alloy 22, according to the first row of Table 8-1, the depth to which the outer weld stress is in compression is about 1.92 mm and the depth to which it is less than 90% of yield stress is about 4.57 mm.

Table 8-1 (part 1 of 3). Summary of Output
(Output DTN: LL030607012251.065)

Output name	Output value or equation	Unit	Note
Yield strength (YS) for Alloy 22 from Table 4.1-4	372 at room temperature 338 at 366K 283 at 477 K	MPa	Linear between temperatures (Section 6.2.1)
Yield strength (YS) for titanium grade 7 from Table 4.1-4	275-450 at room temperature 138-152 at 477K	MPa	Same as above & use average at temperature
Threshold stress (Alloy 22)	0.9 (YS) (Section 6.2.1)	MPa	YS at 200°C (473K) for WP
Threshold stress (Titanium Grade 7)	0.5 (YS) (Section 6.2.1)	MPa	YS at 140°C (413K) for DS
Initial size of incipient cracks	0.05 (Section 6.2.1)	mm	
Depth of plate to be included for embedded flaws	0.25 (Section 6.2.2.2)	Fraction of the plate thickness	
Oblique flaws to be added to radial flaws	0.005 (Section 6.2.2.3)	Fraction of the total flaws	
Mean of repassivation slope, Alloy 22 SDFR model	1.304 (Section 6.3.4)	Dimensionless	
Standard deviation of repassivation slope, Alloy 22 SDFR model	0.16 (Section 6.3.4)	Dimensionless	
Lower bound of repassivation slope, Alloy 22 SDFR model	0.984 (Section 6.3.4)	Dimensionless	
Upper bound of repassivation slope, Alloy 22 SDFR model	1.624 (Section 6.3.4)	Dimensionless	
Crack growth rate, V_t	$V_t = 7.8x10^{-2} n^{3.6}\left(4.1x10^{-14}\right)^n (K_I)^{4n}$ (Section 6.3.4, Eq. 19), where K_I is the SIF in MPa√m	mm/s	n is the repassivation slope
Mean general corrosion rate, Vgc, Alloy 22	7.23 (Section 6.3.5)	nm/y	
Threshold stress intensity factor, K_{ISCC}	$K_{ISCC} = (V_{gc} / \overline{A})^{1/\overline{n}}$ (Section 6.3.5, Eq. 20), where $\overline{A} = 7.8 \times 10^{-2} n^{3.6}\left(4.1 \times 10^{-14}\right)^n$ (Section 6.3.4, Eq. 18) and $\overline{n} = 4n$ (Section 6.3.3, Eq. 16)	MPa $m^{0.5}$	n is the repassivation slope V_{gc} in mm/s

Table 8-1 (part 2 of 3). Summary of Output
(Output DTN: LL030607012251.065)

Output name	Output value or equation	Unit	Note
Radial stress coeff. A_0, WPML, as-welded	181.636 (Section 6.4.2.4, Table 6-5)	MPa	
Radial stress coeff. A_1, WPML, as-welded	-177.592 (Section 6.4.2.4, Table 6-5)	MPa/mm	
Radial stress coeff. A_2, WPML, as-welded	23.385 (Section 6.4.2.4, Table 6-5)	MPa/mm^2	
Radial stress coeff. A_3, WPML, as-welded	-0.900 (Section 6.4.2.4, Table 6-5)	MPa/mm^3	
Hoop stress coeff. A_0, WPML, as-welded	219.908 (Section 6.4.2.4, Table 6-5)	MPa	
Hoop stress coeff. A_1, WPML, as-welded	56.494 (Section 6.4.2.4, Table 6-5)	MPa/mm	
Hoop stress coeff. A_2, WPML, as-welded	-20.848 (Section 6.4.2.4, Table 6-5)	MPa/mm^2	
Hoop stress coeff. A_3, WPML, as-welded	1.083 (Section 6.4.2.4, Table 6-5)	MPa/mm^3	
Radial stress coeff. A_0, WPOL, laser-peened	-265.920 (Section 6.4.4, Table 6-8)	MPa	
Radial stress coeff. A_1, WPOL, laser-peened	103.987 (Section 6.4.4, Table 6-8)	MPa/mm	
Radial stress coeff. A_2, WPOL, laser-peened	-9.857 (Section 6.4.4, Table 6-8)	MPa/m^2	
Radial stress coeff. A_3, WPOL, laser-peened	0.254 (Section 6.4.4, Table 6-8)	MPa/mm^3	
Hoop stress coeff. A_0, WPOL, laser-peened	-292.607 (Section 6.4.4, Table 6-8)	MPa	
Hoop stress coeff. A_1, WPOL, laser-peened	178.277 (Section 6.4.4, Table 6-8)	MPa/mm	
Hoop stress coeff. A_2, WPOL, laser-peened	-14.135 (Section 6.4.4, Table 6-8)	MPa/mm^2	
Hoop stress coeff. A_3, WPOL, laser-peened	0.320 (Section 6.4.4, Table 6-8)	MPa/mm^3	
Mean stress profile at $\theta=0$, $S_0(x)$	$S_0(x) = A_0 + A_1x + A_2x^2 + A_3x^3$ (Section 6.4.2.3, Eq. 23)	MPa	x (in mm) is crack depth
$S_0(x)$, radial stress, WPML, as-welded	Table 8-2, 2nd column	MPa	Calculated from Eq. 23
$S_0(x)$, hoop stress, WPML, as-welded	Table 8-2, 4th column	MPa	Calculated from Eq. 23
SIF, $K_0(x)$, radial stress, WPML, as-welded	Table 8-2, 3rd column	$MPa\ m^{0.5}$	
SIF, $K_0(x)$, hoop stress, WPML, as-welded	Table 8-2, 5th column	$MPa\ m^{0.5}$	

Table 8-1 (part 3 of 3). Summary of Output
(Output DTN: LL030607012251.065)

Output name	Output value or equation	Unit	Note
$S_0(x)$, radial stress, WPOL, laser-peened	Table 8-3, 2nd column	MPa	Calculated from Eq. 23
$S_0(x)$, hoop stress, WPOL, laser-peened	Table 8-3, 4th column	MPa	Calculated from Eq. 23
SIF, $K_0(x)$, radial stress, WPOL, laser-peened	Table 8-3, 3rd column	MPa $m^{0.5}$	
SIF, $K_0(x)$, hoop stress, WPOL, laser-peened	Table 8-3, 5th column	MPa $m^{0.5}$	
WPOL thickness (h)	25 (Section 6.4.2.1, Fig. 8)	mm	
WPML thickness (h)	10 (Section 6.4.2.1, Fig. 8)	mm	
Stress variability, ∇S	17.236893 (Section 6.4.5)	MPa	
Stress profile, $S_\theta(x)$, at angle θ from $S_0(x)$	$S_\theta(x) = S_0(x) - \nabla S(1 - \cos(\theta))$ (Section 6.4.5, Eq. 25a)	MPa	
SIF profile, $K_\theta(x)$, at angle θ from $K_0(x)$	$K_\theta(x) = K_0(x)\,(S_\theta(h) / S_0(h))$ (Section 6.4.5, Eq. 25b)	MPa $m^{0.5}$	
Variation amplitude of $S_0(x)$, ΔS	0.15 (YS) (Section 6.4.5, use YS value at the room temperature)	MPa	Uncertainty for ΔS is represented by a normal distribution truncated at ±3-sigma (±15% YS).
Lower bound of stress variation	$S_\theta(x)\min = S_\theta(x)\left(\frac{S_\theta(h) - \Delta S}{S_\theta(h)}\right)$ (Section 6.4.5, Eq. 26a)	MPa	
Upper bound of stress variation	$S_\theta(x)\max = S_\theta(x)\left(\frac{S_\theta(h) + \Delta S}{S_\theta(h)}\right)$ (Section 6.4.5, Eq. 26b)	MPa	
Lower bound of SIF variation	$K_\theta(x)\min = K_\theta(x)\left(\frac{S_\theta(h) - \Delta S}{S_\theta(h)}\right)$ (Section 6.4.5, Eq. 26c)	MPa $m^{0.5}$	
Upper bound of SIF variation	$K_\theta(x)\max = K_\theta(x)\left(\frac{S_\theta(h) + \Delta S}{S_\theta(h)}\right)$ (Section 6.4.5, Eq. 26d)	MPa $m^{0.5}$	

Table 8-2. Stresses and Stress Intensity Factors for the As-Welded WP Middle Lid (Output DTN: LL030607012251.065, also Section 6.4.2.4, Table 6-7)

Depth, mm	Radial stress (Sx), MPa	SIF due to Sx, MPa-$m^{0.5}$	Hoop stress (Sz), MPa	SIF due to Sz, MPa-$m^{0.5}$
0.1593	153.9288	4.9033	228.3849	7.5754
0.3203	127.1172	6.2685	235.9015	10.9665
0.4797	101.7315	6.8580	242.3296	13.7144
0.6407	77.2206	6.9761	247.8300	16.1330
0.8000	54.0676	6.7631	252.3158	18.3358
0.9593	31.9924	6.3044	255.8750	20.3775
1.1203	10.7596	5.8250	258.5570	22.3816
1.2797	-9.2150	5.2651	260.3330	24.3197
1.4407	-28.3699	4.6000	261.2667	26.1726
1.6000	-46.3322	3.8615	261.3655	27.9459
1.7593	-63.3265	3.0726	260.6697	29.6433
1.9203	-79.5368	2.2534	259.1863	31.2668
2.0797	-94.6509	1.4282	256.9724	32.8922
2.2407	-109.0061	0.5951	254.0088	34.5292
2.4000	-122.3284	-0.2400	250.3830	36.1060
2.5593	-134.7922	-1.0656	246.0945	37.6220
2.7203	-146.5363	-1.8707	241.1150	39.0762
2.8797	-157.3405	-2.6491	235.5736	40.4676
3.0407	-167.4522	-3.4047	229.3818	41.8264
3.2000	-176.6850	-4.1787	222.6938	43.2168
3.3593	-185.1690	-4.9390	215.4749	44.5479
3.5203	-193.0032	-5.6775	207.6685	45.8181
3.6797	-200.0480	-6.3965	199.4620	47.0265
3.8407	-206.4725	-7.0865	190.7114	48.1718
4.0000	-212.1664	-7.7528	181.6234	49.2531
4.1593	-217.2211	-8.2576	172.1366	50.3451
4.3203	-221.7016	-8.7427	162.1726	51.3729
4.4797	-225.5376	-9.2143	151.9633	52.3351
4.6407	-228.8312	-9.6605	141.3230	53.2313
4.8000	-231.5367	-10.0894	130.4975	54.0602
4.9593	-233.7127	-10.4950	119.4050	54.8214
5.1203	-235.3959	-10.9446	107.9526	55.4811
5.2797	-236.5735	-11.4131	96.4029	56.0586
5.4407	-237.2926	-11.8636	84.5422	56.5637
5.6000	-237.5602	-12.3055	72.6415	56.9965
5.7593	-237.4080	-12.7309	60.6057	57.3567
5.9203	-236.8501	-13.1320	48.3342	57.6444
6.0797	-235.9201	-13.7114	36.1065	57.7587
6.2407	-234.6208	-14.4707	23.6946	57.6946
6.4000	-233.0011	-15.2333	11.3811	57.5522
6.5593	-231.0713	-15.9891	-0.9356	57.3322
6.7203	-228.8287	-16.7277	-13.3570	57.0353
6.8797	-226.3414	-17.4611	-25.6005	56.6626
7.0407	-223.5802	-18.4707	-37.8942	56.1419
7.2000	-220.6238	-20.3589	-49.9583	55.3276
7.3593	-217.4669	-22.2128	-61.8935	54.4422
7.5203	-214.0957	-24.0173	-73.7955	53.4878
7.6797	-210.6019	-25.7872	-85.3924	54.6294
7.8407	-206.9348	-27.4989	-96.8987	56.2191
8.0000	-203.1923	-29.1709	-108.0509	57.7865

Table 8-3. Stresses and Stress Intensity Factors for Laser Peened WP Outer Lid (Output DTN: LL030607012251.065, also Section 6.4.4, Table 6-9)

Depth, mm	Radial stress (Sx), MPa	SIF due to Sx, MPa-$m^{0.5}$	Hoop stress (Sz), MPa	SIF due to Sz, MPa-$m^{0.5}$
0.3988	-226.0035	-9.1866	-223.7417	-5.6943
0.8001	-188.9005	-11.7979	-158.8532	-6.4965
1.1989	-154.9833	-13.0189	-98.6408	-6.1528
1.6002	-123.7220	-13.4298	-42.2143	-5.1372
1.9990	-95.4153	-13.2965	9.8344	-3.6697
2.4003	-69.6047	-12.7780	58.2916	-1.8824
2.7991	-46.5198	-12.2958	102.6663	0.1212
3.2004	-25.7687	-11.7214	143.6471	2.2821
3.5992	-7.5170	-11.0116	180.8374	4.5533
3.9980	8.4709	-10.2080	214.6297	6.8939
4.3993	22.3728	-9.3437	245.3299	9.2702
4.7981	34.1098	-8.4525	272.6715	11.6543
5.1994	43.9293	-7.6096	297.1262	14.0165
5.5982	51.8041	-6.8298	318.5068	16.3364
5.9995	57.9323	-6.0675	337.2088	18.6024
6.3983	62.3334	-5.3416	353.1178	20.8003
6.7970	65.1483	-4.6612	366.4827	22.9177
7.1984	66.4775	-4.0331	377.4871	24.9441
7.5971	66.4012	-3.4507	386.1141	26.9023
7.9985	65.0162	-2.8535	392.5969	28.8612
8.3972	62.4372	-2.2745	396.9757	30.7287
8.7986	58.7292	-1.7170	399.4297	32.5008
9.1973	54.0361	-1.1860	400.0499	34.1745
9.5987	48.3961	-0.6829	398.9677	35.7479
9.9974	41.9777	-0.2101	396.3190	37.2200
10.3962	34.8443	-0.3513	392.2239	38.4530
10.7975	27.0415	-0.5163	386.7654	39.5674
11.1963	18.7651	-0.7070	380.1350	40.5636
11.5976	10.0075	-0.9242	372.3715	41.4432
11.9964	0.9766	-1.1690	363.6954	42.2086
12.3977	-8.3447	-1.4403	354.1195	42.8627
12.7965	-17.7414	-1.7949	343.8874	43.4439
13.1978	-27.2353	-2.1728	332.9919	43.9342
13.5966	-36.6092	-2.5554	321.6934	44.3269
13.9954	-45.8267	-2.9438	310.0462	44.6272
14.3967	-54.8472	-3.3378	298.0958	44.8409
14.7955	-63.4595	-3.7396	286.1158	44.9743
15.1968	-71.6755	-4.0160	274.0769	45.0329
15.5956	-79.2941	-4.1354	262.2538	45.0208
15.9969	-86.3145	-4.2182	250.6192	44.9464
16.3957	-92.5507	-4.2696	239.4426	44.8182
16.7945	-97.9528	-4.2904	228.7710	44.6449
17.1958	-102.4495	-4.2805	218.6644	44.4361
17.5946	-105.8869	-4.3087	209.3730	44.2112
17.9959	-108.2109	-4.5204	200.9017	43.9968
18.3947	-109.2950	-4.7313	193.4801	43.7750
18.7960	-109.0551	-4.9400	187.1369	43.5578
19.1948	-107.3973	-5.1487	182.0747	43.3569
19.5961	-104.2024	-5.3536	178.3522	43.1853
19.9949	-99.4140	-5.5551	176.1390	43.0560

9. INPUTS AND REFERENCES

Andresen, P.L. and Ford, F.P. 1994. "Fundamental Modeling of Environment Cracking for Improved Design and Lifetime Evaluation in BWRs." *International Journal of Pressure Vessels and Piping, 59 (1-3),* 61-70. [New York, New York]: Elsevier Science. TIC: 247388.

Arthur, W.J. 2003. "YMP-2003-005, Baseline Change Proposal (BCP) 'Design Changes to Site Recommendation (SR) Waste Package.'" Memorandum from W.J. Arthur (DOE/ORD) to M.Y.S. Chu (DOE), January 28, 2003, 0129035840, with enclosure. [162432]

ASM International. 1987. *Corrosion*. Volume 13 of Metals Handbook. 9th Edition. Metals Park, Ohio: ASM International. TIC: 209807.

ASME (American Society of Mechanical Engineers) 1969. *Criteria of the ASME Boiler and Pressure Vessel Code for Design by Analysis in Section III and VIII, Division 2*. The American Society of Mechanical Engineers. 1969, Library of Congress Catalog Card Number 56-3934.

Beavers, J.A.; Devine, T.M., Jr.; Frankel, G.S.; Jones, R.H.; Kelly, R.G.; Latanision, R.M.; and Payer, J.H. 2002. *Final Report, Waste Package Materials Performance Peer Review Panel, February 28, 2002*. [Las Vegas, Nevada]: Waste Package Materials Performance Peer Review Panel. ACC: MOL.20020614.0035. [158781]

Bradford, S.A. 1987. "Fundamentals of Corrosion in Gases." In *Corrosion,* Volume 13, pp. 61-76 of *Metals Handbook.* 9th Edition. Metals Park, Ohio: ASM International. TIC: 209807.

BSC (Bechtel SAIC Company) 2001. *Aging and Phase Stability of Waste Package Outer Barrier.* ANL-EBS-MD-000002 REV 00 ICN 01. Las Vegas, Nevada: Bechtel SAIC Company. ACC: MOL.20010926.0007. [151550]

BSC (Bechtel SAIC Company) 2001. *Environment on the Surfaces of the Drip Shield and Waste Package Outer Barrier*. ANL-EBS-MD-000001 REV 00 ICN 02. Las Vegas, Nevada: Bechtel SAIC Company. ACC: MOL.20010724.0082. [155640]

BSC (Bechtel SAIC Company) 2001. *Model Validation Status Review*. TDR-WIS-MD-000005 REV 00. Las Vegas, Nevada: Bechtel SAIC Company. ACC: MOL.20011211.0095.

BSC (Bechtel SAIC Company) 2001. *Plugging of Stress Corrosion Cracks by Precipitates*. CAL-EBS-MD-000017 REV 00. Las Vegas, Nevada: Bechtel SAIC Company. ACC: MOL.20011010.0168.

BSC (Bechtel SAIC Company) 2002. *Technical Work Plan for: Waste Package Materials Data Analyses and Modeling*. TWP-EBS-MD-000005 REV 05. Las Vegas, Nevada: Bechtel SAIC Company. ACC: MOL.20021218.0029. [161132]

BSC (Bechtel SAIC Company) 2003. *Analysis of Mechanisms for Early Waste Package/Drip Shield Failure.* CAL-EBS-MD-000030 REV A. Las Vegas, Nevada: Bechtel SAIC Company. [161238]

BSC (Bechtel SAIC Company) 2003. *Drip Shield Structural Response to Rock Fall.* 000-00C-TED0-00500-000-00A. Las Vegas, Nevada: Bechtel SAIC Company. ACC: ENG.20030327.0001. [162598]

Buchalet, C.B. and Bamford, W.H. 1976. "Stress Intensity Factor Solutions for Continuous Surface Flaws in Reactor Pressure Vessels." *Mechanics of Crack Growth, Proceedings of the Eighth National Symposium on Fracture Mechanics, Providence, Rhode Island, 26-28 August 1974.* ASTM Special Technical Publication 590. Pages 385-402. Philadelphia, Pennsylvania: American Society for Testing Materials. TIC: 247548.

Canori, G.F. and Leitner, M.M. 2003. *Project Requirements Document.* TER-MGR-MD-000001 REV 01. Las Vegas, Nevada: Bechtel SAIC Company. ACC: DOC.20030404.0003. [161770]

Chan, S.K.; Tuba, I.S.; and Wilson, W.K. 1970. "On Finite Element Method in Linear Fracture Mechanics." *Engineering Fracture Mechanics,* 1-17. Oxford, United Kingdom: Pergamon Press. TIC: 247507.

CRWMS M&O 1996. *Waste Package Closure Weld Development Report.* BBA000000-01717-2500-00006 REV 00. Las Vegas, Nevada: CRWMS M&O. ACC: MOL.19960909.0188.

CRWMS M&O 1998. *Waste Package Phase II Closure Methods Report.* BBA000000-01717-5705-00016 REV 00. Las Vegas, Nevada: CRWMS M&O. ACC: MOL.19981208.0099.
CRWMS M&O 2000. *General Corrosion and Localized Corrosion of Waste Package Outer Barrier.* ANL-EBS-MD-000003 REV 00. Las Vegas, Nevada: CRWMS M&O. ACC: MOL.20000202.0172. [144229]

CRWMS M&O 1999. *Classification of the MGR Ex-Container System*. ANL-XCS-SE-000001 REV 00. Las Vegas, Nevada: CRWMS M&O. ACC: MOL.19990928.0221.

CRWMS M&O 1999. *Classification of the MGR Uncanistered Spent Nuclear Fuel Disposal Container System*. ANL-UDC-SE-000001 REV 00. Las Vegas, Nevada: CRWMS M&O. ACC: MOL.19990928.0216. CRWMS M&O 1999. Classification of the MGR Uncanistered Spent Nuclear Fuel Disposal Container System. ANL-UDC-SE-000001 REV 00. Las Vegas, Nevada: CRWMS M&O. ACC: MOL.19990928.0216.

CRWMS M&O 2000. *General Corrosion and Localized Corrosion of the Drip Shield.* ANL-EBS-MD-000004 REV 00. Las Vegas, Nevada: CRWMS M&O. ACC: MOL.20000329.1185. [144971]

CRWMS M&O 2001. *Abstraction of NFE Drift Thermodynamic Environment and Percolation Flux*. ANL-EBS-HS-000003 REV 00 ICN 02. Las Vegas, Nevada: CRWMS M&O. ACC: MOL.20010221.0160.

DOE (U.S. Department of Energy) 2003. *Quality Assurance Requirements and Description*. DOE/RW-0333P, Rev. 13. Washington, D.C.: U.S. Department of Energy, Office of Civilian

Radioactive Waste Management. ACC: DOC.20030422.0003. [162903]

Ewalds, H.L. and Wanhill, R.J.H. 1984. *Fracture Mechanics.* New York, New York: Edward Arnold. TIC: 247389.

Fix, D.V; Estill, J.C.; Hust, G.A.;King, K.J.; Day, S.D.; and Rebak, R.B. 2003. "Influence of Environmental Variables on the Susceptibility of Alloy 22 to Environmentally Assisted Cracking." *Corrosion 2003*. The annual conference and corrosion show sponsored by NACE International. Paper No. 03542.

Ford, F.P. and Andresen, P.L. 1988. "Development and Use of a Predictive Model of Crack Propagation in 304/316L, A533B/A508 and Inconel 600/182 Alloys in 288°C Water." *Environmental Degradation of Materials in Nuclear Power Systems—Water Reactors, [Proceedings of the Third International Symposium, Traverse City, Michigan, August 30-September 3, 1987].* Theus, G.J. and Weeks, J.R., eds. Pages 798 - 800. [Warrendale, Pennsylvania: Metallurgical Society]. TIC: 247505.

Harris, D.O.; Lim, E.Y.; and Dedhia, D.D. 1981. *Probabilistic Fracture Mechanics Analysis.* Volume 5 of *Probability of Pipe Fracture in the Primary Coolant Loop of a PWR Plant.* NUREG/CR-2189. Washington, D.C.: U.S. Nuclear Regulatory Commission. TIC: 247333.

Hornbach, D.J. 1999. *X-Ray Diffraction and Ring-Core Determination of the Residual Stress Distributions in One(1) Alloy C22 Welded Plate and One (1) Alloy C22 Test Bar.* 1034-8520. Cincinnati, Ohio: Lambda Research. TIC: 247252.

Jones, R.H. and Ricker, R.E. 1987. "Stress-Corrosion Cracking." *Metals Handbook Ninth Edition.* Volume 13. Corrosion . 145-163. Metals Park, Ohio: ASM International. TIC: 209807.

Klepfer, H.H. 1975. *Investigation of Cause of Cracking in Austenitic Stainless Steel Piping. Volume 1.* NEDO-21000-1 75NED35 CLASS 1. San Jose, California: General Electric. Copyright Requested. Library Tracking Number-247509.

LL000312705924.132. Stress Corrosion Cracking of the Drip Shield, the Waste Package Outer Barrier and the Stainless Steel Structural Material. Submittal date: 03/10/2000.

LL000316205924.142. Stress Corrosion Cracking of the Drip Shield, the Waste Package Outer Barrier and the Stainless Steel Structural Material. Submittal date: 03/22/2000.

LL000319805924.143. Corrosion Cracking of the Drip Shield, the Waste Package Outer Barrier and the Stainless Steel Structural Material. Submittal date: 03/22/2000.

LL000319905924.144. Corrosion Cracking of the Drip Shield, the Waste Package Outer Barrier and the Stainless Steel Structural Material. Submittal date: 03/22/2000.

LL000320005924.145. Corrosion Cracking of the Drip Shield, the Waste Package Outer Barrier and the Stainless Steel Structural Material. Submittal date: 03/22/2000.

LL020603612251.015. Slow Strain Rate Test Generated Stress Corrosion Cracking Data. Submittal date: 08/27/2002.

LL021105312251.023. Stress Corrosion Crack Growth and Initiation Measurements for C-22 and Ti-7, General Electric Global Research Center (GEGRC) 121202. Submittal date: 01/08/2003.

LL030412512251.057. LTCTF Corrosion Rate Calculations for Five-Year Exposed Alloy C22 Specimens Cleaned Under TIP-CM-51. Submittal date: 05/28/2003.

Lu, J., ed. 1996. *Handbook of Measurement of Residual Stresses*. Lilburn, Georgia: Fairmont Press. TIC: 247903.

Lundin, C.D. 2002. "Re: Welding Process Considerations for Waste Package Fabrication." Letter from C.D. Lundin to J.A. Cogar (BSC), September 11, 2002, with attachment. ACC: MOL.20021015.0209.

Macdonal, D.D. and Urquidi-Macdonald, M. 1991. "A Coupled Environment Model for Stress Corrosion Cracking in Sensitized Type 304 Stainless Steel in LER Environments." *Corrosion Science*, 32, 51-82. New York, New York: Pergamon Press.

Macdonald, D.D.; Urquidi-Macdonald, M.; and Lu, Pai-Chuan 1994. "The Coupled Environmental Fractural Model - A Deterministic Method for Calculating Crack Growth Rates." *Corrosion 94*. Paper No. 246, Houston, Texas: NACE International.

MO0003RIB00071.000. Physical and Chemical Characteristics of Alloy 22. Submittal date: 03/13/2000.

MO0003RIB00073.000. Physical and Chemical Characteristics of TI Grades 7 and 16. Submittal date: 03/13/2000.

MO0301SEPFEPS1.000. LA FEP List. Submittal date: 01/21/2003.

Mohr, W.C. 1996. "Internal Surface Residual Stresses in Girth Butt-Welded Steel Pipes ." *Residual Stresses in Design, Fabrication, Assessment and Repair, PVP-Vol. 321,* 37-44. New York, New York: American Society of Mechanical Engineers. TIC: 247502.

NRC (U.S. Nuclear Regulatory Commission) 2003. *Yucca Mountain Review Plan, Information Only.* NUREG-1804, Draft Final Revision 2. Washington, D.C.: U.S. Nuclear Regulatory Commission, Office of Nuclear Material Safety and Safeguards. TIC: 254002. [162418]

Pasupathi, V. 2000. Documentation of Literature on Residual Stress Measurements. Interoffice correspondence from V. Pasupathi (CRWMS M&O) to G.M. Gordon, May 19, 2000, LV.WP.VP.05/00-070, with enclosures. ACC: MOL.20000522.0146.

Reamer, C.W. 2001. "U.S. Nuclear Regulatory Commission/U.S. Department of Energy Technical Exchange and Management Meeting on Total System Performance Assessment and Integration (August 6 through 10, 2001)." Letter from C.W. Reamer (NRC) to S. Brocoum (DOE/YMSCO), August 23, 2001, with enclosure. ACC: MOL.20011029.0281. [158380]

Rice, J.R. 1968. "A Path Independent Integral and the Approximate Analysis of Strain Concentration by Notches and Cracks." *Journal of Applied Mechanics, Transactions of the ASME, 35,* 379-386. New York, New York: American Society of Mechanical Engineers. TIC: 247487.

Shcherbinskii, V.G. and Myakishev, V.M. 1970. "Statistical Distribution of Welding Defects with Respect to Azimuth." *Central Scientific-Research Institute of Technical Engineering. Translated from Defektoskopiya, No. 4., UDC 620.179.16,* 143-144. New York, New York: Plenum Publishing Corporation. TIC: 247890.

SI (Structural Integrity Associates), Inc. 2003. *Evaluation of the CRM-21 PWR and Viability Availability Waste Package*. Report No. SIR-99-094. Revision 1. Prepared for Bechtel SAIC, Las Vegas, Nevada, by Structural Integrity Associates, Inc., San Jose, California. March 2003. ACC: MOL.20030327.0004.

Smith, D. 2003. *Weld Flaw Evaluation and Nondestructive Examination Process Comparison Results for High-Level Radioactive Waste Disposal Container Manufacturing Program.* TDR-EBS-ND-000007 REV 01. Las Vegas, Nevada: Bechtel SAIC Company.

Sprowls, D.O. 1987. "Evaluation of Stress-Corrosion Cracking." *Metals Handbook Ninth Edition.* Volume 13. Corrosion. 245-282. Metals Park, Ohio: ASM International. TIC: 209807.

Structural Integrity Associates. 2002. *Structural Integrity Associates Support of Waste Package Design for Year 2001*. SIR-02-073. San Jose, California: Structural Integrity associates. ACC: MOL.20020709.0389.

Tada, H.; Paris, P.C.; and Irwin, G.R. 1973. *The Stress Analysis of Cracks Handbook.* St. Louis, Missouri: Del Research Corporation. TIC: 247050.

9.1 PROCEDURES

AP-2.27Q, Rev. 0, ICN 0. *Planning for Science Activities.* Washington, D.C.: U.S. Department of Energy, Office of Civilian Radioactive Waste Management. ACC: MOL.20020701.0184.

AP-SI.1Q, Rev. 4, ICN 0. *Software Management*. Washington, D.C.: U.S. Department of Energy, Office of Civilian Radioactive Waste Management. ACC: MOL.20030113.0149.

AP-SIII.10Q, Rev. 1, ICN 0. *Models*. Washington, D.C.: U.S. Department of Energy, Office of Civilian Radioactive Waste Management. ACC: DOC.20030312.0039.

AP-SV.1Q, Rev. 0, ICN 2. *Control of the Electronic Management of Information.* Washington,

D.C.: U.S. Department of Energy, Office of Civilian Radioactive Waste Management. ACC: MOL.20000831.0065.

10. ATTACHMENTS

No attachments.